THE CONTRIBUTIONS OF VIRAL AND CELLULAR ELEMENTS TO ROUS SARCOMA VIRUS BUDDING

A Dissertation

Presented to the Faculty of the Graduate School

of Cornell University

In Partial Fulfillment of the Requirements for the Degree of

Doctor of Philosophy

by

Kari Ann Dilley

May 2009

CONTRIBUTIONS OF VIRAL AND CELLULAR ELEMENTS TO ROUS SARCOMA VIRUS BUDDING

Kari Ann Dilley, Ph. D.

Cornell University 2009

The efficient release of newly assembled retrovirus particles from the plasma membrane requires the recruitment of a network of cellular proteins (the ESCRT machinery) normally involved in the biogenesis of multivesicular bodies (MVBs). It is known that retroviruses, as well as other enveloped viruses, recruit this ESCRT machinery through short motifs termed late domains. Retroviruses use three classes of late domains as docks for the ESCRT machinery: PT/SAP, PPXY, and $LYPX_nL$.

The major late domain of Rous sarcoma virus (RSV) has been mapped to a PPPY motif in Gag that binds members of the Nedd4-family of ubiquitin ligases. RSV Gag also contains a second putative late domain motif, LYPSL, positioned five amino acids downstream of PPPY. $LYPX_nL$ motifs have been shown to support budding in other retroviruses by binding the ESCRT adaptor protein Alix. To investigate the role of this LYPSL motif in RSV budding I measured budding rate and spreading rate, and examined the budding phenotypes with scanning electron microscopy of various PPPY and LYPSL mutants in the context of infectious RSV. Typical of late domain phenotypes, SEM showed an increase number of particles in the process of budding on the plasma membrane when the LYPSL motif was mutated to AAASA. I found that mutating the LYPSL motif alone caused a moderate reduction in the budding rate of RSV. However, the role of the LYPSL motif in budding and

spreading was amplified when the primary PPPY late domain was fully or partially mutated. In this same context I also showed that the related equine infectious anemia virus LYPDL motif acts as a stronger late domain than the LYPSL. Furthermore, I found that the over-expression of Alix increases the budding and spreading rate of wild-type and late domain mutants, especially PPPY mutants in which the LYPSL motif remains intact. Taken together these results support a model of RSV budding in which the LYPSL motif acts as a secondary late domain via its interaction with Alix.

BIOGRAPHICAL SKETCH

Kari Ann Dilley was born in Flint, Michigan on October 23rd 1979 to two school teachers Mary and W. Ray Dilley. She and her ever-patient and much taller older brother Michael grew up playing basketball, soccer, and catching frogs in the creek next to their house. She graduated from Lake Fenton High School in 1998, where she fell in love with Biology and Chemistry in the classes of Mr. Cupal and Mr. Miller.

Kari earned a Bachelor of Science, majoring in cell and molecular biology, from the University of Michigan in Ann Arbor. There she was introduced to biological research studying the molecular mechanisms of apoptosis in the pathology lab of Claudius Vincenz and Peter Ward under the supervision of graduate student Tom Hlaing.

Following graduation Kari got a puppy, Amoeba, and moved to Ithaca to pursue her doctorate at Cornell University. She was tickled to be in the town that her childhood hero Carl Sagan once lived and worked. Kari was lucky enough to be able to join the Vogt lab and study retroviral budding. With the encouragement of Volker, she was able to collaborate with and visit the Ruml lab in Prague for a summer. Kari was proud to be part of the Vogt lab and will treasure her memories of and friendships with her labmates forever.

Kari received a postdoctoral fellowship at the NCI-Frederick to study HIV recombination in the lab of Wei-Shau Hu.

This dissertation is dedicated in its entirety, except for typos, to Mom and Dad.

The typos are for you Volker.

ACKNOWLEDGMENTS

I would like to thank Mom, Dad, and Mike for their endless support through school, college, and graduate school, especially during these last few months, and for always encouraging my interest in science (and for babysitting Amoeba). It means everything to me and I could not have done it without you.

I would like to thank Volker for taking a chance on me and letting me join the lab when the lab was full and the money tight. I appreciate how Volker always seemed to see the best in his students, not their weaknesses, and always gave them the benefit of the doubt. I am eternally grateful for Volker's advice, scientific and otherwise. I always felt better leaving Volker's office than I did when I entered.

I want to thank my committee Bill Brown and Gary Whittaker for helpful experimental and presentation suggestions.

I would like to thank past and present Vogt lab members. Marc Johnson initiated what later became my project and continued to provide invaluable advice, as well as scanning electron micrographs. I am indebted to Danso Ako-Adjei, Judy Phillips, Elena Kamynina, Bob Suran, Amanda Dalton, Gisela Schatz, Paul Keller, Becky Bean, Jany Chan, and Rob Dick for daily scientific discussions and advice. I want to thank Amy Antosh for microscopy help, Zdenek Knejzlik and Tomas Ruml for an enriching collaboration, and Diane Colf for tolerating numerous questions and late abstracts and progress reports.

TABLE OF CONTENTS

LIST OF FIGURES

LIST OF TABLES

LIST OF ABBREVIATIONS

Viruses

ASLV	avian sarcoma and leukemia virus
EBOV	ebola virus
EFV	equine foamy virus
EIAV	equine infectious anemia virus
FFV	feline foamy virus
GALV	gibbon ape leukemia virus
HAV	hepatitis A virus
HBV	hepatitis B virus
HIV-1	human immunodeficiency virus type 1
HTLV-1	human T-cell leukemia virus type 1
HTLV-2	human T-cell leukemia virus type 2
MLV	murine leukemia virus
MMTV	mouse mammary tumor virus
MPMV	Mason-Pfizer monkey virus
RSV	Rous sarcoma virus
SV5 (PIV5)	simian virus 5 (parainfluenza virus 5)
WDSV	walleye dermal sarcoma virus
VSV	Vesicular stomatitis virus

Viral genes and elements

CA	capsid domain of Gag
CTD	C-terminal domain of CA

CTRS	cytoplasmic targeting and retention signal
DIS	dimerization initiation sequence
Env	envelope glycoprotein
Gag	structural protein (group-specific antigen)
IN	integrase
ISD	internal scaffold domain
LTR	long terminal repeat
MA	matrix domain of Gag
MBD	membrane binding domain of MA
MHR	major homology region
NC	nucleocapsid domain of Gag
NRS	negative regulator of splicing
NTD	N-terminal domain of CA
PBS	primer binding site
PIC	preintegration complex
PR	protease
RT	reverse transcriptase
SU	surface glycoprotein
TM	transmembrane glycoprotein
UTR	untranslated regron
VLP	virus-like particle

Cellular proteins and protein domain

AAA	ATPases associated with diverse cellular activities
AIP1	ALG-2-interacting protein 1

Alix	ALG-2-interacting protein X
AMSH	associated molecule with the Src homology 3 domain of STAM
Bro	BCK1-like resistance to osmotic shock
CHMP	charged multivesicular body protein, chromatin modifying protein
CON	connexin-like
CRM1	chromosome region maintenance protein 1
Doa	degradation of alpha2
DUB	de-ubiquitinating enzyme
EAP	ELL Associating Protein
EGFR	epidermal growth factor receptor
Eps15	EGF pathway substrate 15
ESCRT	endosomal sorting complex for transport
FYVE	Fab1, YOTB, Vac1, EEA1
GLUE	GRAM-like ubiquitin-binding in Eap45
HECT	homology to the E6-AP carboxyl terminus
Hbp	Hrs-binding protein
Hrs	hepatocyte growth factor-regulated substrate
Hse	has symptoms of class E mutants; resembles Hrs, STAM, East
ILV	interlumenal vesicles
JAMM	Jab1/MPN domain-associated metalloisopeptidase
LBPA	lysobisphosphatidic acid
MHC-I	Major histocompatibility complex I
MIM	MIT Interaction Motifs
MIT	microtubule interacting and transport
MVB	multivesicular body
MVB12	multivesicular body sorting factor of 12 kilodaltons

Nedd4	neural precursor cell expressed developmentally downregulated 4
NES	nuclear export signal
NLS	nuclear localization signal
NZF	Npl4 zinc finger
PRD	proline-rich domain
RING	really interesting new gene
SH3	src homology-3
SSM	STAM-specific motif
STAM	signal-transducing adaptor molecule
SETA	Src homology 3 domain-containing, expressed in tumorigenic astrocytes
Tsg101	tumor susceptibility gene 101
UBPY	Ub-specific peptidase Y, also known as USP8
UEV	ubiquitin E2 variant
UIM	ubiquitin-interacting motif
VHS	Vps27/Hrs/STAM domain
VPS	vacuolar protein sorting
WH	winged-helix protein motif
WW	tryptophan-tryptophan
YAP	Yes (tyrosine kinase)-associated protein

Miscellaneous

DF1	(Doug Foster) chicken fibroblasts ev-0 cell line
DMEM	Dulbecco's modified Eagle medium
EDTA	ethylenedinitrilo tetraacetic acid

FBS	fetal bovine serum
GFP	green fluorescent protein
GST	glutathione *S*-transferase
MT4	T-cell cell line transformed with HTLV-1
NMR	nuclear magnetic resonance
PAGE	polyacrylamide gel electrophoresis
PBS	phosphate buffered saline
PCR	polymerase chain reaction
$PI_{(4,5)}P_2$	phosphatidylinositol 4,5-bisphosphate
SDS	sodium dodecylsulfate
SEM	scanning electron microscopy
TEM	transmission electron microscopy
TIRF	total internal reflection fluorescence

CHAPTER ONE

INTRODUCTION

Being obligate parasites, viruses have adapted strategies for commandeering host cellular pathways to perform steps in their own replication cycles. Because the virus and the host cell are using the same pathways, elucidating viral mechanisms for utilizing cellular pathways often leads to insightful breakthroughs in understanding the cell itself. For example, the recent link discovered between enveloped virus budding, such as that of Human Immunodeficiency Virus (HIV-1), and the cellular ESCRT pathway required for the biogenesis of multivesicular bodies (MVBs), has accelerated the progress in understanding the complex network of proteins that make up the ESCRT pathway. Driven by the necessity to understand and fight a threatening human pathogen, such as HIV-1, researchers have expanded the known functions of the ESCRT machinery to those beyond MVB formation and virus budding, to that of cytokinesis and autophagy.

The work presented in this thesis examines the role of viral elements (late domains) and their interactions with the cellular proteins (the ESCRT pathway) in the budding of Rous sarcoma virus.

Classification of Retroviruses

Retroviruses are a family of enveloped viruses that contain two copies of a single-stranded RNA genome. The retroviridae family was named for a signature step in its replication cycle in which the RNA genome is reverse transcribed into double-stranded DNA (dsDNA) and integrated into the cell genome. Retroviral genomes are between 7-13 kb and encode at least three major proteins: Gag, Pol and Env (Figure 1.1A) (37). Gag is the structural polyprotein that directs particle assembly and ultimately makes up the matrix,

capsid and nucleocapsid of the virion. Pol contains the enzymes reverse transcriptase and integrase responsible for the reverse transcription of the genome and integration of the resulting DNA into the host chromosome, respectively. Retroviruses are further divided into two categories, simple or complex, based on whether they contain additional genes that encode accessory proteins. These auxiliary proteins play a variety of roles in viral replication and pathogenesis. Retroviruses can also be classified into seven genera: alpharetroviruses (e.g. Rous sarcoma virus, RSV), betaretroviruses (e.g. Mason-Pfizer monkey virus and Mouse mammary tumor virus), gammaretroviruses (e.g. Murine leukemia virus), deltaretroviruses (e.g. Bovine leukemia virus), epsilonretroviruses, lentiviruses (e.g. Human immunodeficiency virus and Equine Infectious Anemia virus), and spumaviruses (e.g. Human foamy virus). The focus of this thesis, Rous sarcoma virus (RSV), is the prototypic alpharetrovirus and it lacks accessory proteins. However, the genome does carry the free standing v-src gene (Figure 1.1C) that is responsible for the transforming property of RSV, though it is dispensable for viral replication.

Retroviral Replication

Entry

Retroviral infection is initiated with the envelope-mediated binding of the virion to a specific cell surface receptor followed by virus/cell membrane fusion (Figure 1.2) (46). The binding and fusion steps are mediated by the external glycosylated polypeptide (SU) and the membrane-spanning protein (TM), products of the *env* gene. Env is translated, glycosylated, and oligomerized in the rough endoplasmic reticulum and is transported to the plasma membrane via membrane trafficking. A trimer of this SU/TM heterodimer makes up the

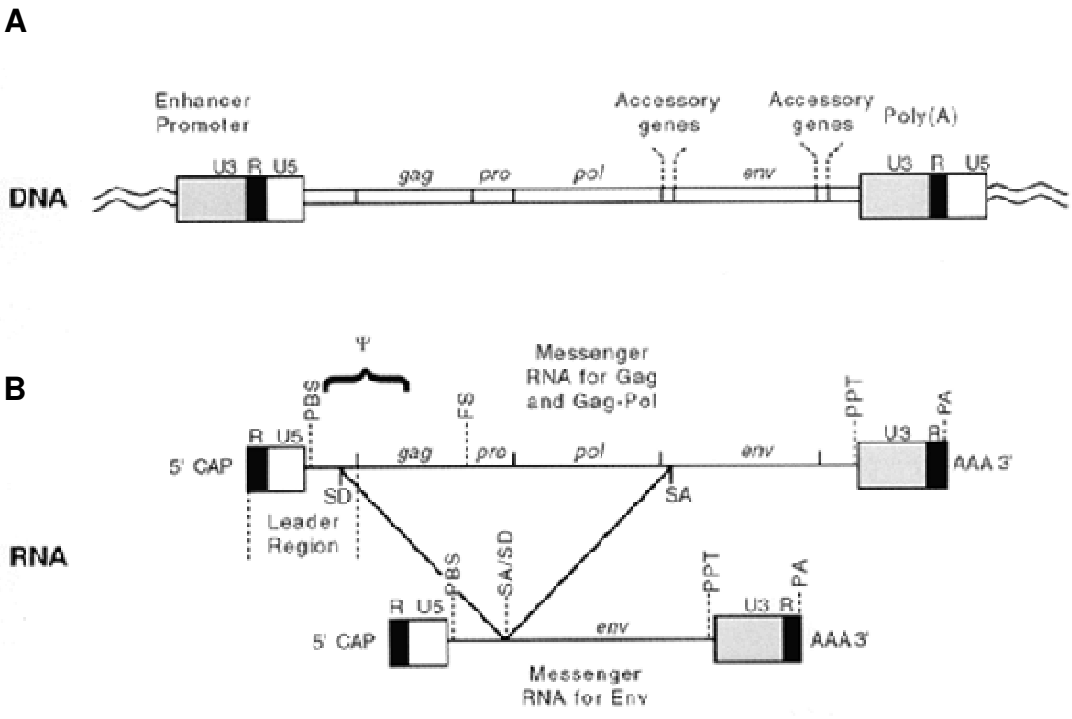

Figure 1.1 Genetic Ogranization of Retroviruses. (A) Proviral DNA from a generic retrovirus. LTRs are made up of U3, R, U5 elements. (B) Primary transcription product. (PBS) primer-binding site, (Ψ) Psi packaging signal, (SD) splice donor, (FS) frameshift, (PA) poly-adenylation signal, (SA) splice acceptor, (PPT) polypurine tract, (AAA) poly(A) tail. (C) Genetic organization of RSV. Reprinted from Coffin et al. (37).

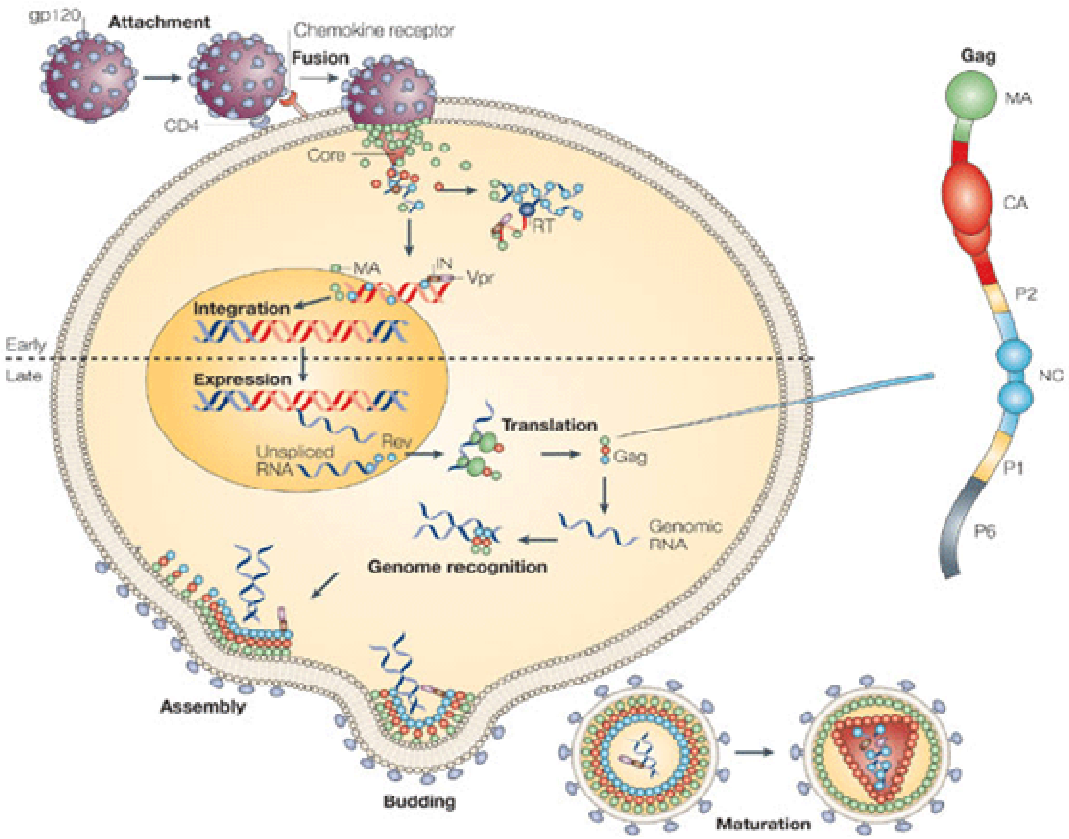

Figure 1.2 The retroviral replication cycle. A virion binds a specific cellular receptor via the Env glycoprotein leading to membrane fusion and the release of the viral core into the cytoplasm. Viral reverse transcriptase copies RNA genome into dsDNA for integration into host chromosome. Host transcription machinery transcribe and translate viral genes. Gag is targeted to the membrane for assembly. Two copies of the genome are packaged into each nascent particle that buds from the plasma membrane. Shortly after budding the viral protease cleaves Gag yielding an infectious particle. Reprinted from D'Souza et al. (46).

functional Env “knob” required to mediate viral entry (50). Rous sarcoma virus Env is translated as a Pr95 precursor that is proteolytically processed in the Golgi into its SU (gp85) and TM (gp37) products (47, 50). The binding of RSV surface glycoprotein (SU) to the cellular receptor induces exposure and insertion of a portion of TM fusion peptide into the lipid bilayer. TM is refolded and primed for triggering which occurs at low pH in an acidified endosome (130). Once fusion occurs the viral core is released into the cytoplasm of the infected cell and the signature step of retroviruses, reverse transcription takes place.

Reverse Transcription

Reverse transcription was discovered independently by Howard Temin and David Baltimore, who showed that purified particles (RSV and Rauscher mouse leukemia virus) possessed DNA polymerase activity that incorporated ^{3}H-TTP into a DNA product (10, 206). They showed that the template was sensitive to RNase and the product was sensitive to DNase. The RNA-dependent DNA polymerase, reverse transcriptase (RT) contains an RNase H domain (125) as well as the polymerase domain. Reverse transcription is primed by the binding of a host tRNA to the primer binding site (PBS) near the 5’ end of the RNA (Figure 1.3). This tRNA is specific to each genus of retrovirus. For example, RSV uses tryptophan tRNA (72, 153, 216), HIV-1 uses lysine tRNA (168) and MLV uses proline tRNA to prime reverse transcription (157). Although tRNAs and other RNA are passively incorporated into particles, specific primer tRNA is packaged through its association with RT (158, 177). After tRNA anneals, minus-strand DNA synthesis is initiated and continues until the 5’ end of the RNA, yielding the minus-strand “strong stop” DNA (-sssDNA). The RNaseH activity of RT then

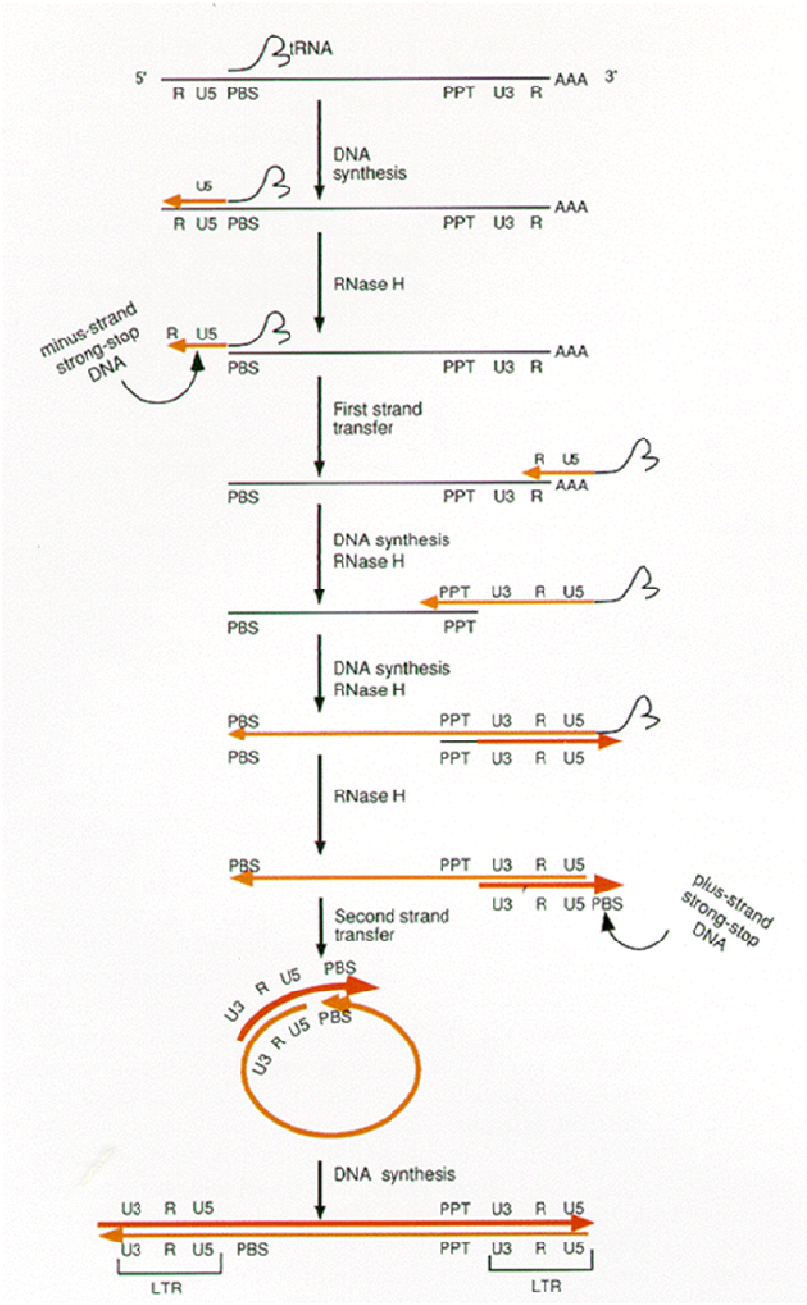

Figure 1.3 Steps of reverse transcription of the retroviral genome. (Black lines) RNA; (light orange) minus-strand DNA; (dark orange) plus-strand DNA; (PPT) polypurine tract; (U3) part of LTR unique to 3' end of genome; (U5) part of LTR unique to 5' end of genome; (R) part of LTR repeated at both ends of genome. Reprinted from Coffin et al. (3).

degrades the RNA of the DNA:RNA duplex, and the minus-strand "strong stop" DNA is transferred to the 3' end of the RNA in what is termed the first strand transfer. The R, or repeated sequence that is at both ends of the RNA genomes allows the minus-strand strong stop DNA to bind the 3' end of RNA. Next, DNA polymerization and RNaseH activity continue to the 5' end of the RNA template. The RNaseH leaves a short polypurine tract (PPT) undigested that becomes important for priming DNA polymerization using the newly synthesized DNA strand as the template. The plus-strand strong stop DNA (+sssDNA) is polymerized using the PPT as a primer. The second strand transfer occurs when the complementary PBS segment in the +sssDNA and the minus strand DNA anneal. RT then completes plus- and minus-strand synthesis using the other strand as template.

Two characteristics of reverse transcription make it a powerful driver of evolution. First, RT lacks proofreading ability, having neither 3' nor 5' exonuclease activity, and thus is error-prone. Second, retroviral RTs are able to jump from one RNA genome to the other. If a cell is infected with genetically distinct but related viruses, and both of their genomes are packaged into the same particle, the resulting DNA provirus often is a recombinant of the two viruses.

Integration

Reverse transcription results in a double-stranded DNA copy of the genome that is flanked by viral long terminal repeats (LTRs) (Figure 1.3). The viral integrase (IN) protein recognizes short 12-20 bp sequences called attachment (att) sites at the ends of the LTRs and catalyzes two distinctreactions. The first reaction, 3' processing, hydrolyzes a dinucleotide from each end and creates recessed 3' OH groups that then act as

nucleophiles to promote the second reaction, the DNA strand transfer. Host cell enzymes then repair the DNA intermediate. Once integrated, the provirus replicates along with the host genome and is used as a template for transcription by the cell machinery.

Integration-site selection varies among retroviruses. Avian sarcoma-leukosis virus (ASLV) exhibits an almost random integration-site selection in chromosomes, with only a slight preference for transcription units (but not transcription start sites) (124, 137). Gammaretroviruses, such as MLV, tend to integrate near the 5' ends of transcription units and CpG islands (226). Lentiviruses, such as HIV-1, do not prefer the 5' end of genes but do prefer active transcription units for integration (124, 184). Using MLV/HIV-1 chimeras Lewinski et al. determined that IN is the main determinant for integration-site selection, though Gag may have minor influence (109). A cellular protein, lens epithelium-derived growth factor (LEDGF/p75), contributes to the targeting of active genes for HIV-1 integration, acting as a tether between IN and the DNA (32).

Viral Transcription, Translation

Cis elements in the LTRs of the proviral DNA and cellular transcription factors mediate synthesis of viral genomic RNA, and cellular RNA processing machinery caps 5' ends, polyadenylates 3' ends and splices viral transcripts. Some complex retroviruses carry viral trans-activators for transcription. For example, the HIV-1 *tat* gene, whose product (Tat) binds to a stem loop (called TAR) in the 5' end of nascent RNAs, enhances elongation several hundred-fold. Unspliced viral RNA serves as template for translation of Gag and Gag-Pol-Pro (or Gag-Pol in RSV as protease is part of the Gag polyprotein) and for packaging into newly assembled virus as genomic RNA. Spliced RNA serves

as a template for Env translation, Src translation (in RSV) or the translation of other accessory proteins (in complex retroviruses). Free cytoplasmic ribosomes translate the viral proteins Gag and Gag-Pol-Pro (Gag-Pol in RSV) while ribosomes on the rough endoplasmic reticulum translate Env.

Assembly

The assembly of retrovirus particles is driven by the Gag polyprotein (Reviewed in (61)). Gag alone can assemble into virus-like particles (VLPs) *in vitro* in the presence of nucleic acid (21) and can assemble and bud *in vivo* in the absence of all other viral components. Retroviral Gag polyproteins share three common domains MA, CA, and NC, but differ in additional cleavage products (p2a, p2b, p10, SP in RSV). RT, and IN are targeted to the site of assembly and incorporated into assembling particles as part of the Gag-Pol polyprotein. Particle assembly is the result of thousands of Gag molecules arranged radially at the plasma membrane with the N-terminal MA domain of Gag associated with the membrane and the C-terminal NC domain toward the center of the particle (Figure 1.4). During or shortly after budding, the viral protease is activated and cleaves Gag into its smaller domains resulting in an infectious particle with core composed of CA enclosing the NC associated RNA genome (Figure 1.4).

Most retroviruses assemble using the C-type assembly pathway where Gag molecules are targeted to the plasma membrane by the MA domain (54, 86, 219) (Figure 1.5). RSV MA contains a patch of basic charges and is responsible for targeting Gag to the membrane, mostly through ionic interactions (41, 42). Most Gag proteins, not including that of RSV, are also post-translationally myristylated at the N-terminal glycine of MA (76). The myristate it thought to assume two positions, one where it is sequestered

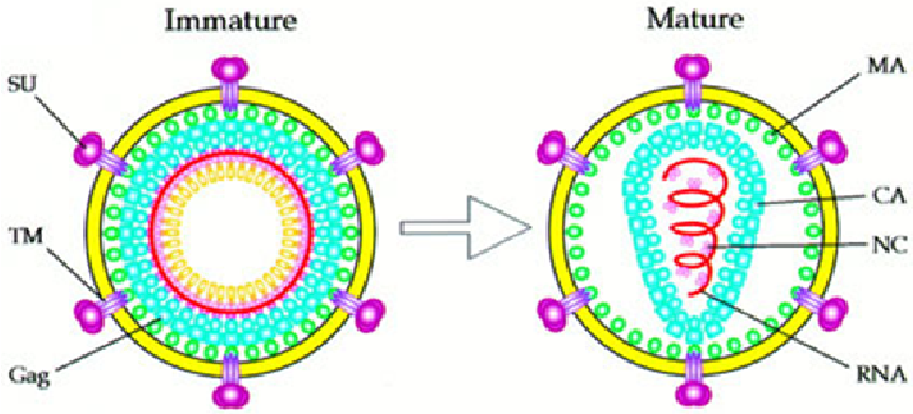

Figure 1.4 Models of immature and mature retroviral structure. During or shortly after budding the viral protease is activated cleaving the Gag polyprotein. This results in a dramatic change in arrangement. Yellow is membrane, green is MA, cyan is CA, purple is NC, red is RNA genome, orange is p6. HIV-1 particles, seen here, have a mature cone-shaped capsid core (cyan). However, the shape of the core varies with retrovirus. RSV and MLV have roughly spherical cores approximately centered in the particle. MMTV particles have a round core that is placed eccentrically. MPMV cores are bar shaped. Reprinted from Coffin et al. (37).

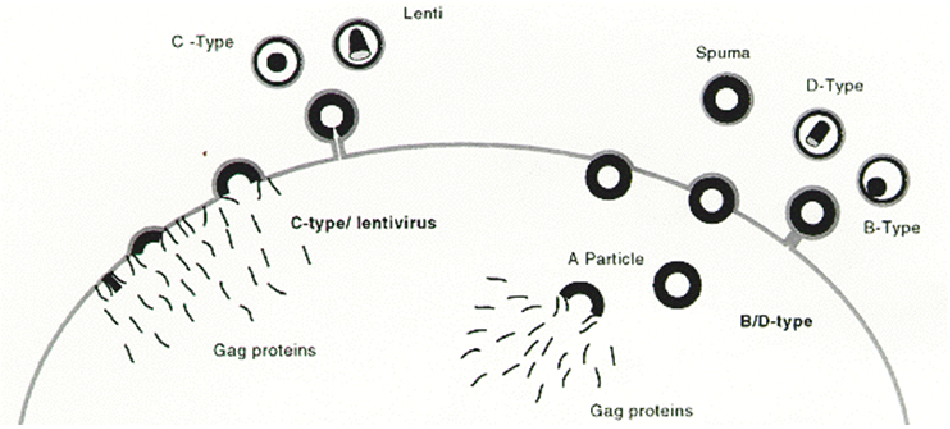

Figure 1.5 Two assembly pathways for retroviruses: C-type and B/D-type. HIV-1 and RSV are examples of viruses that assembly using the C-type assembly pathway where Gag is targeted to the plasma membrane for assembly and budding. In contrast to MPMV (type-D) and MTMV (type-B) capsids that assemble in a perinuclear region and traffick to the plasma membrane where they bud. Reprinted from Coffin et al. (37).

within Gag and one where it is exposed (190, 240). The myristate exposure, or “myristyl switch”, may be induced by multimerization of Gag (205) or by Gag binding to $PI(4,5)P_2$ on the inner leaflet of the plasma membrane (172). A newly assembled immature virus particles is composed of thousands of Gag molecules arranged radially with the N-terminal MA domain associated with the inner leaflet of the viral membrane. The newly assembled immature retroviral particle that buds from the plasma membrane is morphologically distinct from the mature particle that infects a new cell.

Mouse mammary tumor virus (MMTV) and Mason-Pfizer monkey virus (MPMV) particles assemble using the alternative B/D-type assembly pathway (Figure1.5). Gag accumulates and immature capsids assemble at perinuclear regions. The naked capsids (lacking membrane) are then targeted to the plasma membrane via an Env-dependent mechanism where they then bud from the cell. B-and D-type Gag proteins carry a conserved 18-amino acid sequence in MA that it responsible for cytoplasmic assembly and thus is called the cytoplsmic targeting-retention signal (CTRS). This signal is the dominant signal directing Gag on the B/D-type assembly pathway and its presence in MLV Gag in an analogous position is enough to cause MLV to assemble intracytoplasmically (33). A second sequence element termed the internal scaffold domain (ISD) in the p12 domain of MPMV Gag also contributes to D-type assembly (96, 175, 189). The ISD is thought to be a strong self-interacting domain and promote cytoplasmic assembly of particles by promoting Gag multimerization and thus bypassing the need for the Gag-concentrating role membrane plays in C-type assembly. MMTV lacks a specific self-interacting domain such as the ISD, but instead seems to have multiple regions that contribute to Gag-Gag interactions (235).

After translation, RSV Gag is trafficked transiently through the nucleus by a noncanonical nuclear localization signal (NLS) located in the MA domain (178). In the nucleus Gag binds to unspliced RSV genomic RNA which may promote Gag-Gag interactions (92) and is then exported. A nuclear export signal (NES) (179) and the soluble CRM1 export adaptor are critical for Gag transport back to the cytoplasm (178). A Gag mutant in which two acidic residues in MA are mutated to basic residues, thereby increasing its affinity for acidic ligands in the inner leaflet of the plasma membrane, is able to bypass the nuclear entry step in Gag trafficking. The resulting particles packaged only $1/10^{th}$ the amount of genomic RNA found in wild-type particles and were noninfectious, implying that the transient nuclear localization is an essential step for RNA packaging (20).

The largest Gag domain, CA, contributes significantly to Gag-Gag interactions. The CA domain is also the defining element in the size and morphology of virus particles (2) and the CA-CA interactions are important for the assembly of both immature and mature particles. CA is organized into two α-helical domains, the N-terminal domain (NTD) and the C-terminal domain (CTD) separated by a flexible linker. In the mature core the NTDs interact with other NTDs to form the hexamers that make up the lattice and the CTDs form dimers with the CTDs of CA molecules in neighboring hexamers (128, 225).

The most highly conserved stretch of amino acids in Gag, termed the major homology region (MHR) is about 20 amino acids long and is located in the CTD of CA. The exact function of the MHR is unknown, but the MHR has been shown to be important for assembly and infectivity (39).

The NC domain of Gag plays integral roles in assembly and packaging of viral RNA. NC is mostly non-structured and usually located at the C-terminus of Gag (except in RSV Gag which has PR at the C-terminus after NC). NC harbors one or two zinc fingers that are responsible for specifically recognizing the packaging sequence (Ψ) in the 5'UTR of the viral genomic RNA. The binding of NC to RNA also promotes Gag-Gag interactions, nucleating assembly and acting as a scaffold for the assembly of a particle.

Budding

Gag is the only *viral* requirement for the budding of VLPs. The one exception in the retroviral family is foamy virus which also requires the expression of Env for budding (9, 55). However in this case, Env seems to play an important role in targeting Gag to membrane, since adding the Src myristylation signal to the N-terminus of Gag allows VLPs to bud without Env (49, 111). Thus the block in the absence of Env is probably occurring at assembly, not budding.

Though Gag is the only viral component required for budding, a whole network of cellular proteins must also participate. The Gag sequences that are required for the final membrane fission step of budding are short (four or five amino acid) modular recognition sequences. Deletion or mutation of these short sequences in Gag results in a block in particle release (Figure 1.6). The viral particles are fully assembled but remain attached to the cell through a thin membranous stalk and display immature morphology, implying protease activation has not occurred (1.6A, middle and right panels). Because of their role in the late stages of budding, they have been termed "late domains". Late domains can be classified on the basis of sequence consensus, fitting into three groups: PT/SAP, PPXY, and $LYPX_nL$ (Figure 1.7). Late domains tend to

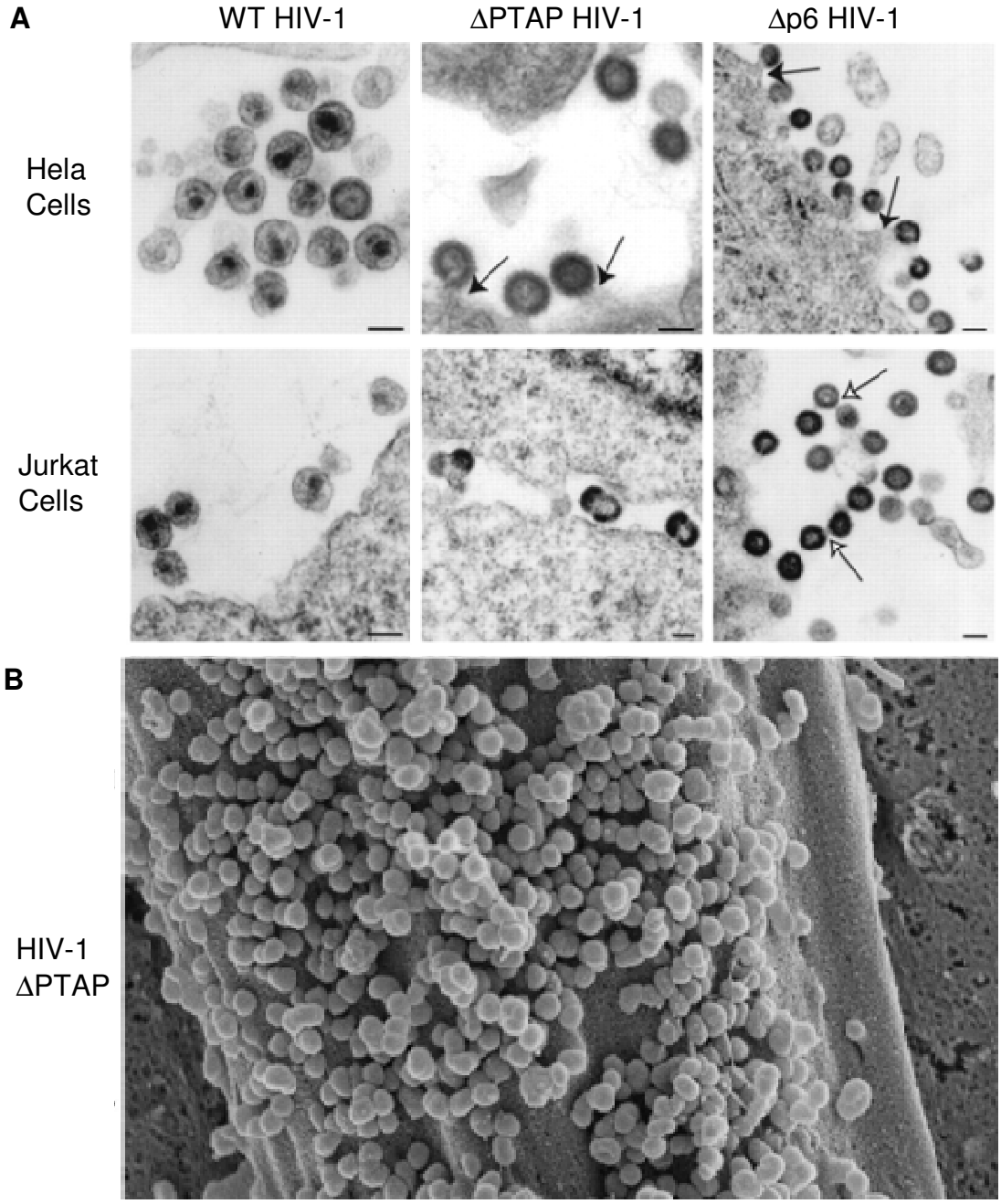

Figure 1.6 Late domain phenotype by electron microscopy. (A) TEMs of HIV-1 budding. Left column is TEM of mature wild-type HIV-1 particles from Hela (upper) and Jurkat (lower) cells, respectively. Middle column shows immature tethered HIV-1 particles that lack the PTAP late domain from Hela and Jurkat cells, respectively. Right column shows immature HIV-1 particles lacking p6 tethered to membrane and to each other in Hela and Jurkat cells. Reprinted from Demirov et al. (44). (B) SEM of cell surface decorated with fully assembled HIV-1 particles lacking PTAP. Courtesy of Marc C. Johnson.

be located in one of two places in retroviral Gag proteins, either between MA and CA (Figure 1.7, RSV, MLV, HTLV-1, and MPMV) or at the C-terminus (Figure 1.7, HIV, EIAV, and FIV). Another defining property of late domains is that they can often be swapped among different retrovirus, and maintain their function (118, 154, 233). The small size of late domains, their placement in unstructured regions of Gag, as well as their ability to be moved within Gag and even moved between viruses, suggested that late domains may function by recruiting host proteins. Later studies identified the interacting partners of late domains as components of the cellular pathway that is responsible for the formation of multivesicular bodies.

Multivesicular Body (MVB) Biogenesis and the ESCRT Pathway

Overview of ESCRT pathway

The multivesicular body (MVB) biogenesis pathway, also called the ESCRT pathway (Endosomal Sorting Complex Required for Transport), is a membrane trafficking network responsible for the budding of transmembrane cargo-containing intralumenal vesicles (ILVs) into an endosome, forming a multivesicular body (MVB) (for review (81, 159, 223) (Figure 1.8) (3). Once in the intralumenal vesicle, the cargo proteins have a few different potential fates. The resulting MVB can fuse with or mature into a lysosome where local lipases and hydrolases digest the intralumenal vesicles and transmembrane cargo. Post-Golgi transmembrane proteins marked for degradation as well as resident lysosomal hydrolases use this pathway en route to the lysosome. Alternatively, as in the case of class II MHC-containing ILVs, the MVBs traffic to and fuse with the plasma membrane, releasing the vesicles outside of the cell (34). Like other membranous components of the cell, MVBs or late endosomes are defined by their location in the cell, cargo, morphology by

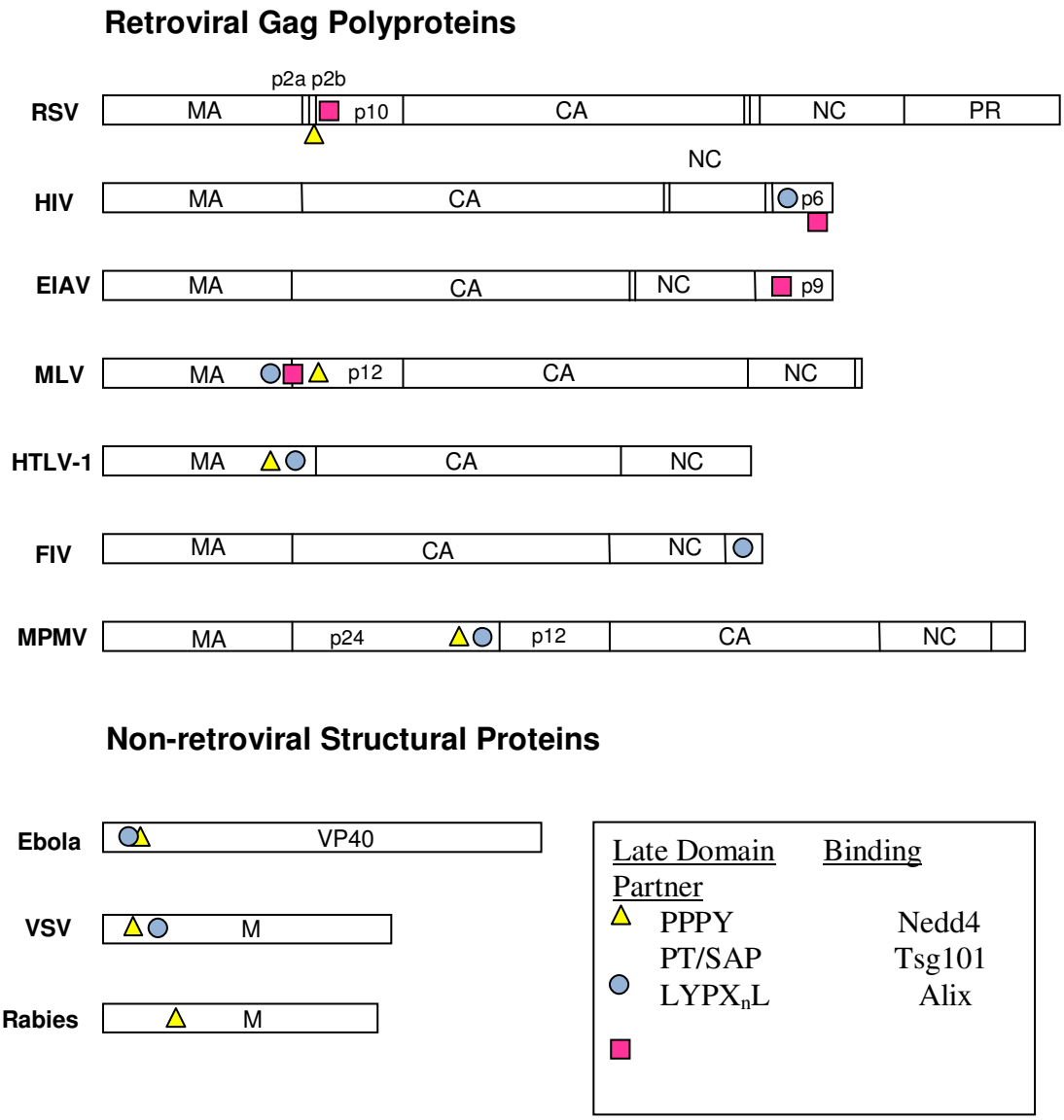

Figure 1.7 Positions of late domains within retroviral Gag proteins and other viral structural proteins. Late domains are located either between the MA and the CA domain or at the C-terminus of retroviral Gag proteins. Non-retroviral enveloped viruses, such as Ebola virus and Vesicular stomatitis virus (VSV) also harbor late domains in their structural proteins.

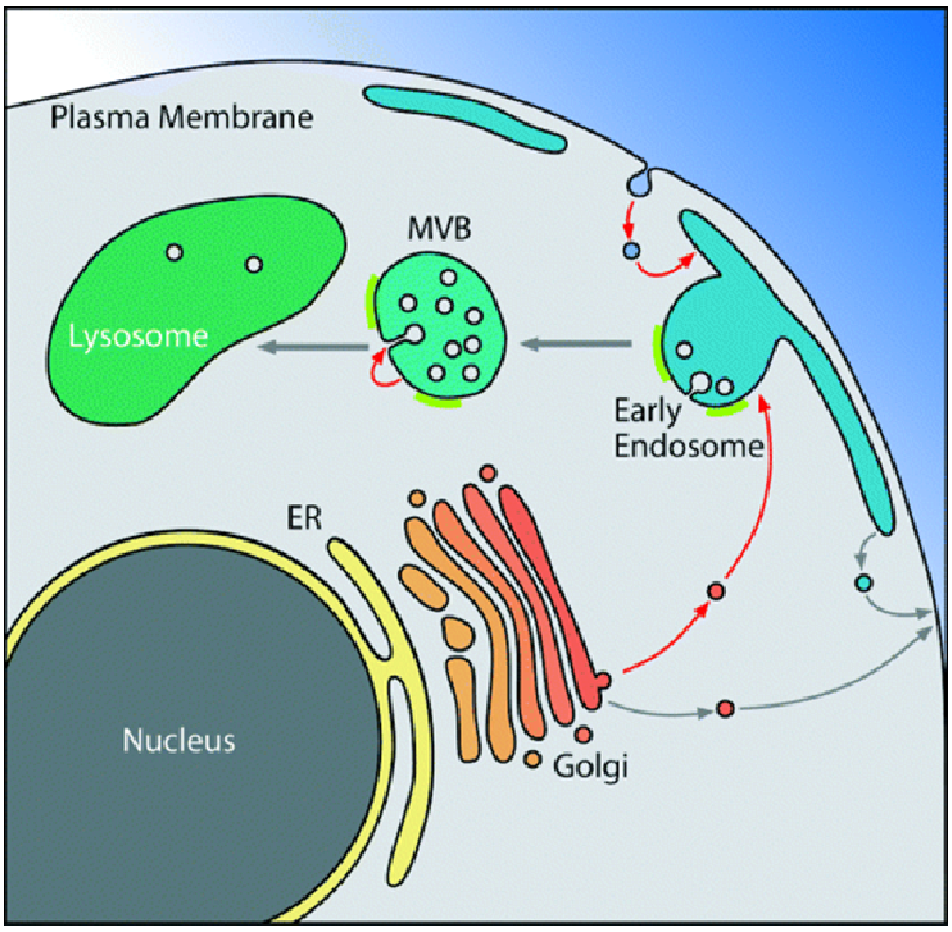

Figure 1.8 Protein Sorting Pathways. Cargo proteins can be delivered to the endosome from the endocytosis from the plasma membrane or from the secretory pathway. Cargo protein and lipids intended for degradation as well as resident lysosomal hydrolases bud into late endosomes called multivesicular bodies (MVBs) which then fuse with or mature into lysosomes. Reprinted from Babst et al. (3).

electron micrsoscopy, pH, and protein and lipid composition. Specifically, MVBs are located in the perinuclear region of the cell and exhibit multiple internal vesicles by visualization by EM. The internal vesicles vary from 30-100 nm in diameter (~20-30 nm in yeast) (Figure 1.9) (134).

The protein network involved in transmembrane cargo selection, cargo sorting, and the budding of cargo-containing vesicles is conserved across all eukaryotes (108, 223) and requires the sequential recruitment of four high molecular weight hetero-oligomeric complexes ESCRT-0, ESCRT-I, ESCRT-II and ESCRT-III (Table 1.1). MVB biogenesis also requires proteins that are not part of any ESCRT complex. Members of the Nedd4-family of ubiquitin ligases are responsible for the initial ubiquitination of the cargo protein (Figure 1.10) (204). Adaptors also play a role in regulating and bridging the ESCRT complexes. For example, the adaptor protein Alix acts as a bridge between ESCRT complexes by binding ESCRT-I component Tsg101 and ESCRT-III components CHMP4A,B,C. Finally, de-ubiquitinating enzymes (DUBs) deubiquitinate the transmembrane cargo prior to vesicle budding.

Ubiquitination of transmembrane cargo protein

Monoubiquitination is sufficient to signal cargo entry into the ESCRT pathway. There is also evidence that diubiquitination via K63-links functions during vacuolar sorting in yeast (59). This is in contrast to polyubiquitin chains of four or more K48-linked ubiquitin molecules that serve to target proteins to the 26S proteasome for degradation. The K63-linked ubiquitin adopts a more open conformation allowing for binding of ubiquitin-interacting domains, such as the UIM (Ubiquitin-interacting motif), UEV (Ubiquitin E2 variant), and VHS (Vps27/Hrs/STAM) domains found in some components of the ESCRT complexes. The E3 ubiquitin ligases of the Nedd4-family and Rsp5p are

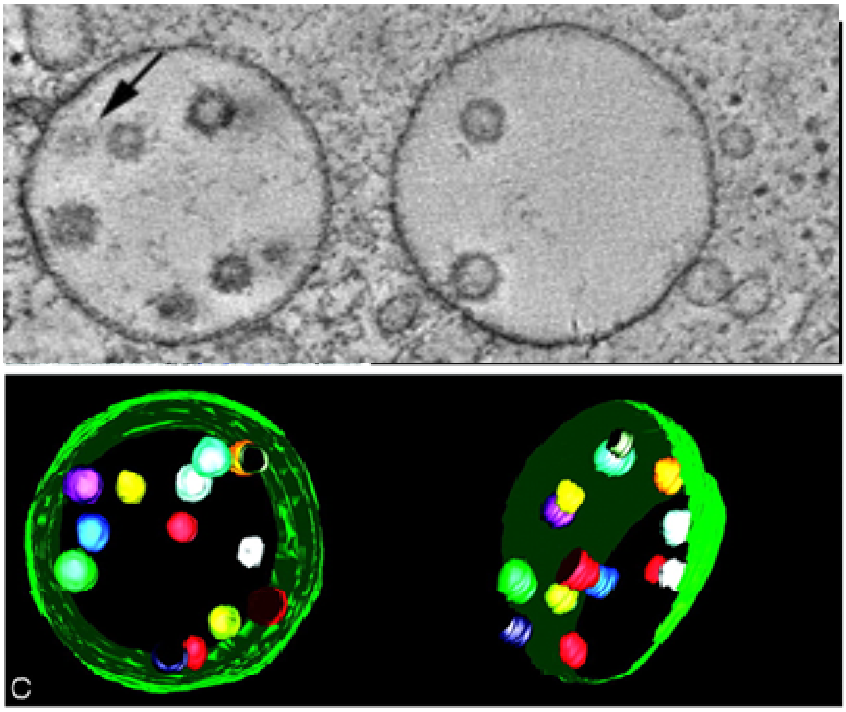

Figure 1.9 Morphology of multivesicular bodies. (A) Tomographic slice through a three-dimensional electron tomographic reconstruction of two MVBs in a human B cell. (B) Model of the left MVB pictured in (A) tilted along two different angles. Internal vesicles are not perfectly spherical due to manual tracing. Reprinted from Murk et al. (134).

Table 1.1 ESCRT Machinery

Complex or Function	Yeast Protein	Mammalian Protein	Domains	Interactors	Role in Viral Budding
Ubiquitin Ligase	Rsp5p	Nedd-4	C2 WW HECT	PPPY motifs Bro1	Yes (RSV, HIV, MLV, FIV)
ESCRT-0	Vps27p	Hrs	UIM VHS FYVE PPEY PSAP PRD Clathrin box motif	Ubiquitin PI(3)P Tsg101 Vps37A Vps37B Vps37C Clathrin Eps15	
	Hse	STAM1, STAM2	SSM Coiled-coil UIM	Hrs Clathrin Ubiquitin	
ESCRT-I	Vps23p	Tsg101	UEV PRD Leu-Zipper Steadiness-Box	PTAP motifs Ubiquitin Hrs, Alix Vps37p Vps28p Tsg101 EAP30 EAP45	Yes (HIV, SIV, FIV, Ebola)
	Vps37p	Vps37A Vps37B Vps37C Vps37D	PTAP	Hrs Tsg101 Vps28p (Vps37A only) Vps20p (Yeast only) Alix (?)	Yes (HIV)
	Vps28p	Vps28		Vps37A Vps36 Vps20p (Yeast only) Tsg101	
	Mvb12p	MVB12A MVB12B		Tsg101-Vps37 complex	Yes/No (HIV)

Table 1.1 (Continued)

Complex or Function	Yeast Protein	Mammalian Protein	Domains	Interactors	Role in Viral Budding
ESCRT-II	Vps25 (2 copies)	EAP20 (2 copies)	WH(winged-helix) motif	Vps22p (EAP30) Vps36p (EAP45) CHMP6	No
	Vps22p	EAP30	WH motif Coiled-coil	Vps25p (EAP20) EAP30 Tsg101 CHMP6	No
	Vps36p	EAP45	GLUE NZF (Yeast only) WH motif	Ubiquitin VPS28 Vps25 (EAP20) Tsg101 CHMP6	no
ESCRT-III	Vps2/Did4	CHMP2A CHMP2B	Charged coiled-coil	Vps4B	
	Vps24p	CHMP3	Charged coiled-coil		
	Vps32/Snf7	CHMP4A,B,C	Charged coiled-coil	Alix, CHMP6 CHMP7 (CHMP4B only)	
	Vps20p	CHMP6	Charged coiled-coil myristyl	EAP20 EAP30 EAP45 CHMP4B Vps4	No (HIV) by depletion Yes (HIV) by overexpression of DN
		CHMP1A		Vps4B	
		CHMP5		LIP5 CHMP5	No (HIV) by depletion, Yes (HIV) by overexpression of DN

Table 1.1 (Continued)

Complex or Function	Yeast Protein	Mammalian Protein	Domains	Interactors	Role in Viral Budding
Adaptors	Bro1/Vps31p	Alix (AIP1)	Bro1 V-domain PRD	LYPXnL motifs Tsg101 CHMP4A, B,C Alix AMSH VPS37 (?) LBPA Doa4 Nedd4/Rsp5 Endophilins	Yes (HIV, EIAV, MLV, RSV)
Vps4 activator	Vta1p	LIP5	MIT	Vps4 CHMP5 CHMP6?	Yes
		CHMP7		UBPY	
	Did2	CHMP1A,B			
	Vps60p	CHMP5		Vta1(LIP5?)	
Sodium/proton exchanger	Vps44p/Nhx1	SLC9A6		Vps4	
DUBs		AMSH	MIT Rhodanese JAMM MADS Coil Mov34 CON	STAM CHMP1A,B CHMP3 CHMP4A,B Alix clathrin	
	Doa4 /Ubp4p	UBPY	MIT Rhodanese	STAM Hbp CHMP1A,B CHMP7 CHMP4C	
AAA-ATPase	Vps4p	Vps4A, B	MIT	LIP5 CHMP1A CHMP2A,B CHMP6	Yes (HIV, RSV, EIAV, PIV5, MPMV, HTLV-1, PFV, Lassa, Sendai, HBV, HSV-1, EBOV)

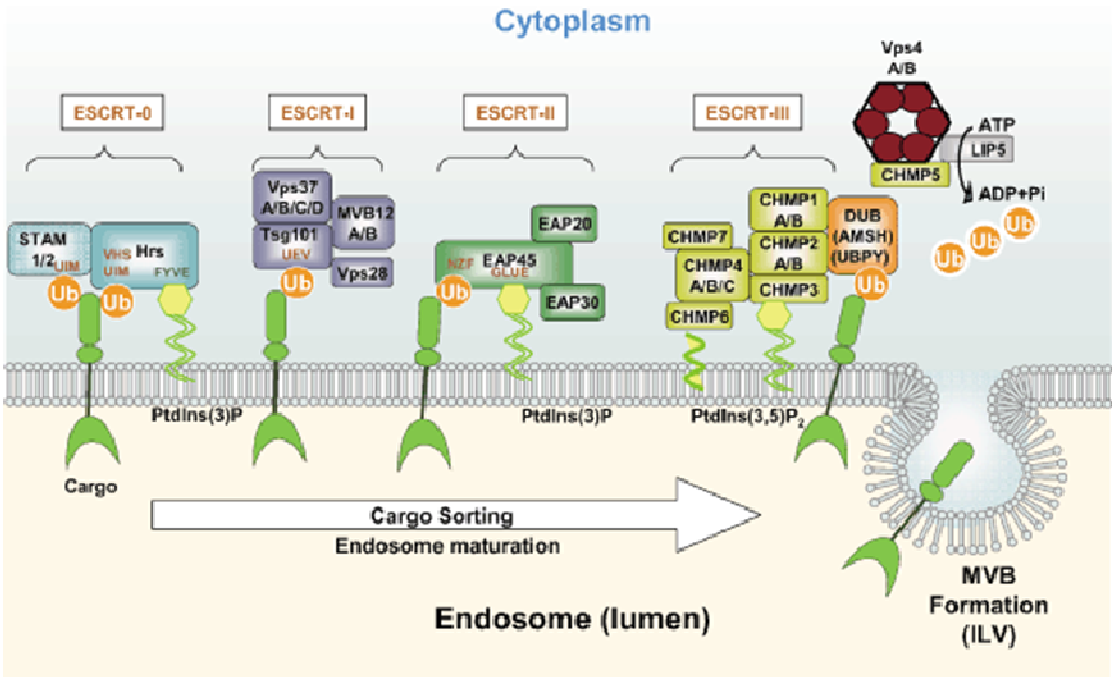

Figure 1.10 Schematic overview of the Endosomal Sorting Complex Required for Transport (ESCRT) pathway's role in the formation of Multivesicular Bodies (MVBs). Ubiquitinated transmembrane cargo proteins are recognized by the ESCRT-0 complex. ESCRT-0 recruits ESCRT-I, which recruits ESCRT-II, which recruits ESCRT-III. Cargo is deubiquitinated by deubiquitases and the Vps4 AAA-ATPase disassembles the ESCRT-III complex resulting in the budding of a cargo-containing vesicle away from the cytoplasm and into a late endosome yielding a MVB. Reprinted from Tanaka et al. (204).

responsible for ubiquitinating cargo bound for MVBs in mammals and yeast, respectively. First, the ubiquitin is recognized by the Ubiquitin-Interacting Motif (UIM) of Hrs (187) and STAM (77) which are members of the ESCRT-0 complex, and later in the pathway by members of the ESCRT-I and –II complexes, as well.

The post-translational covalent attachment of ubiquitin to a protein is mediated by three groups of enzymes, E1, E2, and E3. E1 acts as an activating enzyme that transfers ubiquitin to an E2 conjugating enzyme. The E2 then interacts with an E3 which is responsible for target protein selection. E3s of the "really interesting new gene" (RING) domain family require an association with an E2 to transfer the ubiquitin to the target protein. E3s of the "homology to the E6-AP carboxyl terminus" (HECT) domain family have ubiquitin-ligase activity by themselves. Nedd4 has an N-terminus C2 domain important for membrane binding, 2-4 protein interacting WW domains and a C-terminal HECT domain responsible for catalyzing the actual ubiquitin ligation. WW domains were first identified in YAP (Yes-associated protein) (199) and later in many modular proteins involved in various regulatory or signal transduction functions and thus were suspected to be peptide-interaction domains (14). The suspected role of mediating protein/protein interactions was confirmed when the WW domains of YAP were shown to interact with PPXY sequences in partner proteins (31). Since then, the WW domains of many diverse proteins have been shown to interact with proline-rich regions.

WW domains can be divided into six groups based on ligand sequence preferences (180). The largest group, which includes that of the Nedd4 family, binds the PPXY consensus sequence (27, 75, 129, 193, 208). The structure of WW domains forms a shallow binding site for linear peptide motifs

with a three-stranded antiparallel β-sheet (112). The WW domain is defined as a 38 residue sequences that contains, among other semi-conserved amino acids, two invariant tryptophans spaced 20-23 amino acids apart. WW domains are also rich in polar amino acids and have prolines located at each terminus (14, 200). For Nedd4-family of ubiquitin ligases, the WW domain is thought to mediate its interaction with its PPXY-containing substrates. Both the C2 domain and the WW domains of Nedd4 are able to interact with the HECT domain and auto-inhibit ligase activity (17, 221). When they couple one ubiquitin molecule to another, typically Nedd4-family members catalyze K63 ubiquitin links (94).

De-ubiquitination early in ESCRT pathway

As an added layer of regulation, two unrelated DUBs, UBPY and AMSH (associated molecule with the Src homology 3 domain of STAM), bind a noncanonical SH3-binding motif (PXV/ID/NRXXKP) (87) on STAM, perhaps to de-ubiquitinate and rescue incorrect cargo from lysosomal degradation (87) (reviewed in (36, 97)). AMSH is a member of the JAMM domain metalloprotease family of DUBs (119, 120) that processes K63-linked ubiquitin chains but not K48-linked polyubiquitin chains (120). UBPY is a member of the UBP family of cysteine proteases and can process K63- and K48-linked ubiquitin chains equally well (170). The actual substrates of AMSH and UBPY are unknown. Thus, these DUBs could be de-ubiquitinating MVB machinery, MVB cargo or both. A catalytically inactive AMSH (D348A) (120), but not UBPY (170), causes the accumulation of a higher molecular mass form of STAM (+14 kDa) that is recognized by anti-ubiquitin antibodies, implying AMSH may de-ubiquitinate STAM. However, in UBPY knockdown cells, STAM is depleted (170). UBPY may contribute to STAM stability by de-

ubiquitinating polyubiquitin chains on STAM and thus preventing proteasomal degradation. There is evidence from the epidermal growth factor receptor (EGFR) downregulation pathway that AMSH and UBPY may have opposite consequences. Knockdown of AMSH enhances EGFR degradation (120) while knockdown of UBPY inhibits degradation (16, 170). DUBs also have a reappearing role near the completion of the ESCRT pathway, removing ubiquitin from cargo before vesicle budding (48). Instead of a regulatory role, this function seems to be important for maintaining pools of free ubiquitin (48).

ESCRT-0 complex

The ESCRT-O complex is the first high molecular weight complex recruited to the ubiquitinated cargo and is composed of the Hrs and STAM proteins. Hrs contains an N-terminal phosphatidylinositol 3-phosphate-(PI(3)P) binding FYVE domain responsible for its endosomal membrane targeting. Both Hrs and STAM interact with clathrin and have a VHS (Vps27/Hrs/STAM) domain (121, 166, 174). It has been speculated that clathrin acts to corral the Hrs/STAM complex and the ubiquitinated cargo for interaction with ESCRT-I (223). Hrs assembles into a hexameric cylinder (164). However, the structure of STAM and its stoichiometry relative to Hrs is unknown.

ESCRT-I complex

The ESCRT-I complex is composed of the four proteins Tsg101, Vps28, Vps38 and MVB12 in a 1:1:1:1 heterotetramer (126) (Table 1.1). Tsg101 is the central component of the ESCRT-I complex, binding to all other ESCRT-I subunits. In addition, the N-terminal UEV (Ubiquitin E2 Variant) ubiquitin binding domain of Tsg101 also binds to the PT/SAP sequence in Hrs (and to two PSDP sequences in yeast Vps27) of the ESCRT-0 complex (8, 13, 91)

and to the ubiquitinated cargo directly (90, 117). Downstream from ESCRT-I, Tsg101 interacts with EAP30 and EAP45 of the ESCRT-II complex and with the adaptor Alix (195, 215).

ESCRT-II complex

The ESCRT-II complex is composed of three proteins EAP30 (ELL Associating Protein 30), EAP25, and EAP45. EAP45 is able to bind ubiquitin via a NZF and a GLUE domain. ESCRT-II recruits ESCRT-III through the C-terminus of EAP45 which binds ESCRT-III component CHMP6. The exact function of the ESCRT-II is unknown and this complex is dispensable for some degradation pathways. For example, some research groups reported it had no effect on EGFR degradation (16), while others reported it had an intermediate phenotype (102). While the ESCRT-I complex might be important for initial shunting of the cargo into the MVB pathway, and the ESCRT-III complex may be important for the actual membrane invagination and/or fission, ESCRT-II may play a less essential or phenotypically obvious role such as corralling or concentrating cargo. ESCRT-II does interact with ESCRT-III and thus helps mediate the progression to the next step in the pathway. However, the adaptor protein Alix is able to bind Tsg101 (ESCRT-I) and CHMP4 (ESCRT-III) and thus could bridge the two complexes in the absence of ESCRT-II.

ESCRT-III complex

There are eleven mammalian ESCRT-III members (six in yeast) called CHMPS (charged multivesicular body proteins) (5, 99, 176). All ESCRT-III components share a similar structure. They are small (200-250 amino acids), alpha helical and highly polar. The N-terminal third is highly basic while the C-terminal two-thirds is highly acidic (135). Unlike ESCRT-I and ESCRT-II, proteins of the ESCRT-III complex do not bind ubiquitin and are monomeric

and in a “closed” confirmation in the cytoplasm, and they assemble only after membrane binding and transition into the “open” conformation (4, 188). The closed conformation is the result of the highly specific interaction between the basic and acidic domains (104, 236). Multimerization of ESCRT-III complexes is believed to deform the membrane, perhaps causing the invagination of the nascent vesicle (71).

De-ubiquitination late in MVB pathway

Prior to the vesicle budding, cargo proteins are deubiquitinated by DUBs (48). In yeast this step appears to serve the purpose of sparing the ubiquitin the fate of the cargo, namely degradation. Yeast cells lacking the DUB homologous to UBPY (Doa4) are able to generate MVBs but display a growth defect, and the over-expression of ubiquitin rescues the defect. This implies that the de-ubiquitination is not important for the process of MVB formation, but is instead important for maintaining pools of free ubiquitin in the cell. Knocking down mammalian UBPY, the closest mammalian DUB to Doa4 and its likely homologue, actually results in more and larger MVBs, although the MVBs seem to be tethered to each other by electron dense structures as seen by TEM (170). AMSH (1, 210) and UBPY (169) contain MIT domains that interact with CHMP proteins. Doa4 binds the proline-rich domain of Bro1, the yeast homolog of Alix (141). In addition, myc-tagged Xp95, the *Xenopus* orthologue of Alix binds GST-AMSH in cell lysates (43). Perhaps the interaction requires post-translational modification such as phosphorylation because this result could not be recapitulated *in vitro* (43). Another interpretation could be that the interaction between Alix and AMSH is indirect or transient.

Adaptor proteins of the ESCRT pathway

Some proteins required for the sorting of cargo proteins into MVBs are not part of any ESCRT complex. One example is Alix (ALG-2-interacting protein X), also known as AIP1 (ALG-2-interacting protein 1) and XP95 in *Xenopus*, which is a highly-conserved 869 amino acid adaptor protein that resides in the cytoplasm. Among the proteins of the MVB pathway, Alix interacts with the highest number of other components, consistent with this adaptor role (Table 1.1). Crystal structures have revealed that Alix is composed of three domains: an N-terminal Bro1 domain, a central V-domain, and a C-terminal proline-rich region (56, 95, 107, 238) (Figure 1.11).

The Bro1 domain is named for its yeast analog Bro1 and is composed of ten alpha helices and one beta sheet that are arranged into three helical hairpins flanked on one side by an alpha helix and the other by a small beta sheet. Overall, the Bro1 domain is curved, about 100 Å long, and resembles a banana shape like its yeast analog Bro1 (56, 95) (Figure 1.11B). It has been suggested that its convex face possibly allows Alix to sense negative curvature in membranes. Two hydrophobic patches reside on the surface of the Bro1 domain. The first patch is the site of Src kinase docking (182). The second hydrophobic patch is responsible for binding the ESCRT-III components CHMP4A, B, and C and thus links Alix to the ESCRT-III complex (88, 89).

The structure of Alix's central V domain is appropriately a V, with each arm of the V composed of a three-helix bundle (56) (Figure 1.11B). The two arms of the V are oriented at a 30° angle to each other but do seem to exhibit some conformational flexibility, perhaps upon ligand-binding (56). Hydrophobic side-chain-packing interactions or "knobs into holes" side chain

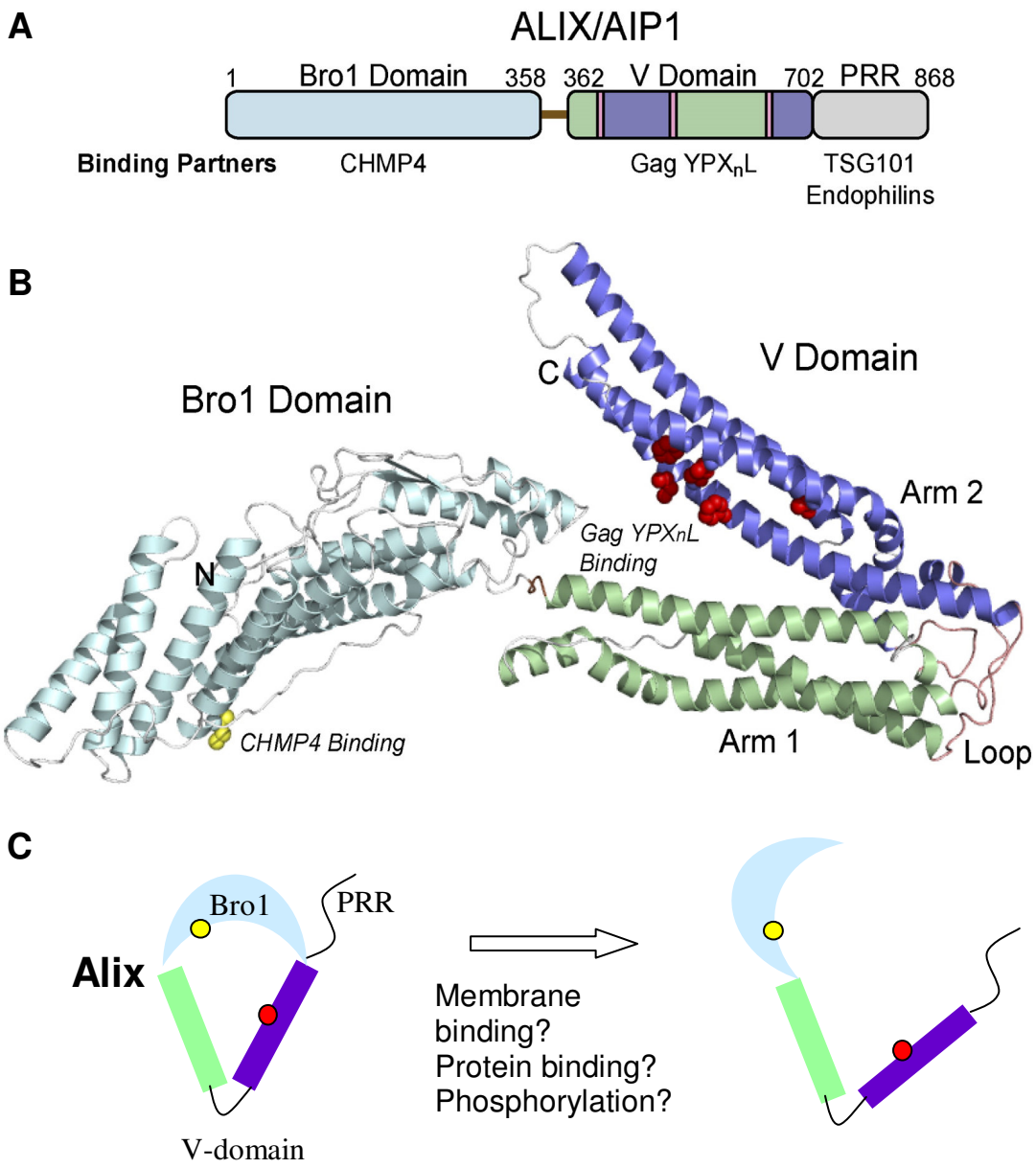

Figure 1.11 Alix structure. (A) Domain layout of Alix. N-terminal Bro1 domain, linker, V-domain, and Proline-rich domain at C-terminus (B) Ribbon representation of the N-terminal Bro1 domain and central V-domain of Alix. Yellow residues are implicated in CHMP4 binding and red residues are implicated in $LYPX_nL$ binding. (C) Model of Alix autoinhibition. CHMP4 binding surface is obstructed in Alix at native conditions. CHMP4-binding surface becomes available possibly after Src binding, phosphorylation, or membrane associate. (A) and (B) are reprinted from Fisher et al. (56). (C) is adapted from Zhou et al. (241).

packing is mostly responsible for stabilizing each of the arms. Almost solely hydrophobic interactions from the backbone atoms are responsible for stabilizing the three strands in the loop between the two arms.

The proline-rich region is 58% proline and glutamine residues and thus assumed to be unstructured. While there are crystal structures of Alix containing just the Bro and V domains, there are no crystal structures of full-length Alix containing the PRR because this protein does not express well (56). The PRD (or PRR) of Alix binds endophilins, which regulate membrane shape during endocytosis via their curved BAR domain and their lysophosphatidic acid acyltransferase activity, or possibly through their interaction with other enzymes like synaptojanin and dynamin (28). The Tsg101 UEV domain is able to bind to a PTAP motif in the PRD of Alix (117, 215).

Vps4-mediated release of ESCRT-III and vesicle budding

ESCRT-III's association with membrane is irreversible without the input of energy. The disassembly of the ESCRT complexes is an ATP-dependent process mediated by the AAA ATPase Vps4 (6, 7). In the absence of nucleotides Vps4 is a dimer in the cytosol (57, 185, 229). Yeast has one Vps4 protein and mammals have two isoforms, VpsA, and Vps4b (SKD1) (11, 232). Vps4 is composed of five elements: an N-terminal MIT (Microtubule Interacting and Trafficking) domain, a central large AAA ATPase domain and a smaller C-terminal AAA ATPase domain, a three-stranded anti-parallel β-domain inserted into the smaller AAA ATPase domain and a C-terminal helix (185, 198). Vps4 is recruited to endosomes and interacts with the C-terminus of ESCRT-III components through the three-helix bundle that makes up the MIT domain (185). Fourteen Vps4 monomers form a heptameric double ring with

ATPase activity. The two rings have hydrophobic pore diameters of 40 Å and 55 Å, respectively (73). One model proposes that the assembled Vps4 tetradecamer may roll like a barrel on the membrane so that both rings are accessible (73). According to this model, ESCRT complexes are fed through the two rings of the Vps4 tetradecamer by the MIT domains on flexible tethers and disassembled into individual proteins (185). Both rings are able to hydrolyze ATP, but take turns, as ATP binding in one ring inhibits ATP binding in the other (7, 73). It is unclear how ESCRT disassembly is coupled with budding of vesicles into the MVB. But it is known that when local nucleotides are depleted, the Vps4 rings disassemble into cytoplasmic dimers.

Often the ESCRT pathway is represented as a linear pathway where early ESCRT components hand off cargo to later ESCRT components. This "conveyor belt model" has recently been replaced with the "concentric circle model" which proposes an Hrs (ESCRT-0) hexamer nucleates the recruitment and assembly of the ESCRT-I, -II, and –III complexes around it (140). The rings of the polymerized ESCRT complexes could serve to concentrate the cargo with ESCRT-0 at the center and ESCRT-III at the perimeter (Figure 1.12). ESCRT-0, -I, and –II are thought to dissociate from the cargo before the vesicle forms, allowing the cargo to diffuse near ESCRT-III and associated ubiquitin hydrolases and trigger de-ubiquitination of cargo. The invagination and formation of vesicles seems to result from the constriction by ESCRT-III. Indeed circular arrays of CHMP4A (ESCRT-III) have been observed on the surface of cells over-expressing CHMP4A, and the co-expression of only CHMP4A and a dominant negative version of VPS4 leads to protruding buds and tubules from the plasma membrane (71). Vps4-mediated contraction of ESCRT-III would drive the vesicle release.

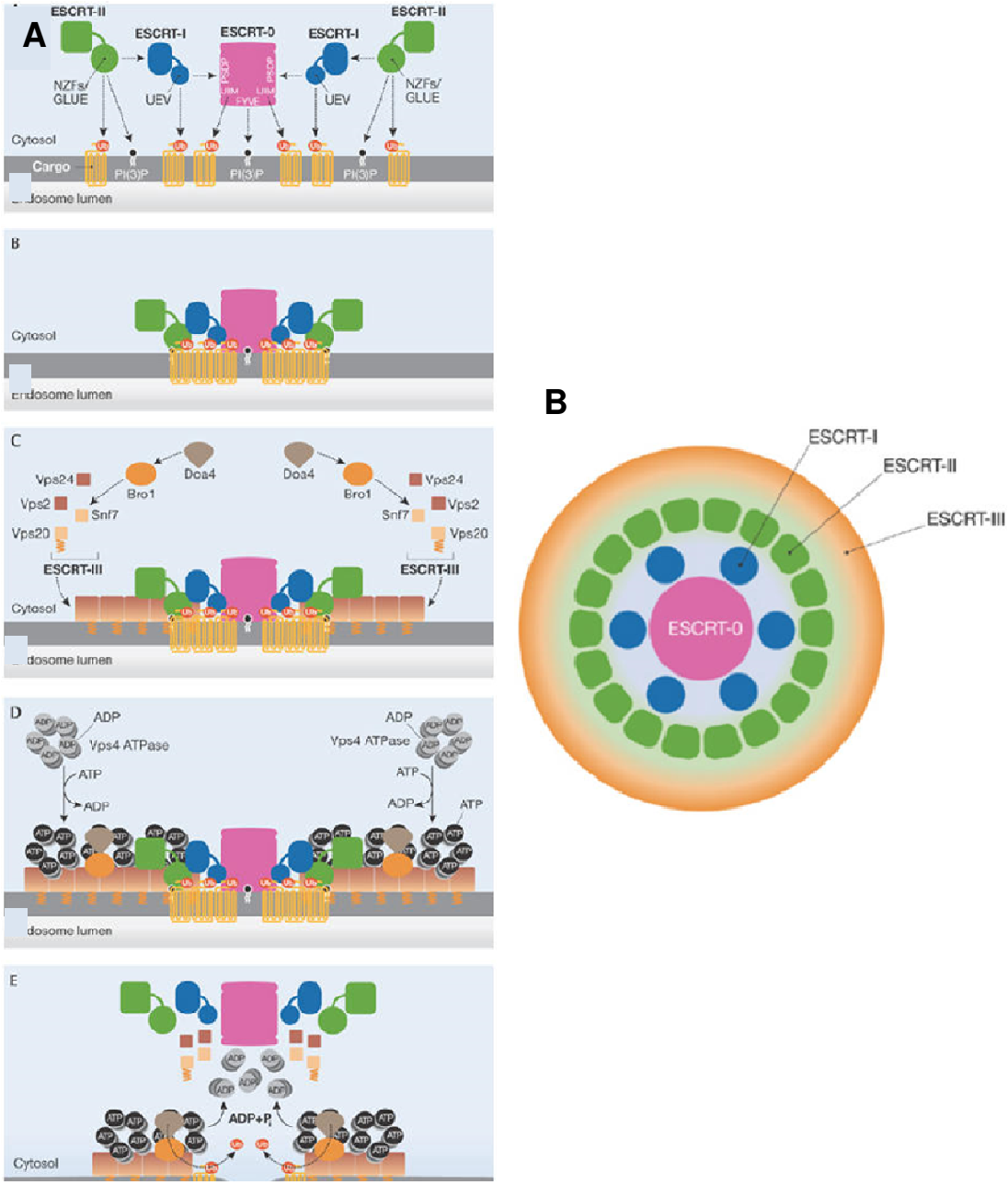

Figure 1.12 The concentric circle model of ESCRT machinery function. ESCRT-0 binds to ubiquitinated cargo and endosomal lipids and nucleates the assembly of the ESCRT-I, -II, -III complexes around the cargo/ESCRT-0 “hub”. ESCRT-III recruits the deubiqitinases and Vps4. Cargo-containing vesicles bud into lumen of endosome after Vps4 releases ESCRT-III. (A) Cross-section of model. (B) Top-down view of model. Reprinted from Nickerson et al. (140).

Non-endosomal functions of ESCRT proteins

Some members of the ESCRT machinery also help mediate the terminal membrane fission event associated with cell division. Yeast two-hybrid screens and affinity purification experiments identified ten proteins implicated in centrosome and midbody function that interact with Hrs, Alix or Tsg101 (127, 211). The ESCRT-I component MVB12A has also been observed concentrated on centrosomes (126).

Cytokinesis begins with the constriction of an acto-myosin contractile ring creating a cleavage furrow. The furrow continues inward until the two daughter cells are connected only through a thin midbody. The midbody is a microtubule-rich stalk formed late in mitosis. At the center of the midbody is the Flemming body that is defined as the densely proteinaceous central region of the midbody that lacks α-tubulin staining. Cep55 (Centrosome protein, 55kDa) is a microtubule bundling protein (239) that provides a protein recruiting and organizing role at the Flemming body and is required for membrane abscission during cytokinesis (52). Cep55 as well as other proteins involved in cytokinesis are located at the centrosome during interphase, and relocate to the midbody during late mitosis (25). During interphase Cep55 recruits both Tsg101 and Alix from the centrosome to the Flemming body during the late states of mitosis (25, 127, 230). Mutating (192) or knocking down (230) Tsg101 causes abnormalities in mitosis and an increase in multinucleated cells. Cep55 recruits Tsg101 through a PPNTS motif in the proline-rich region of Tsg101 (24) and Alix through a PxY motif in the proline-rich region of Alix (24, 127). Failure to recruit Alix causes a disruption in Flemming body morphology (24), and prevention of abscission (24, 127). Alix/Tsg101 interaction is required for cytokinesis (25) but Alix

multimerization is dispensable (24). Cep55 itself does not seem to have a role in viral budding (25). ESCRT-III also participates in the membrane fission step of cytokinesis (24, 25). Alix must maintain its CHMP4 binding in order to function in cytokinesis, implicating ESCRT-III in cell division (24). Specifically, dominant negative N-terminal YFP fusions of CHMP4 isoforms act as inhibitors of cytokinesis (24). In contrast to viral budding, which is most strongly inhibited by YPF-CHMP4B, cytokinesis is most strongly inhibited by YFP-CHMP4C. It has been speculated that the different isoforms of CHMP4 might specialize and perform only certain functions of the ESCRT machinery.

The ESCRT-III component Vps36 was detected in a screen for mutations that disrupt anterior-posterior patterning in *Drosophila melanogaster* (83). The N-terminal GLUE domain of Vps36 is able to interact with the 3' UTR of bicoid mRNA and is responsible for its anterior localization in oocytes.

The deubiquitinating enzymes of the ESCRT pathway have also been implicated in cytokinesis. AMSH and UBPY display concentrated localization as a single or double band at the Flemming body during cytokinesis, respectively (70, 131). Furthermore, depletion of AMSH or UBPY caused an increase in multinucleated cells and cells displaying atypically long spindles (131).

Although the actual fission mechanism of cytokinesis is yet to be understood, Vps4 is localized to the midbody and required for abscission (25, 127), implying a mechanism analogous to vesicle and virus budding.

ESCRT proteins also function in many other cellular processes. For example, Tsg101 is involved in transcriptional regulation of steroid hormone receptors (18, 201). ESCRT proteins (171), Hrs (203), and Vps4 (136), have also been implicated in macroautophagy, which is the process of degrading

organelles and long-lived proteins through double membrane vacuoles that fuse with endosomes and then lysosomes (51). Some CHMP proteins have nuclear localization and instead of being named as CHarged Multivesicular body Proteins, are named for CHomatin Modifying Proteins. For example, CHMP1 functions in MVB formation in the cytoplasm (78) but also functions in chromosome sequestering during mitosis in the nucleus (194). Vps25 (EAP20) of the ESCRT-II complex contains a WH (winged-helix) protein motif that is known to bind nucleic acid, specifically the major groove of DNA (220).

Alix plays a role in diverse functions dependent on its participation in distinct protein networks. Although it was originally identified as pro-apoptotic interactor of ALG-2 (apoptosis-linked gene 2) (123, 214), its ALG-2-associated function is among its least characterized.

Alix has been linked to cell architecture. For example it interacts with MAP (merlin-associated protein) (82), the focal adhesion kinases PYK2 and FAK, α-tubulin (181), and F-actin (152). Extracellular Alix that has been secreted regulates integrin-mediated cell adhesion and extracellular matrix assembly (151). The secretion of Alix has not been corroborated by other groups.

The role of ESCRT pathway in virus budding

PT/SAP late domain binds Tsg101

Tsg101 was first identified by a yeast two-hybrid screen as the cellular binding partner of the PT/SAP late domain of HIV-1 Gag (213). Truncation mutants allowed the identification of the UEV domain and the PTAP motif as being the important interaction domains in Tsg101 and HIV-1 Gag, respectively (64, 197, 213). Depletion of cellular Tsg101 impairs HIV-1 budding (62). Over-expression of the N-terminus of Tsg101 (termed Tsg- 5')

also disrupted HIV-1 virus release as this mutant can bind p6 but not Vps28 (44, 65).

In addition to the direction interaction betweenTsg101and HIV-1 Gag, there is evidence that an intact ESCRT-I complex is required for budding. Tsg101 mutants that lack the binding site for Vps28 are unable to rescue HIV-1 budding in cells that were depleted of wild-type Tsg101 (197). In addition, fusion of the ESCRT-I component Vps37B to HIV-1 Gag lacking a PTAP motif rescues budding (197). This implies that it is the ESCRT-I complex, not Tsg101 specifically, that is required for Gag entry into the ESCRT pathway.

PPPY late domain binds Nedd4-family of ubiquitin ligases

Gross truncations followed by smaller deletions and mutations of RSV Gag helped identified the PPPY motif in p2b domain as a late domain (224, 228). The cellular binding partner of the PPXY late domain was uncovered using three tandem copies of the p2b sequence from RSV as a probe for a chicken cDNA phage expression library (93). The screen identified two unique cDNA clones, denoted LDI-1 and LDI-2 for late domain interactor-1 and -2, that mostly likely correspond to the chicken homologs of the Nedd4–family of E3 ubiquitin ligases, Nedd4-2 (or Nedd4-2s, Elena Kamynina, personal communication) and human WWP1 (murine Itch) ((35, 93). However, the clones were incomplete. Specifically, the LDI-1 lacked the C-terminal half of the protein containing the HECT domain and LDI-2 lacked the N-terminal C2 domain. Both LDI-1 and LDI-2 retained the central WW domain-containing region, implying the WW domains were responsible for the interaction with the p2b peptides probes. In fact, WW domains have independently been shown to interfere with RSV budding when placed in cis in Gag, presumably by binding the late domain (156). Furthermore, RSV Gag interacts with

endogenous Nedd4 family members in a late domain-dependent manner and is co-immunoprecipitated with a peptide containing the WW domains of LDI-1 (93, 212). Over-expression of the full length LDI-1 protein has no effect on RSV budding (212). However, the WW domain of LDI-1 (93), as well as full length LDI-1 containing a HECT active site mutation do inhibit RSV budding. (212).

Nedd4-family members have been detected inside MPMV particles (68), but not HIV-1particles (197). Viruses that harbor the PPXY late domain motif include RSV, MLV, HTLV-1, MPMV, Ebola virus, VSV, Rabies virus (Figure 1.7).

Given that the PPXY late domain binds ubiquitin ligases (93, 115) there has been an intense effort to link ubiquitination to budding. Indeed entry into the ESCRT pathway by a late domain induced ubiquitination of Gag is an attractive model since members of ESCRT-O (Hrs, STAM) and ESCRT-I (Tsg101) have ubiquitin-binding motifs. Yet the data remain conflicting. Linking ubiquitin to the PTAP-encoding portion of HIV-1 increased its affinity for Tsg101, implying it may encourage interactions with the ESCRT machinery (62).

A ubiquitin mutant (K63R) that affect endocytosis but not mutants that affect proteasome degradation (K48R) reduced VLP production modestly from a minimal Gag (196). Both conjugated (146, 147, 150) and unconjugated (165) ubiquitin have been found in retroviral particles, even retroviruses that do not harbor the PPXY late domain. It is estimated that free ubiquitin is present at levels equivalent to about 10% of that of Gag in HIV-1, SIV and MuLV particles and about 2% of mature Gag (p6, p12, or p9 domain) is ubiquitinated in HIV-1, SIV-1, MuLV (147) and EIAV(149), and about 1% of

MMTV Gag are ubiquitinated (150) . Lysines in proximity to the late domain in HIV-1 have been shown to be important for budding efficiency. While no specific lysine is required, mutating all lysines to arginine in NC, sp2, and p6 (14 in all) results in reduced budding efficiency and late domain phenotype, as seen by TEM (69).

Some retroviral budding, such as that of HIV-1, HIV-2, RSV, SIV, and MLV (150), has been shown to be sensitive to proteasome inhibitors, presumably because the inhibitors reduce the amount of free ubiquitin in the cell required for viral budding. The budding of EIAV (149, 155) and MMTV (150) seem to be exceptions, being relatively resistant to proteasome inhibitors. It has been speculated EIAV is able to bypass the requirement for ubiquitin because it utilizes a LYPXL motif that binds Alix. Alix is downstream of Nedd4 and Tsg101 and the other ubiquitin-binding proteins of the ESCRT pathway and does not bind ubiquitin. However, MMTV Gag lacks a $LYPX_nL$ motif (although it has a PTAP motif). It must be noted that both EIAV and MMTV have been shown to be monoubiquitinated, raising the question of whether ubiquitination could be a side effect of budding, not a requirement.

Ubiquitin fused to the C-terminus of EIAV Gag lacking its YPDL late domain rescues budding to levels about 60-70% that of wild type (84). This ubiquitin fusion seems to be recruiting other ESCRT components to achieve rescue because mutating hydrophobic residues Leu-8 and Ile-44 in the fused ubiquitin, which are important for interaction with ubiquitin interacting motifs (UIMs), prevents the Ub-mediated budding rescue, implying that a host protein is recognizing and binding the ubiquitin. The ubiquitin fusion renders the budding of the ΔYPDL Gag, but not EIAV Gag containing PPPY or PTAP, sensitive to the proteasome inhibitor MG-132. Maximum budding rescue is

achieved through 1:1 transfection of ΔYPDL to ΔYPDL-Ub DNA. This is higher than the percent of Gag estimated to be ubiquitinated in normal retroviral budding (5-10%).

Making lysine to arginine mutations in Gag, especially when lysine residues are so numerous (38 in HIV-1 Gag) can have other affects on assembly and budding. To avoid this problem a derivative of the prototypic foamy virus (PFV) Gag that is devoid of lysines was used to study the role of ubiquitination in budding. A ubiquitin ligase WWP1, but not catalytically inactive mutants, was shown to stimulating the budding of PFV, even though it lacked lysines for ubiquitination (237). Thus the ubiquitination of other cellular factors, but not necessarily that of viral proteins, might be important for budding.

Our lab and other labs (J. Wills, personal communication) have failed to show RSV Gag to be ubiquitinated. However, RSV Gag has been shown to be mono- and polyubiquitinated in cell lysates, but primarily monoubiquitinated in virions (212). Less than 10% of Gag is estimated to be ubiquitinated in virions. In both cases the ubiquitination does not occur in the absence of the p2b domain. Furthermore, RSV budding is reduced when all five lysines in the MA and p2 are mutated to arginines, a defect that is alleviated when any one of the arginines is restored to lysine (191).

LYPX$_n$L late domain binds Alix/AIP1

The third class of late domains, LYPX$_n$L, was identified in equine infectious anemia virus (EIAV). Despite lacking a PT/SAP or PPPY motif, the C-terminal p9 domain of EIAV Gag (Figure 1.6) was able to function as a late domain in late domain-lacking RSV and HIV-1 Gags (154). The EIAV p9 sequence responsible for late domain function was finally mapped to a YXXL

motif (162). The cellular binding partner of the new late domain motif, Alix, was then identified by the microsequencing of a ~96 kDa protein incorporated into SIVagm VLPs made of wild-type Gag, but not incorporated into p6 mutant Gag (195). It was also identified by yeast-two hybrid (117, 215). Alix also was also found to be incorporated into HIV-1 VLPs in a p6-dependent manner, and GST pull-down assays mapped the important binding consensus residues to be LYPXXXLXXLF. Alix has been detected in HIV-1 and EIAV particles (30), and it is roughly estimated that about 3-12.5 molecules of Alix are incorporated into subtilisin-treated HIV-1 particles (215). Though mutating the $LYPX_nL$ in full-length HIV provirus had only a moderate effect on virus release (67), mutating this site had a more dramatic effect in the context of a truncated Gag that forms particles as efficiently as wild type Gag but lacks the globular domain of MA and the NTD of CA. The Alix binding motif in EIAV was found to be LYPDL.

A conserved hydrophobic pocket centered around phenylalanine 676 in the interior of the second arm near the apex of the V is responsible for binding the $LYPX_nL$ late domains of HIV-1 p6 and EIAV p9 (56). The pocket is about 10 Å deep and is made up of highly conserved residues. Mutating the Phe676 to Asp abolishes any binding of HIV-1 p6 and EIAV p9 to the V domain in biosensor binding experiments (56). Since the LYPXL binding surface is located near the apex of the V, it is predicted that membrane association or another modification may encourage further opening of the V and exposure of the $LYPX_nL$ docking site (56, 241) (Figure 1.11C).

Although both HIV-1 and EIAV Gag bind Alix using the $LYPX_nL$ consensus motif, context differences in p6 and p9 lead to differences in structural relationships and affinity. Isothermal titration calorimetry assays on

15- and 16- residue peptides of p6 and p9 binding to Alix yielded comparable K_d values (133) despite full-length EIAV p9 having a higher Alix V-domain-binding affinity (i.e. lower dissociation constant) than full length HIV p6 (56). It has been postulated that p9 binding to Alix is less structurally stringent. The proline-rich region of Alix is important for HIV-1 p6 binding in yeast two-hybrid studies, but is not important for EIAV p9 binding (105). Furthermore, the V509A mutation in Alix abrogates p6 binding but is tolerated for p9 binding (105). Part of this may be due to a predicted hinge region in HIV-1 p6. There are contradicting data on the role of the first L in the $\underline{L}YPX_{\underline{n}}L$ motif. Budding assays showed that mutating the L preceding the Y had only a minor effect on EIAV particle production (162). However, in Alix binding assays mutating the first L completely abrogated Alix binding to EIAV p9 but only decreased Alix binding to HIV-1 p6 less than two-fold (133).
Despite the importance of the tyrosine residue in the $LYPX_nL$ motif, replacement of the tyrosine (Y) with phenylalanine (F) had no effect on Alix binding to either HIV-1 p6 or EIAV p9 (133).

Other evidence that HIV Gag and EIAV Gag bind Alix differently includes that Alix multimerization is required for Alix-dependent budding of HIV-1 ΔPTAP mutants but not for a HIV-1 ΔPTAP mutant carrying the p9 domain (24). Perhaps Alix multimerization is needed for avidity effects to compensate for the low-affinity $LYPX_nL$ motif of HIV-1, and is dispensable with the high affinity interaction with LYPDL of EIAV. Alix also interacts with itself (24). Oligomerization has been mapped to two tyrosine residues (Y864 and Y865) in its C-terminus and is important for Tsg101 interaction and Alix-dependent HIV-1 ΔPTAP release (24). Fusion of the GCN4 leucine zipper tothe C-terminus of Alix-multimerization mutants rescues its ability to

interactwith Tsg101 and to mediate Alix-dependent rescue of HIV-1 ΔPTAP budding (24).

Alix interactions with viral components

In addition to the interaction between the V-domain of Alix and the $LYPX_nL$ motif in HIV-1 p6, the N-terminal Bro1 domain of Alix also binds the zinc finger CCHC motifs in HIV-1 NC (160). Deletion of one or both CCHC motifs reduces and completely abolishes incorporation of Alix into HIV-1 particles, respectively. It has been previously shown that over-expression of Alix can rescue the budding defects of HIV-1 PTAP mutants (56, 211). However this Alix-mediated budding rescue is blocked if the CCHC motifs are mutated to CCHS or deleted, making the NC-Alix interaction functionally relevant (160). Though one of the main functions of the NC domain is to bind the RNA genome, the *in vitro* interaction between HA-Alix with GST-NC-p1 was unaffected by treatment with the nuclease benzonase, apparently ruling out the possibility that the interaction is mediated by nucleic acid (160). The significance of this interaction remains unclear.

The HIV-1 accessory protein Nef binds Alix *in vitro* and *in vivo*. The Alix-Nef interaction is dependent on a YPLTF sequence in Nef and allows a Nef-Gag fusion to rescue the budding of a p6 deletion (38).

Alix may be able to interact with ubiquitin. Full-length Alix as well as the V-domain of Alix are able to be precipitated from cell lysates by ubquitin-agarose, though this interaction may be indirect (84). Likewise EIAV Gag lacking the YPDL motif does not immunoprecipiate with Alix or the V-domain, but an EIAV Gag-Ub fusion lacking the YPDL motif does immunoprecipitate with Alix and the V-domain (84).

Relationship between late domains

Often retroviruses have multiple late domains that exist in a functional hierarchy (15, 68, 113, 114). The three known late domains are represented in every combination in the Gag polyproteins of different retroviruses. For example, as described above, in addition to its PT/SAP motif HIV-1 p6 that binds the ESCRT-I component Tsg101 (118), HIV-1 p6 also harbors a $LYPX_nL$ motif that binds Alix and functions in budding (117, 118, 195, 213). However, mutating this $LYPX_nL$ motif or siRNA-mediated depletion of Alix results in only modest reduction in HIV-1 budding (117). However, the effects of mutating the $LYPX_nL$ motif become more obvious in the context of a minimal Gag in which the globular domain of MA and the N-terminal domain of CA are absence (195). Alternatively, a role of $LYPX_nL$ can be illustrated by the ability of Alix over-expression to rescue budding of HIV-1 PTAP mutants (56). Furthermore, the role of the $LYPX_nL$ motif also seems to vary between cell types, as deleting it decreases particle production two-three fold in COS-7 cells, but has no consequence on budding in HeLa cells (45).

MLV contains a PPPY motif, a PSAP motif, and a YPAL motif. The PPPY acts as the dominate late domain, with the PSAP and YPAL motifs playing supportive roles (173). The Ebola virus VP40 structural protein harbors an overlapping PTAPPEY, where the PPEY is most important. Although viruses seem to be able to enter the ESCRT pathway at different steps (by interacting with Nedd4, Tsg101, or Alix) the late domain that interacts with the protein most upstream in the pathway without exception seems to be the dominant late domain.

A possible forth class of late domain was identified in the paramyxovirus SV5 (183). SV5 lacks any of the known late domain

sequences but requires Vps4 for budding. The late domain activity of the structural protein was mapped to an FPIV sequence that was able to mediate budding of a PTAP mutant of HIV-1 Gag. The cellular binding partner to this FPIV sequence is unknown.

The nature of the relationship between the two late domains in viral Gag proteins is unknown. It is possible that they are partially redundant, are cooperative, since they act at slightly different steps in the ESCRT pathway, or are cell-type specific. But it has been observed for a variety of retroviruses that mutating one late domain invariably has a larger effect on budding than mutating the other, implying a hierarchy of function. Only two retroviruses have been found to rely only on a single motif for late domain function, EIAV and Feline immunodeficiency virus (FIV-1) (Figure 1.6). Whether these Gag proteins harbor cryptic late domains is uncertain.

Interestingly none of the late domains recruit ESCRT-II components and none of the ESCRT-II components seem necessary for virus budding (117). Even CHMP6, an ESCRT-III component which links ESCRT-III with ESCRT-II, is dispensable for retroviral budding.

Though the $LYPX_nL$ motif of HIV-1 is considered secondary to the PT/SAP motif, a truncated form of Alix that includes just the V-domain acts as a dominant negative inhibitor of HIV-1 release (133). In addition, the budding of a minimal Gag that lacks NC and p6 cannot be rescued by merely fusing a PTAP domain to the C-terminus (196). The explanation of these observations is probably that HIV-1 Gag also needs either NC or the $LYPX_nL$ sequence to recruit Alix. Interestingly, fusing the PTAPPEY Ebola late domain sequence to the C-terminus of the minimal Gag does rescue budding, presumably because the PPXY motif is supplementing PTAP (196). In other words, although PTAP

is “necessary” and its mutation has dramatic affects on budding, it is not “sufficient” and other elements are required for optimal budding.

THESIS OUTLINE

In this dissertation, I describe my experiments to analyze of the late domain requirements for RSV budding in an infectious system. Chapter Two describes the materials and methods I employed for this study.

In Chapter Three, the *budding* of various late domain mutants is characterized quantitatively by measuring the budding rates by pulse-chase metabolic labeling and qualitatively by analyzing the budding phenotype by electron microscopy. These two complementary techniques identified the LYPSL sequence as a late domain and helped define the relative importance of the two late domains (PPPY and LYPSL). The importance of LYPSL late domain was further supported by the partial budding rate rescue of the PPPY mutants in the presence of over-expressed Alix. Furthermore, I examined the extent that heterologous late domains could function in place of RSV late domains. The LYPDL motif of EIAV proved to be superior to the LYPSL motif of RSV in rescuing the budding rate of PPPY mutants.

In Chapter Four, I describe my studies concerning the *replication* of late domain mutants. Both the effects of the mutations on replication (rate of viral spread), and the effects of replication on the late domain mutants (reduction in viral protein expression), were examined. Overall, the rate at which a given late domain mutant spread through tissue culture correlated well with the budding rates measured by pulse-chase. The notable exceptions were the LYPDL mutants. I also observed a rescue in the spreading rate of PPPY

mutants in the presence of over-expressed Alix, consistent with the budding rates, and with the idea that LYPSL contributes to RSV budding. All the data from Chapters Three and Four are integrated and interpreted in Chapter Five.

CHAPTER TWO

MATERIALS AND METHODS

Plasmids

The Rous sarcoma virus (RSV) proviral constructs were derived from the RCAS vector system (53) and contained the Schmidt-Ruppin-A strain of RSV and a GFP marker expressed as a separate gene, translated from a separately spliced RNA in place of v-src. Mutations in p2 and p10 of Gag were introduced by two-step PCR. The first step involves two PCR reactions. One reaction invariably used the primer KAD23 and the reverse primer that introduces the given late domain mutation. The other reaction invariably used the primer KAD34 and the forward primer that introduces the same late domain mutations. The two PCR products from step one were then used as template for the second step using the flanking KAD23 and KAD34 primers. The PCR product was digested with SacI and SacII resulting in a 1547 bp fragment that was inserted between a unique SacI site (nucleotide 261 of RCAS) located 110 nucleotides upstream from the *gag* open reading frame (ORF) and a unique SacII site (nucleotide 1807 of RCAS) located in the sequence that encodes the C-terminus of the CA domain of Gag. Sequences of all PCR-derived regions of the contructs were verified by DNA sequencing (Cornell University Life Sciences Core Laboratories Center).

Cell culture

The ev-0 derived chicken fibroblast cell line DF1 (ATCC, catalog # CRL 12203) was grown in Dulbecco's modified Eagle medium (Invitrogen) supplemented with 5% fetal bovine serum (Gemini Bio-Products), 5% NuSerum (BD Biosciences), 2% heat inactivated chicken serum (Invitrogen),

1% glutamine (Invitrogen), and 1% vitamins (Invitrogen). Transfection was achieved with Fugene HD (Roche) according to product recommendations. Infection was initiated by filtering medium from cells transfected with proviral DNA through 0.45 μm syringe filters (Pall) and applied to virgin cells.

Measurement of virus budding kinetics

Measurement of virus budding kinetics was done by transfecting DF1 cells with either wild type or mutant proviral RSV DNA and allowing the viral infection to spread. Spread of infection was confirmed by detection of the GFP marker by fluorescence microscopy or flow cytometry. Infected DF1 cells growing on 60mm plates were labeled with 100-300 μCi ^{35}S-Methionine for 30 minutes in met-free DMEM supplemented with 5% fetal bovine serum (Gemini Bio-Products), 5% NuSerum (BD Biosciences), 2% heat inactivated chicken serum (Invitrogen), 1% glutamine (Invitrogen), and 1% vitamins (Invitrogen). About 1 ml of medium covers the bottom of a 60mm plate. The plates were rocked every 5-10 minutes to assure even distribution of labeling medium. Then the radioactive medium was discarded and replaced by prewarmed unlabeled medium. A bottle of medium was warmed by placing in cell incubator with its lid slightly loosened to allow CO_2 levels of the medium to reach those in the incubator. Virus-containing medium was collected serially at various time points and then stored at 4° C. Debris was cleared from the collected medium by low speed centrifugation at 5000 rpm for 5 min. Virus was collected from the medium by centrifugation for 20 minutes at 70,000 rpm in a TLA 100.4 rotor (Beckman) through a 15% sucrose cushion. Virus pellets were dissolved in SDS sample buffer and the viral proteins were resolved by SDS-PAGE. The gel was dried and analyzed using a phosphorimager. Virus release over time was measured by quantitating the band corresponding to CA

from the medium collected at each time point using ImageQuant software (Molecular Dynamics). Budding half-time, or the time at which half of the labeled virus has been released, was calculated using the equation Y=A*(1-exp(-B*x)), where Y equals CA signal (ImageQuant units), X equals time. Budding rate was ultimately expressed as rate relative to wild-type.

Generation of Alix over-expressing DF1 cell line

The human Alix coding sequence was originally obtained in the pCI-neo mammalian expression vector (Promega) as a gift from Wesley Sundquist. The hAlix gene was recloned into the pQCXIP vector (Clontech) using the NdeI and BamHI sites that already flanked hAlix. The 293-based packaging cell line Phoenix-ampho was co-transfected with the pQCXIP retroviral vector expressing human Alix (hAlix) and with a plasmid expressing the G-protein of vesicular stomatitis virus. The medium was collected one to two days later and used to infect DF1 cells. A population of transduced hAlix-expressing DF1 cells was selected in the presence of 2 μg/ml puromycin. Control PuroDF1 cells were established by transduction with the empty vector and also selected with puromycin. The DF1 cells stably-expressing dsRed used in the growth curve were generated in the same way by Danso Ako-Adjei.

Measurement of Viral Spread

DF1 cells were transfected with wild type or mutant proviral RSV DNA carrying a GFP marker. For most experiments, one day post-transfection the cells were trypsinized, diluted 1:10 with non-transfected cells, and reseeded onto fresh plates. For Alix rescue experiments the non-transfected cells were either DF1 cells transduced to express human Alix or control DF1 cells transduced from virus transfected with the empty pQCXIP vector and thus expressing the puromycin resistance gene. Trypsinized and washed cells were fixed for flow

cytometry by incubation in 3.7 % formaldehyde in PBS for 15 minutes. Cells were centrifuged and resuspended in 0.5ml PBS and stored in the dark at 4° for up to a week until flow cytometry analysis.

Flow Cytometry

The spread of infection was monitored by flow cytometric detection of GFP-positive cells using a FACSCalibur system (BD Biosciences). Data acquisition and analysis were performed using CellQuest software (BD Biosciences).

Transmission Electron Microscopy

For each mutant examined, two 100 mm cell culture plates of confluent infected cells were washed with PBS and fixed in 2.5% gluteraldehyde for 1 hour. Cells were then washed with PBS and incubated in 2% osmium tetroxide for at least 1 hour. Osmium tetroxide (OsO_4) was removed and cells were washed at least 5 times with double distilled water. Cells were then dehydrated by sequential 15 minute washes with 10%, 20%, 30%, 50%, 75%, and 100% ethanol. Cells were then washed an additional 3 times with 100% ethanol. Fixed and dehydrated cells were then scraped from plates and collected in microfuge tubes. Cells were incubated in 50:50, 75:25, 100:0 ratios of epoxy [Spurr's low viscosity embedding mixture, Firm Standard: 9.09 ml vinyl cyclohexane dioxide (ERL 4206), 5.26 ml diglysidyl ether of polypropylene glycol (DER 736), 25.24 ml nonenyl succinic anhydride (NSA), 337 µl dimethylaminoethanol (DMAE)] to ethanol for at least 30 minutes each. Cells were allowed to settle or gently centrifuged to bottom of tube. Epoxy was removed from the top of the cells and then the cells were transferred into an embedding capsule and overlayed with epoxy that was allowed to harden at 70° for 16 hours. Sections were cut from the solidified blocks using the microtome. Sections were collected on 400-mesh square copper EM grids

and stained with 2% uranyl acetate for 10 minutes, washed in water, incubated in 0.1% lead citrate for 10 minutes, and washed again in water. Samples were imaged using a Phillips 301 TEM.

Scanning Electron Microscopy

SEM analyses were performed as described previously (103). DF1 cells were plated onto glass coverslips containing a gold finder grid for cell identification, then transfected using Fugene (Roche) with wild- type or mutant RSV proviral DNA. Nineteen hours after transfection, cells were fixed in 4% paraformaldehyde and imaged by fluorescence microscopy to identify the transfected cells and assess relative transfection levels. The cells were then fixed in 2.5% glutaraldehyde, dehydrated, critical point dried, coated with a thin layer of platinum, and imaged at the University of Missouri Electron Microscopy core facility on a Hitachi S4700 Cold-cathode SEM.

Measurement of relative Alix expression in hAlixDF1 cells versus control PuroDF1 cells

Control DF1 cells carrying the puromycin resistance gene and DF1 cells carrying human Alix were cultured separately, each in one well of a 6-well plate. After reaching near confluency, cells were washed, trypsinized, collected in microfuge tubes, gently centrifuged and resuspended in a known volume (1 ml) of PBS. Cells were counted using a hemocytometer and centrifuged again. The similar plated density of control DF1 cells and hAlixDF1 cells was confirmed (calculated PuroDF1= 249,000 cells/ml, hAlixDF1= 250,000 cells/ml). PBS was aspirated and cells from one well of a 6-well plate were resuspended in 80 µl of 1X SDS buffer. To resolve cellular proteins with SDS PAGE, 2.5 µl, 5 µl, 10 µl, and 20 µl (3.125%, 6.25%, 12.5%, and 25% of the total cells from one cell) of the cells lysates were loaded. Alix was

detected by immunoblotting with hAlix antibody obtained from Wesley Sundquist.

Cell Growth curves for DF1, dsRedDF1, PuroDF1, and hAlixDF1 cells

DF1, dsRedDF1, PuroDF1, and hAlixDF1 cells were trypsinized and counted by hemacytometer. Approximately forty thousand cells of each cell type were plated separately in multiple wells of a 6-well plate. Each day one of the wells from each cell type was trypsinzed and counted. Cell number was followed over 4 days until the cells were confluent.

Reverse Transcription of Viral Genomes

Medium was removed from infected cells and cleared through a 0.45 μm syringe filter (Pall). About 1.5 ml of medium was centrifuged at 70 K rpm for 20 minutes using the Beckman Coulter TLA 100.4 rotor. Medium was aspirated and the pellet was washed gently with PBS. The virus pellet was resuspended in 140 μl of virus resuspension buffer (10mM Tris pH 8, 20mM NaCl). RNA was extracted from virus using the QIAamp Viral RNA kit (Roche) according to manufacturer's suggestions. Viral RNA was eluted in a final volume of 60 μl of AVE buffer. Primers were annealed to RNA by heating 5 μl of viral RNA, 1 μl of random hexamers (100μM), and 4 μl ddH_2O for 70° C for 5 minutes and then returning to ice. To this, 4 μl of 5X AMV buffer (Roche), 1 μl of dNTPs (10mM) (Roche) and 0.5 μl of AMV reverse transcriptase (Roche) were added and mixed. A no-RNA and a no-RT control reaction were included. The reverse transcription reaction was allowed to proceed for 1 hour at 42° C followed by heat activation at 85° C for 5 minutes. One to 5 μl of the resulting reaction was used as cDNA template for 50 μl PCR amplifications and primer sets KAD41 and KAD42 or KAD47 and KAD48 were used to amplify the region of Gag between the end of MA and the middle of CA, and

thus included the late domains. Template and no template reactions were included as PCR controls. Often PCR products were re-amplified in 100 µl reactions. The resulting PCR products were gel purified and sequenced at Cornell University Life Sciences Core Laboratory Center using the same primers. In addition, the primers were designed with flanking XbaI (KAD41 and KAD47) and XhoI (KAD42 and KAD48) sequences for insertion into pBlueScript KS II + vector, if needed.

Sequence Alignments

Alix amino acid sequences from Homo sapiens, Equus caballus (horse), and Gallus gallus (chicken) were aligned using the ClustalW server, www.ebiac.uk/clustalw. The accessions for the Alix sequences are NP_037506 for Human, NW_001867381 for horse, and AJ720564 for chicken.

Statistics

P-values were obtained by Student's t-test performed with Microsoft Excel.

CHAPTER THREE:

KINETIC AND ELECTRON MICROSCOPY ANALYSIS OF RSV LATE DOMAIN MUTANT BUDDING

Multimerization of Gag on the inner leaflet of the plasma membrane induces curvature of the membrane resulting in the wrapping of the nascent virus particle in what will become, once it has budded, its own membrane envelope**.** Just as the multimerization of Gag and the assembly of virus particles depends on Gag/nucleic acid and Gag/membrane interactions, the membrane fission step that separates the virus membrane from the cell membrane also depends on a Gag interaction. In order to bud, Gag must recruit a network of cellular proteins that are normally responsible for analogous cellular membrane fission events - the budding of vesicles into multivesicular bodies (MVBs) and the separation of two daughter cells during cytokinesis. Collectively this protein network is called the ESCRT (Endosomal Sorting Complex Required for Transport) machinery and is composed of four high molecular weight complexes (ESCRT-0, -I, -II, and –III) as well as regulatory proteins that are not part of any one complex.

In the case of transmembrane-cargo proteins bound for the lysosome, the ESCRT pathway begins when the cargo protein is tagged for entry into the pathway by mono-ubiquitination by an ubiquitin ligase. The mono-ubiquitin is then recognized and bound by the ESCRT-0 complex, followed by the sequential recruitment of ESCRT-I, -II, and –III complexes. Ultimately, the cargo protein is de-ubiquinated, an ATPase, Vps4, disassembles the ESCRT-III complex and the cargo-containing vesicle buds into the lumen of the late endosome forming a MVB. Finally, the MVB fuses or matures into a lysosome, degrading the internal vesicles and their contents.

To complete their own budding, newly assembled virions recruit the ESCRT machinery to perform membrane fission. While over thirty cellular proteins are implicated in the cellular process of sorting cargo into MVBs, retroviruses are known to interact with only three of them directly, a ubiquitin ligase of the Nedd4-family, Tsg101 that is a component of the ESCRT-I complex, and an adaptor protein, Alix, that interacts with components of ESCRT-I and ESCRT-III complexes. Retroviral Gag proteins harbor short motifs termed late domains that bind these three proteins. Late domains are classified into three classes based on sequence consensus, 1) PPXY, 2) PT/SAP, and 3) $LYPX_nL$. The PPXY late domain sequence binds members of the Nedd4 family of ubiquitin ligases. The PT/SAP late domain motif binds the ESCRT-I component Tsg101. Finally, the $LYPX_nL$ consensus sequence binds the ESCRT adaptor protein Alix.

Since late domains are protein-binding motifs, they are often positionally independent. In other words, late domains can mediate particle release even when placed in alternative locations within Gag. Furthermore, heterologous late domain of one class (PPXY, PTAP, or $LYPX_nL$) from one retrovirus can often functionally replace the late domain of a different class in a different retrovirus.

Each retrovirus depends on one or more (up to three) late domains to mediate release from the cell (Figure 1.7). No pattern exists as to which late domains are required together or which act alone. In other words, the three late domains exist in every combination in some retroviral Gag protein (Figure 1.7). Evidence is emerging that when more than one late domain contributes to the budding of a given virus, the late domains exist in a functional hierarchy, with one serving as primary late domain, and the other(s) serving as a

secondary late domain(s). For example, HIV-1 budding depends heavily on a PTAP motif that recruits, Tsg101, and also, but to a lesser extent, on a $LYPX_nL$ motif that recruits Alix. EIAV, in contrast, relies solely on a single LYPDL late domain for particle egress.

Thus far, the budding of RSV has been credited to a single late domain. Specifically, a PPPY motif in the p2b segment of RSV Gag has previously been shown to play a critical role in budding (224) by engaging members of the Nedd4-family of ubiquitin ligases (93). However, RSV Gag also possesses a putative, but yet uncharacterized, LYPSL late domain motif in p10, five amino acids downstream from the PPPY late domain (Figure 3.1). Since late domains often reside in close proximity to each other (15, 68, 74, 110, 118) and since the $LYPX_nL$ consensus sequences have been shown to be important for release of other retroviruses (163, 195), I sought to determine the role of this LYPSL sequence in RSV budding.

In order to characterize the general late domain requirements for RSV budding, including the role of the LYPSL sequence and the relationship between the established PPPY late domain and the LYPSL motif, infectious RSV mutants were constructed. Mutants were created in which the entire PPPY and/or LYPSL late domain sequence were mutated (ie. AAAA-LYPSL, PPPY-AAASA, AAAA-AAASA), the late domain sequences were partially mutated (ie. APPY-LYPSL, APPY-LYPDL, APPY-AAASA), or entire late domain sequences were replaced with heterologous late domain motifs (ie. PTAP-LYPSL, FPIV-LYPSL, PPPY-LFPIV, PPPY-LYPDL) (Figure 3.1). The late domain mutants were characterized by measuring budding rate and by electron microscopy.

Rous sarcoma virus provirus

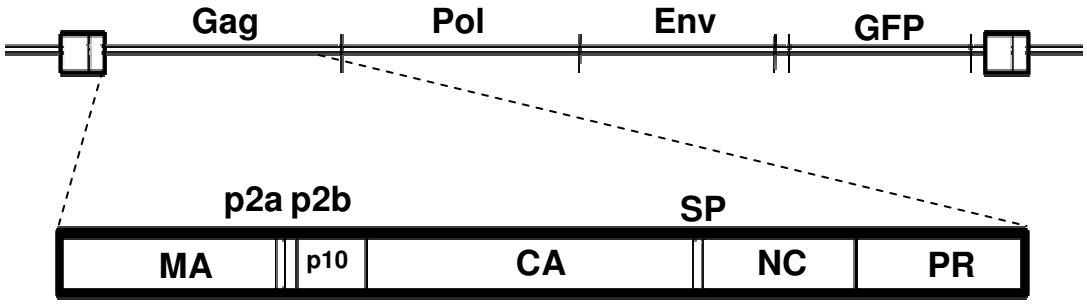

	p2a p2b **PPPY**VG**I**SG**LYPSL**	Mutation Description
1)	**PPPY-LYPSL**	**Wild-type**
2)	PPPY-LYPDL	EIAV LYPDL
3)	APPY-LYPSL	weakened PPPY
4)	PPPY-AAASA	no $LYPX_nL$
5)	APPY-AAASA	weakened PPPY, no $LYPX_nL$
6)	APPY-LYPDL	weakened PPPY, EIAV LYPDL
7)	AAPY-LYPSL	further weakened PPPY
8)	AAPY-LYPDL	further weakened PPPY, EIAV LYPDL
10)	AAAA-LPYSL	no PPPY
11)	PTAP-LYPSL	PTAP in place of PPPY
12	FPIV-LYPSL	FPIV in place of PPPY
13)	FPIV-LYPDL	FPIV in place of PPPY, EIAV LYPDL
14)	PPPY-LFPIV	LFPIV in place of LYPSL
15)	APPY-LFPIV	weakened PPPY, LFPIV in place of LYPSL
16)	AAAA-LFPIV	no PPPY, LFPIV in place of LYPSL
17)	AAAA-AAASA	no PPPY, no $LYPX_nL$
	(**FPAV)**	**Wild type sequence in PR**
18)	(GPAV)	GPAV in place of FPAV in PR
19)	AAAA-AAASA (GPAV)	no PPPY, no LYPSL, mutated FPAV in PR

Figure 3.1 Overview of late domain mutants constructed in the context of infectious RSV provirus DNA carrying a GFP reporter gene. Underlined amino acids represent mutations.

Measurement of budding rate

In earlier reports from diverse labs budding defects were detected and characterized by measuring the amount of Gag in the medium at a fixed time point after metabolic labeling. Budding efficiency then could be expressed as a ratio of the amount of Gag immunoprecipitated from the medium to the amount of total Gag (Gag immunoprecipitated from the cells and from the medium). Specifically for RSV, cells were transfected with Gag expression vectors. Fourty-eight hours post-transfection cells were metabolically labeled with ^{35}S-methionine. Cells and cell medium were then subjected to immunoprecipitation after 2.5 hours of labeling (224, 228). HIV-1 budding efficiency was measured by a similar method except the cells were metabolically labeled for longer periods, such as for 12 hours (67), or overnight (79). In contrast, my analysis describes budding defects of various late domain mutants in terms of "budding rate" (i.e. budding half-time) instead of by the classical "budding efficiency". Instead of measuring the amount of Gag in the medium at one time point as has been done previously, I measured Gag in the medium at many time points and was thus able to follow viral release over time. By examining the kinetics of budding using pulse-chase, where the time was long enough for all of the labeled Gag to exit, as illustrated by the plateauing of the CA plots (Figure 3.2.B), the immunoprecipitation of Gag from the cells and normalization to this population of Gag becomes unnecessary.

All of the late domain mutants I constructed were measured using the kinetic approach described above. Cells susceptible to RSV infection, DF1 chicken fibroblasts, were transfected with wild-type or late domain mutant proviral RSV DNA, and the infection was allowed to spread for at least one

Figure 3.2 Overview of the method used to measure the budding rates (budding half-times) of late domain mutants. (A) Examples of viral proteins resolved by SDS-PAGE. Each lane represents the virus collected from the medium at a time point (6 timepoints for each experiment). The bands containing the viral CA protein are boxed and were used to quantitate virus release at each time point. (B) A plot of the cumulative CA signal collected from the medium over time from the quantitation of the CA bands on the gells in (A). (C) Budding half-time was calculated for each virus and normalized to wild-type (virus A). The budding rate of Virus C was slower than this budding assay can measure and thus the bar representing its budding rate is below the dashed line representing the detection level of this assay.

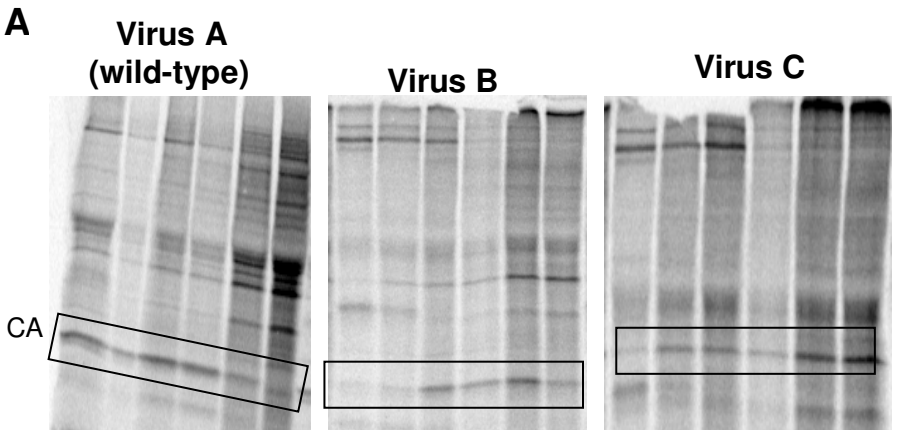
A
Virus A
(wild-type)
Virus B
Virus C
CA

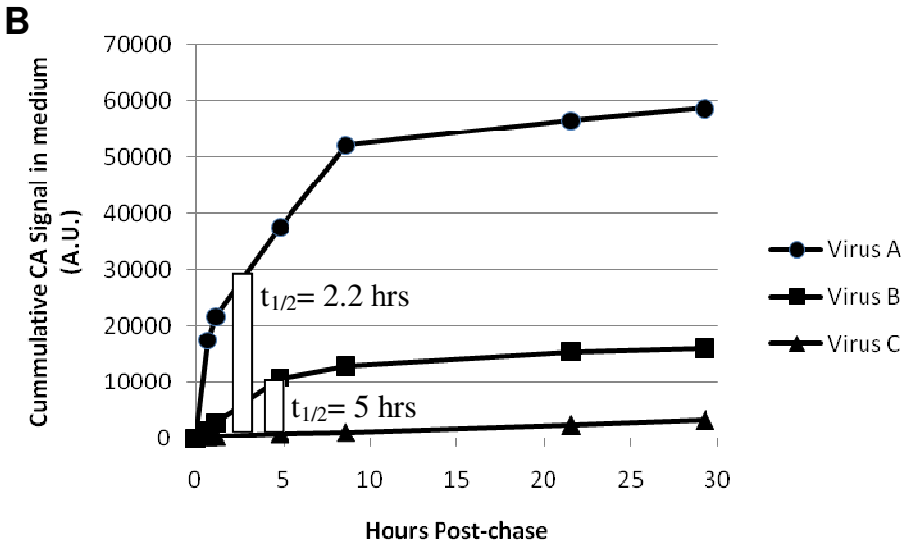
B
Cummulative CA Signal in medium
(A.U.)
70000
60000
50000
40000
30000
20000
10000
0
0
5
10
15
20
25
30
Hours Post-chase
t1/2= 2.2 hrs
t1/2= 5 hrs
Virus A
Virus B
Virus C

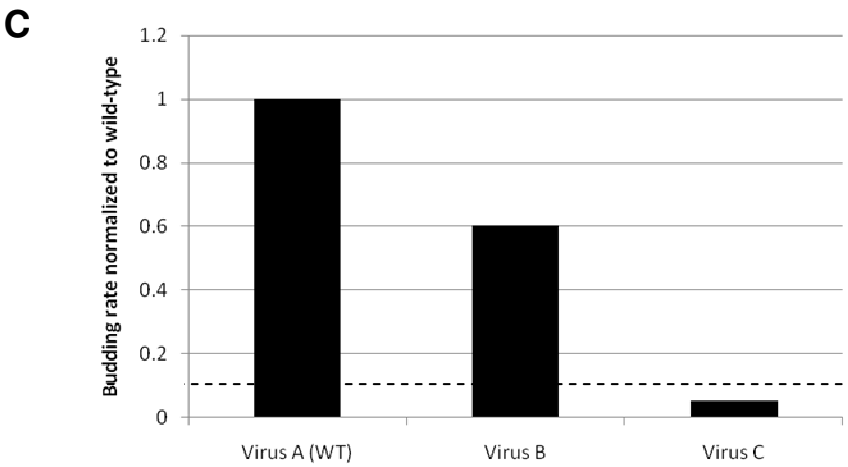
C
Budding rate normalized to wild-type
1.2
1
0.8
0.6
0.4
0.2
0
Virus A (WT)
Virus B
Virus C

week. Infection of the majority of cells was confirmed by detection of the GFP marker by flow cytometry or fluorescence microscopy. All mutants proved to be infectious and able to spread in DF1 chicken fibroblasts, as evidenced by western blot against the CA domain and detection of GFP marker by fluorescence microscopy. Even a double knockout of the PPPY and LYPSL motifs (AAAA-AAASA) was able to spread throughout the culture (Chapter 4, Figure 4.1).

All budding assays were done using infected cells, to avoid expression differences often resulting from transient transfection. Infected cells were pulsed with ^{35}S-Methionine for 30 minutes, and chased with fresh medium. Virus-containing medium was collected serially approximately every hour. In other words, at each time point the medium was collected and replaced with new medium, allowing me to quantitate virus release during each period. The virus was collected by centrifugation of the collected medium and the viral proteins were resolved by SDS-polyacrylamide gel electrophoresis (PAGE) (Figure 3.2A). The gel was exposed to a phosphor-screen and the band corresponding to CA (Figure 3.2A, box) was quantitated with the ImagQuant program and used as a proxy for the amount of particles released. Plotting the cumulative amount of virus released over time (Figure 3.2B) allowed me to calculate the budding half-time, or the time at which half of the labeled virus had been released from the cell. The calculated budding half-time was then normalized to the budding half-time of wild-type RSV (Figure 3.2C). The average budding half-time for wild-type RSV was measured to be approximately 2 hours (130 minutes).

It is important to note that the budding half-time measurement is not strictly the time it takes for a virus to pinch off from the membrane. The

budding half-time includes all steps following the incorporation ^{35}S-methionine into viral proteins, including Gag trafficking to the plasma membrane, particle assembly, and budding. It is unknown how long it takes newly synthesized RSV Gag to traffic to the membrane and assembly. It is known that following synthesis on cytoplasmic ribosomes, RSV Gag undergoes trafficking through the nucleus mediated by an NLS within the MA domain and an NES at the C-terminus of the p10 domain before being targeted to the membrane (178). Unlike RSV Gag, HIV-1 Gag does not traffick through the nucleus. Pulse-chase experiments followed by gradient fractionation of cell lysates showed that approximately 80% of HIV-1 Gag is associated with membranes only 5 minutes after synthesis but assembly into particles occurs over several hours (209). In contrast, *de novo* assembly of an HIV-1 particle occurs in about 5-10 minutes as observed by total internal reflection fluorescence (TIRF) microscopy (85). Limitations in experimental methods have made it difficult to distinguish distinct steps in Gag trafficking and assembly and have been the source of conflicting conclusions. My method for evaluating budding is also unable to separate the various steps.

In order to give enough information to predict budding half time, this method of measuring budding rate requires that the plot of virus release over time plateaus (i.e. all the radiolabeled virus is released). If the plot does not plateau and a best fit curve is not able to predict when the plot will plateau, it is not possible to know at what time half of the labeled virus was released. Some of the late domain mutants tested budded so slowly, given the time of the experiment, I was not able to predict when all of the virus would be released, and thus calculate the budding half-time. Thus, these viruses were considered to bud at a rate below the level of measurement for this assay

(Figure 3.2C, Virus C). I estimate this rate to be lower than 1/10th the budding rate of wild-type RSV. This threshold is denoted on the budding rate graphs by a dashed line (Figure 3.2C).

The LYPSL motif functions in RSV release

The LYPX$_n$L late domain motif that binds Alix is present in many retroviral Gag proteins (Table 3.1). In some cases, such as in EIAV, the LYPX$_n$L sequence is the sole late domain. In other retroviral Gag proteins, such as HIV-1 and HTLV-1, LYPX$_n$L acts in conjunction with the PTAP and/or PPPY late domains to promote budding. RSV Gag harbors a putative LYPX$_n$L late domain five amino acids downstream from the PPPY late domain. Preliminary data from our lab (not shown) and other labs failed to show a major role for this motif in RSV release. I hypothesized that this result is due to their method of measuring budding efficiency and the presence of the strong primary late domain PPPY. To uncover the contribution of the LYPSL motif to budding I weakened the primary PPPY late domain, as has also been done for HIV-1 (56, 211) and for MLV (115) and used a pulse-chase-based budding kinetics assay.

To examine the role of the LYPSL motif in RSV budding, I first mutated the LYPXL consensus motif to alanines, yielding the amino acid sequence AAASA in place of LYPSL (Figure 3.1, line 4). Although just the YPXL is often considered the core consensus sequence of this motif class, I chose to also mutate the preceding L residue because it has been shown to contribute to Alix binding and in other viruses is present just upstream of the YPXL motifs implicated in budding (105, 133, 195).

Table 3.1 Consensus of $LYPX_nL$ motifs in the presence and absence of other late domains

Virus	**$LYPX_nL$ Motif**	**Location**	**Other late domains Sequences**	**Location**
EIAV	LYPDL	p9	None	N/A
HIV-1	LYPXXXLXXLF	P6	PTAP	p6
MLV	LYPAL	MA-CA border	PPPY, PTAP	p12
Maedi-Visna virus	LYPNL	end of MA	PTAP	C-term
BIV	IYPSL	End of MA	PSAP	C-term
SIVgsn	LYPSL	p6	PTAP	p6
SIVdeb	LYPDL	p6	none	NA
RSV	LYPSL	p2b	PPPY	p10

EIAV, equine infectious anemia virus; MLV, murine leukemia virus; BIV, bovine immunodeficiency virus; SIVgsn, simian immunodeficiency virus (greater spot-nosed monkeys) SIVdeb, simian immunodeficiency virus (De Brazza's monkeys).

Mutating the entire LYPSL consensus motif to alanines, (PPPY-AAASA), led to less than a two-fold reduction in budding rate, which was barely statistically significant with a $p<0.05$ (Figure. 3.3, compare bars 1 and 2). P values for the budding rates for each compared mutant pairs are reported in Table 3.2. By contrast, just weakening the PPPY late domain by mutating only the first proline, APPY-LYPSL, reduced budding rate about three-fold, with $p<0.005$ (Figure 3.3, compare bars 1 and 3). In other words, mutating just a single amino acids of the PPPY motif (APPY-LYPSL) reduces budding more dramatically than mutating *all* of the LYPXL consensus sequence (PPPY-AAASA), confirming the strength of the PPPY late domain in RSV budding.

Because of the strength of the PPPY late domain in promoting budding, I thought it was possible that any contribution of the LYPSL motif to budding could be partly obscured in the presense of the PPPY late domain. To address this, I made the same LYPSL mutations (AAASA) in the context of a partially weakened PPPY motif (APPY). The budding of this mutant (APPY-AAASA) became more sensitive to mutations in LYPSL (Figure 3.3, compare bars 3 and 4), with at least a ten-fold reduction in budding rate for the APPY-AAASA mutant as compared with wildtype (Figure 3.3, compare bars 1 and 4). Thus, I conclude that the LYPSL sequence functions in RSV release and its contribution to budding is more easily observed when the primary PPPY late domain is compromised.

Heterologous late domains support RSV budding to varying degrees

Since late domains are modular protein binding motifs and often retain their ability to promote virus budding when placed in different regions of Gag

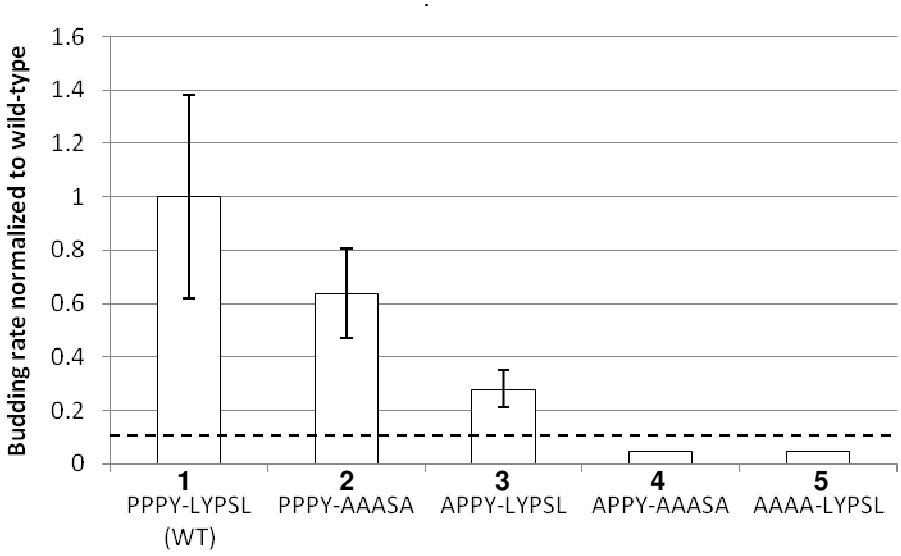

Figure 3.3 Budding rates (budding half-times) of late domain mutants normalized to wild-type RSV. Budding half-times were calculated using pulse-chase labeling of cells infected with wild-type or late domain mutants. The budding rates of mutants APPY-AAASA (bar 4) and AAAA-LYPSL (bar 5) were slower than the threshold of detection of this experiment, denoted by the dashed line. The p value obtained from Student's t-test for wild-type budding rate and PPPY-AAASA, and wild-type budding rate and APPY-LYPSL budding rates were both significant ($p < 0.05$).

Table 3.2 Budding rate p values obtained from Student's t-test

Mutant Pair	p value
1 PPPY-LYPSL (WT): PPPY-AAASA	0.0073
2 PPPY-LYPSL (WT): APPY-LYPSL	0.0024
3 PPPY-LYPSL (WT): PPPY-LYPDL	0.6745
4 PPPY-LYPSL (WT): APPY-LYPDL	0.0033
5 PPPY-LYPSL (WT): AAPY-LYPSL	0.0274
6 APPY-LYPSL: AAPY-LYPSL	0.1705
7 PPPY-LYPSL (WT): (GPAV)	0.0412
8 PPPY-LYPSL (WT): AAPY-LYPDL	0.5915
9 APPY-LYPSL: APPY-LYPDL	0.0094
10 AAPY-LYPSL: AAPY-LYPDL	0.0296
11 APPY-LYPDL: AAPY-LYPDL	0.0446
12 PPPY-LYPSL (WT): PPPY-LYPSL (WT)(ALIX)	0.6625
13 APPY-LYPSL: APPY-LYPSL(ALIX)	0.0119
14 PPPY-AAASA: PPPY-AAASA(ALIX)	0.7165
15 AAAA-LYPSL: AAAA-LYPSL(ALIX)	NA
16 PPPY-LYPSL (WT): PPPY-LFPIV	0.4054
17 PPPY-AAASA: PPPY-LFPIV	0.0846

or in different viruses (116, 148, 154, 228), I investigated how well late domain motifs from other viruses could satisfy the requirements for RSV budding. Though others have examined the effects of exogenous late domains on RSV budding using transient transfection of Gag constructs into COS-1 cells (154), I did so using infectious RSV in the more relevant DF1 chicken fibroblast cell line.

According to isothermal calorimetry assays, Alix binds the LYPDL-containing p9 sequence of EIAV more tightly than the LYPLTSL p6 sequence of HIV-1 (56, 133, 238). To investigate whether the LYPDL would act as a "stronger" late domain than the native LYPSL sequence in the context of RSV, I substituted the LYPDL motif of EIAV in place of the LYPSL sequence. No difference in budding rate was observed when the primary PPPY late domain motif remained intact (Figure 3.4, compare bars 1 and 2). However, when PPPY motif was handicapped by mutating it to APPY, the LYPDL then was able to partially rescue the budding rate (Figure 3.4, compare bars 3 and 4), and thus acted as a stronger late domain than the normal LYPSL sequence. Likewise, the LYPDL sequence also partially rescued the budding rate of the AAPY mutant (Figure 3.4, compare bars 5 and 6). The LYPDL-mediated rescue was statistically significant by Student's T-test in the presence of APPY or AAPY ($p<0.05$) (Table 3.2, lines 9 and 10). These data correlate well with the reported higher Alix-binding affinity of LYPDL compared to LYPLTSL *in vitro*, supporting the idea that LYPDL may represent the optimized Alix-binding motif, and thus may be a stronger late domain.

The budding rate of the AAPY-LYPSL mutant and the APPY-LYPSL mutant were comparable (not significantly different, $p>0.1$) (Figure 3.4, compare bars 3 and 5). Both mutations merely handicapped the PPPY late

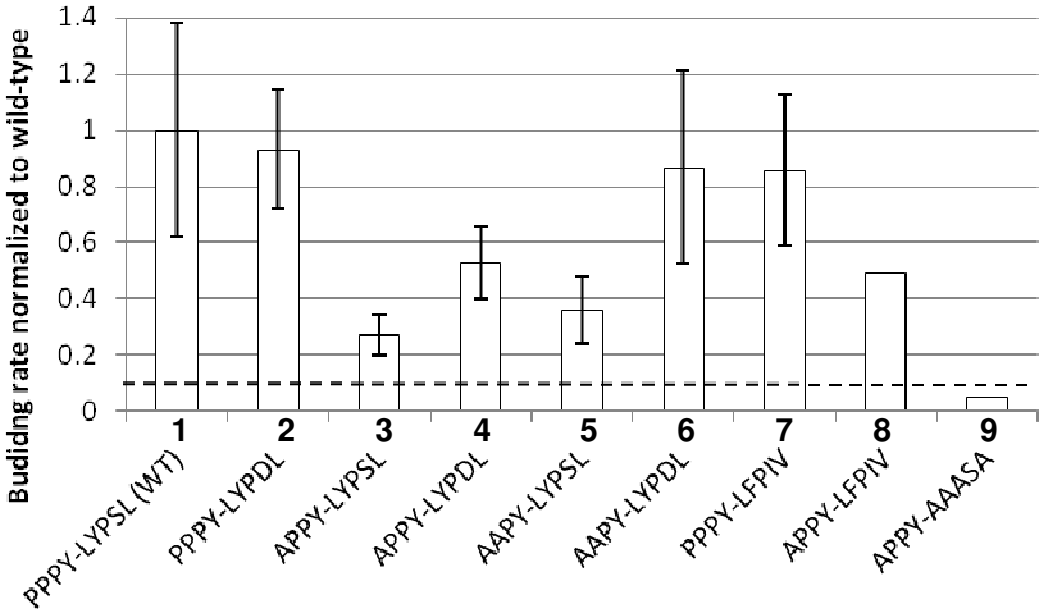

Figure 3.4 The budding rates of late domain mutants in which the LYPSL motif is replaced with the LYPDL motif of EIAV or the LFPIV sequence of parainfluenza 5 (SV5). The budding rates of LYPSL mutants were examined in the context of wild-type PPPY motif (bar 2) or of weakend PPPY motif (APPY), bars 3 and 4, and (AAPY), bars 5 and 6. Budding rate was calculated as budding half-time using pulse-chase, and then was normalized to wild-type. The APPY-LFPIV bar (bar 8) lacks error bars because it was measured once. The p values obtained for wild-type budding rate and APPY-LYPSL, APPY-LYPDL, AAPY-LYPSL budding rate from the Student's t-test were significant ($p<0.05$). The p value for APPY-LYPSL and APPY-LYPDL budding rate was also significant . The p value for AAPY-LYPSL and AAPY-LYPDL was $p< 0.05$.

domain motif, but did not slow budding as severely as the AAAA-LYPSL mutation (Figure 3.3, bar 5). However, the LYPDL-mediated rescue was more dramatic for AAPY-LYPDL than for APPY-LYPDL (Figure 3.4, bars 3-6). If one assumes that the rescue is the result of stronger Alix binding, perhaps AAPY-LYPDL buds at a faster rate than APPY-LYPDL because AAPY binds less Nedd4 than APPY, and thus physically obstruct Alix binding less. Since the PPPY motif and the LYPSL motif are only 4 amino acids apart, the simultaneous binding of Nedd4 and Alix to Gag is unlikely.

A novel class of late domains with the consensus sequence of FPXV has been identified in the paramyxovirus parainfluenza virus 5 (SV5) (183). Despite being sensitive to dominant negative VPS4 and proteasome inhibitors, SV5 budding does not rely on any of the three known classes of late domains. The budding activity was mapped to a FPIV sequence in the matrix structural protein. It has been speculated that FPIV could be another variation of an Alix-binding motif. LYPSL and FPIV could be lumped together in a ΦPXη consensus, where Φ is a large hydrophobic residue (Y or F), X is any residue, and η is a non-polar residue (V or L). A tyrosine (Y) substitution for the phenylalanine (F) in the FPIV motif maintains late domain function in SV5. In both the YPXL and FPXV motif, the X position is tolerant of many amino acids (183) and in both sequences the upstream amino acid (L and A) are nonpolar. However, GST-pulldown and yeast-2-hybrid experiments failed to detect an interaction between the FPIV sequence and Alix (183).

In order to examine the possibility that FPIV could function as a late domain in RSV, I measured the budding rate of mutants in which the YPSL was replaced with FPIV (PPPY-LFPIV and APPY-LFPIV) (Figure 3.1).

Mutating the LYPSL to LFPIV reduced the budding rate modestly, but this reduction was not statistically significant (Figure 3.4, compare bars 1 and 7). This is not unexpected since mutating all of the LYPSL sequence to AAASA causes only a modest decrease in budding rate. To rule out the possibility that the primary PPPY late domain was obscuring the role or lack of role of the FPIV sequence, I constructed the FPIV mutant in the context of a weakened PPPY motif (APPY-LFPIV). This mutant budded faster than a mutant in which the PPPY was weakened and the LYPSL motif was replaced with alanines (APPY-AAASA), implying that the FPIV may have late domain function in this context (Figure 3.4, compare bars 8 and 9). However, this budding rate was measured only one time and later data suggest that this data is a result of the mutant APPY-LFPIV reverting to PPPY-LFPIV (Chapter 4, Figure 4.5). Thus, from the budding rate data, I cannot conclude whether FPIV can substitute for LYPSL.

I also wanted to test if the primary PPPY late domain could be functionally replaced with heterologous late domain motifs. The PPPY sequence was replaced with the PTAP late domain from HIV-1, the FPIV motif from SV5, or ablated by mutation to AAAA. Measuring the budding rates of these mutants suggested that neither the PTAP motif nor the FPIV motif performs any better than AAAA in place of PPPY (Figure 3.5, compare bars 3 to 4 and 5). The budding experiments were performed three times for the AAAA-LYPSL and PTAP-LYPSL mutants and twice for the FPIV-LYPSL mutant, with none of the experiments yielding budding rates fast enough for this assay to measure. The primary PPPY late domain proved to be optimal and irreplaceable at this position.

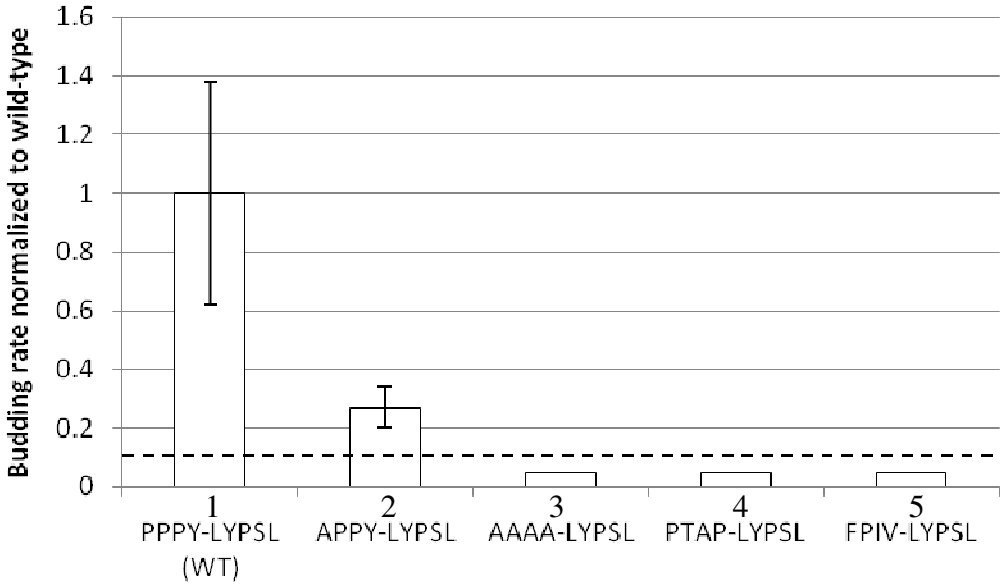

Figure 3.5 The budding rates of mutants in which the LYPSL is replaced with the paramyxovirus FPIV late domain motif. The budding rates of LFPIV mutants were examined in the context of a wild-type PPPY motif (bar 2) or of a weakend PPPY motif (APPY) (bar 5). Budding rate was calculated as budding half-time using pulse-chase, and then was normalized to wild-type. The budding rates of mutants AAAA-LYPSL (bar 3), PTAP-LYPSL (bar 4), and FPIV-LYPSL (bar 5) were slower than the threshold of detection in this experiment, denoted by the dashed line. The budding experiments were done three times for AAAA-LYPSL (bar 3) and PTAP-LYPSL (bar 4), and two times for FPIV-LYPSL (bar 5).

As mentioned above and to follow in chapter 4 (Figure 4.1), I found that RSV is infectious and can spread through tissue culture even when both the PPPY primary late domain and the secondary LYPSL late domain are mutated to alanines (AAAA-AAASA). This suggested that RSV may harbor a third late domain to mediate budding. Upon examination of RSV amino acid sequence, I located a FPXV motif in the PR domain of Gag. Furthermore, sequences similar to the FPIV motif were identified in other retroviruses (Table 3.2) and tended to fall in regions where late domains normally lie (i.e. between MA and CA or at C-terminus of Gag). In the case of RSV, the sequence was FPAV and was near the C-terminal in the PR domain. Danso Ako-Adjei mutated an F residue to G in protease and tested protease function *in vitro*. Protease function was unaffected by this F→G mutation and thus is not expected to affect infectivity. Next, I moved the mutation to infectious RSV provirus and measured budding. The GPAV mutant did bud about two-fold slower than wild-type RSV ($p < 0.05$) (Figure 3.6). Thus, the FPAV sequence in PR of Gag may be important for budding. The possibility that this mutation affected another step in trafficking or assembly cannot be excluded and thus further studies will be needed.

Over-expression of Alix rescues budding of PPPY mutants

Based on the budding assays, I conclude that the LYPSL motif does contribute to RSV budding. To corroborate this data, I chose to investigate the effects of the over-expression of Alix, the cellular LYPSL-binding partner, on RSV budding. Previous work showed that the over-expression of Alix could compensate for a lack of the primary PTAP motif in HIV-1 Gag, rescuing budding to wild-type levels (56, 211). If the RSV LYPSL late domain mediates

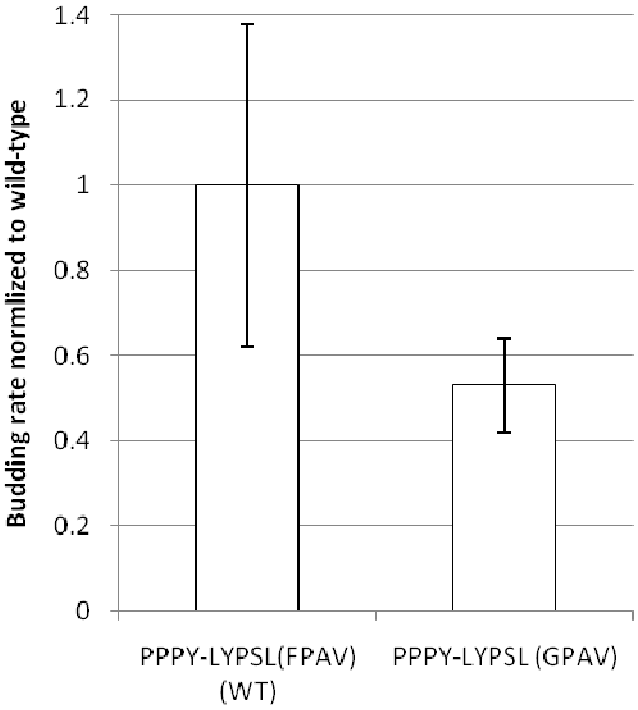

Figure 3.6 Budding rate of mutant in which the FPAV sequence in PR was mutated to GPAV. Budding half-times were calculated using pulse-chase labeling of cells infected with wild-type or GPAV mutant. T-test gives a p value of < 0.05.

budding through an interaction with Alix, Alix over-expression could also rescue the budding defect observed in PPPY mutants. Thus, I established a DF1 cell line that over-expresses human Alix, denoted as hAlixDF1 cells, using a MLV-based vector carrying the human Alix gene (hAlix). Alix is highly conserved, with human and chicken Alix sharing 83% identity and 92% similarity (Figure 3.7). Since the processes of transduction and selection of cells expressing hAlix might alter cellular properties, control DF1 cells were transduced with the same retroviral vector used to transduce the hAlix cellsexcept carrying only the puromycin resistance gene. The control cells are denoted as PuroDF1s.

To confirm Alix over-expression, Alix expression was detected by immunoblot of hAlixDF1 and control puroDF1 cells (Figure 3.8A). Assuming α-hAlix antibodies recognize endogenous chicken Alix and human Alix equally well, immunoblotting of cell lysates from hAlixDF1 and PuroDF1 cells normalized for cell number, it is estimated that hAlixDF1 cells express Alix at a levels about 20-fold above that of endogenous Alix (Figure 3.8A).

Aside from the ESCRT pathway, Alix functions in a variety of cellular processes. Thus, constitutive Alix over-expression could conceivably have a wide variety of effects on the DFI cells. Although, the hAlixDF1 cells appeared overall healthy, exhibiting normal rate of cell division (Chapter 4, Figure 4.8), they displayed morphological differences from wild-type DF1 and puroDF1 cells. While wild-type DF1 cells and PuroDF1 cells were more square with multiple contact points with the plate (Figure 3.8B, top and middle rows), over-expression of hAlix cells caused the DF1 cells to elongate and have fewer points of contact (Figure 3.8B, bottom row). A link between Alix and cell morphology has been reported previously. WI38 cells (derived from human

Figure 3.7 Alignment of Homo sapiens (first line), Equus caballus (second line) and Gallus gallus (third line) Alix amino acid sequence. (*)residue match; (blank) residues do not match and are not similar; (.) two of three residues match; (:) residues are similar. Blue represents acidic amino acids, pink represents basic residues, green represents polar residues, and red represents non-polar residues. Alignment was performed using ClustalW server, www.ebiac.uk/clustalw.

Figure 3.7 (Continued)

```
EKMVPVSVQQSLAAYNQRKADLVNRSIAQMREATTLANGVLASLNLPAAIEDVSGDTVPQ 415
EKMVPVSVQQALAAYNQRKADLVNRSIAQMREATTLANGVLASLNLPAAIEDVSGDTVPQ 415
EKMVPLQVQQSVSVYNQRKADLVNRLIAQMREATNLANGVLASLNLPAAIEDVSGDTVPQ 419
*****:.***:::.********** ********.************************

SILTKSRSVIEQGGIQTVDQLIKELPELLQRNREILDESLRLLDEEEATDNDLRAKFKER 475
SILTKSTSVIEQGGIQTVDQLIKELPELLQRNREILDESLRLLDEEEATDSDLRAKFKER 475
SILNKSKAVIEQGGVQTIDQLIKDLPELLQRNKEILDESLRLLDEEETTDNELRTKFKER 479
***.** :******:**:*****:********:**************:**.:**:*****

WQRTPSNELYKPLRAEGTNFRTVLDKAVQADGQVKECYQSHRDTIVLLCKPEPELNAAIP 535
WQRTPSNELYKPLRAEGNNFRAVLDKAVQADGQVKERYQSHRDTIALLCKPEPELNAAIP 535
WQRTPSNDLYKPLRAEGANFHNILNKAVQADGQVREGYQSHRDTIALLCKPEAELNAAIP 539
*******:********* **: :*:*********:* ********.******.*******

SANPAKTMQGSEVVNVLKSLLSNLDEVKKEREGLENDLKSVNFDMTSKFLTALAQDGVIN 595
SANPAKTMQGSEVVNVLKSLLTNLDEVKKEREGLENDLKSVNFDMTSKFLTALAQDGVIN 595
SANPAKTLQGSEVVNVLKTLLASLDEVKKEREQLENDLKSVNFDMTNKFLTALAQDGAIN 599
*******:**********:**:.********* ************.**********.**

EEALSVTELDRVYGGLTTKVQESLKKQEGLLKNIQVSHQEFSKMKQSNNEANLREEVLKN 655
EEALSVTELDRIYGGLTTKVQESLKKQEELLKNIQVSHQEFSKMKQSNNEANLREEVLKN 655
EEAISVTELDRIYGSYTQKVQESLKKQEELLKNIQNAHQDFSKMKQSNNESNLREEVLKN 659
***:*******:**. * ********** ****** :**:**********:*********

LATAYDNFVELVANLKEGTKFYNELTEILVRFQNKCSDIVFARKTERDELLKDLQQSIAR 715
LATAYDNFVELVANLKEGTKFYNELTEILVRFQNKCSDIVFARKTERDELLKDLQQSIAR 715
LAVANDNFVELLANLKEGTKFYNELTEILLKFQNKCSDIVFARKTERDELLKDLQQSIAR 719
**.* ******:*****************::*****************************

EPSAPSIPTPAYQSSPAGG---HAPTPPTPAPRTMPPTKPQPPARPPPPVLPAN-RAPSA 771
EPSAPSIPTPAYQSSPAAG---HAPTPPTPAPRTMPPTKPQPPARPPPPVLPAN-RAPSA 771
EPSAPSIPLPTYQTTPAGGSKPAASSTPTPAPRTMVGTKPQPPARPPPPVISAASSSPSA 779
******** *:**::**.*    *.:.********  *************:.*   :***

TAPSPVGAG--------TAAPAPSQTPGSAPPPQAQGPPYPTYPGYPGYCQMPMPMGYNP 823
TAPAPVATG--------TTAPAPSQTPGSAPPPQAQGPPYPTYPGYPGYCQMPMPMGYNP 823
SAPSGTAAAPPSAPTPAAPTPAPGASASSTAPSQAQGPPYPTYPGYPGYCQMPMPIGYNP 839
:**: ..:.        :.:***. :..*:.*.**********************:****

YAYGQYNMPYPP-VYHQSPGQAPYPGPQQPSYPFPQPPQQSYYPQQ 868
YAYGQYNMPYPP-VYHQSPGQAPYPGPQQPSYPFPQPPQQSYYPQQ 868
YMYGQYNLPYAPSPVFQNPGQPPYPAPQQPGYPFPQQP---YFPQQ 882
* *****:**.*   .*.***.***.****.***** *   *:**
```

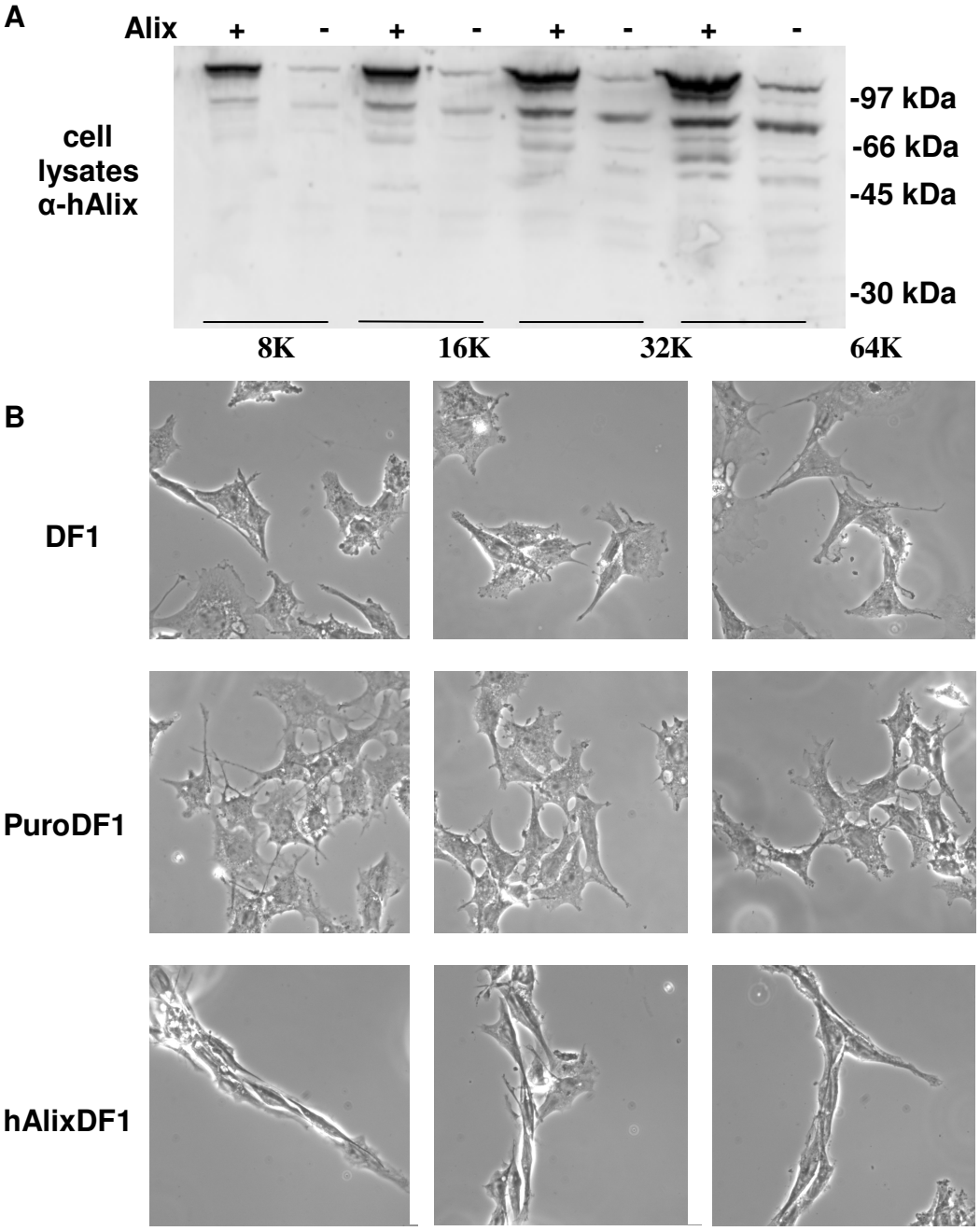

Figure 3.8 Alix Over-expression in DF1 cells. (A) Immunoblot against hAlix in DF1 cells (-) or in DF1 cells constituatively overexpressing hAlix (+). Cells number was normalized by hemocytometer, so that approximately equal number of cells are represented in each pair of wells. The pairs of lanes have approximately 8,000 (8K), 16,000 (16K), 32,000 (32K), and 64,000 (64) cells loaded respectively. (B) Phase contrast microscopy of DF1 cells, DF1 cells carrying puromycin-resistance (PuroDF1), and DF1 cells over-expressing human Alix (hAlixDF1).

lung fibroblasts) subcultured after transfection with siRNA against Alix exhibited a rounded up morphology compared to control cells (152). Similarly, NIH3T3 cells looked larger and flatter upon over-expression of Alix and more rounded up upon siRNA against Alix (227). The difference in hAlixDF1 cell morphology could also possibly be due to Alix interactions with the actin cytoskeleton and cytoskeleton regulators (152, 181) or Alix deposition on the substratum, since it is reported to regulate integrin-mediated cell adhesions and fibronectin matrix assembly (151).

Based on the known function of the $LYPX_nL$ late domain in other retroviruses, the RSV LYPSL motif presumably mediates budding by recruiting Alix to the site of budding. In order to confirm this model, and implicate Alix in RSV budding, I measured and compared the budding rates of various late domain mutants in control puroDF1 cells to their budding rates in hAlixDF1 cells. Specifically, I hypothesized that the role of Alix in budding, like the role of the LYPSL motif, could be uncovered when the primary PPPY late domain is muted (APPY) or ablated (AAAA).

Budding assays were performed on infected hAlixDF1 or puroDF1 control cells. The budding rate of wild-type RSV was not significantly affected by Alix over-expression (Figure 3.9, bars 1 and 2). However, Alix over-expression increased the budding rate of both PPPY mutants (APPY-LYPSL and AAAA-LYPSL). The budding rate of the APPY-LYPSL mutant increased of about two-fold in hAlixDF1 cells compared to control cells ($p<0.05$) (Figure 3.9, bars 3 and 4). Furthermore, Alix over-expression rescued the budding rate the PPPY mutant, AAAA-LYPSL, from a rate too low to measure (Figure 3.9, bar 7) to a rate comparable to the modest effect seen for the PPPY-AAASA mutant (Figure 3.10, bars 8 and 5). Statistical analysis could not be

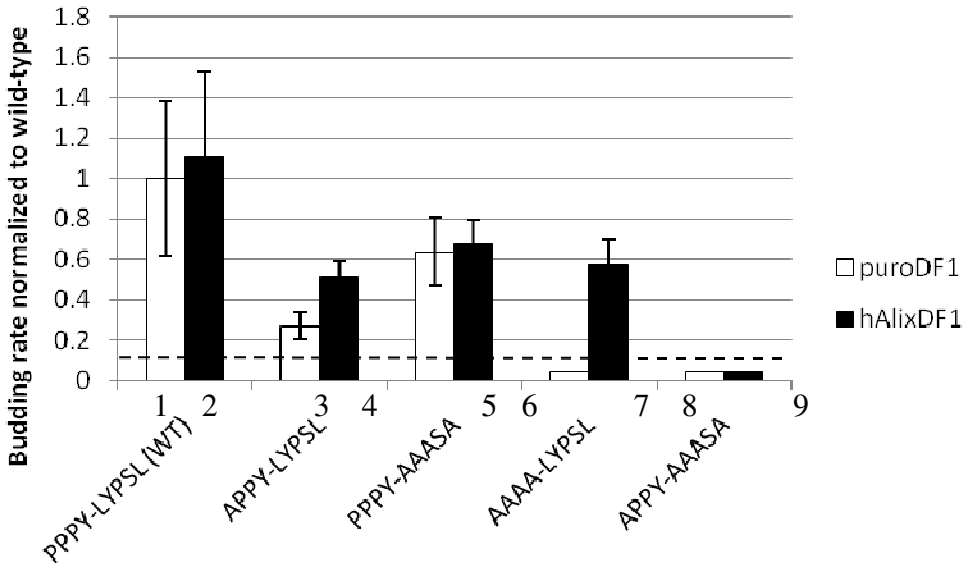

Figure 3.9 Partial rescue of the budding rate of the PPPY mutants by over-expression of human Alix. DF1 cells or DF1 cells constituatively over-expressing human Alix (hAlixDF1) were infected with wild-type or late domain mutants. Budding rate was calculated as budding half-time using pulse-chase, and then was normalized to wild-type. The p value obtained by Student's t-test for APPY-LYPSL budding rate in DF1 and hAlixDF1 cells was significant ($p>0.05$). The p value for AAAA-LYPSL budding rate in DF1 and hAlixDF1 cells was not able to be calculated because in DF1 cells budding rate is below the assays sensitivity.

performed on this set (AAAA-LYPSL) because budding was too slow to obtain a measurable budding rate in control cells.

To exclude the possibility that the increase in budding rate was the result of the late domain mutations reverting back to wild-type late domains the viral RNA from the APPY-LYPSL and AAAA-LYPSL mutants collected from the hAlixDF1 cells was reverse transcribed and sequenced. In each case, the mutations were still present and no second site mutations existed in a ~750 nucleotide region surrounding the late domains.

An increase in budding rate in hAlix over-expressing cells was not observed for the APPY-AAASA mutant in which the presumed Alix binding LYPSL motif was absent (Figure 3.9, bar set 9 and 10). The APPY-AAASA mutant buds at a rate below the level of detection for this assay, in both hAlixDF1 and puroDF1 cells. Likewise, the budding of the PPPY-AAASA mutant, which lacks the Alix binding site and displays only a modest but statistically significant retardation in control cells, is not rescued by Alix over-expression (Figure 3.9, bars 5 and 6).

These data support the model that the LYPSL motif in RSV Gag helps mediate budding via an interaction with the cellular protein Alix, and its effect can be observed when the primary PPPY late domain is handicapped and the LYPSL is present (APPY-LYPSL and AAAA-LYPSL).

Virus budding visualized by electron microscopy

As an independent method to evaluate budding, electron microscopy was employed to examine the budding phenotype of the various late domain mutants. The pulse-chase budding experiments measurements include the time of all steps from the time of the translation of viral proteins, to trafficking

of viral proteins, to assembly and finally budding. Thus, the slowed budding rates measured for the late domain mutants do not exclude the possibility that the mutations also perturb other steps in retrovirus replication, such as trafficking or assembly. To confirm that the observed defects were due to a block specifically at the membrane scission step of budding two types of electron microscopy analysis, transmission (TEM) and scanning electron microscopy (SEM), were performed.

First, thin sections of DF1 cells infected with mutants PPPY-AAASA, APPY-LYPSL, APPY-AAASA, or AAAA-AAASA were examined by transmission electron microscopy. Due to the rapid budding rate of RSV and the fact that this technique can only observe particles in a thin plane, wild-type particles are rarely observed in the act of budding from the plasma membrane by this technique. In fact, I was unable to observe any budding particles on cells infected with the PPPY-AAASA or the APPY-LYPSL mutant. Apparently, the modest reduction in budding rate observed for these mutants in the pulse-chase assays is not sufficient to increase the number of particles on the surface as observed in thin sections. It is possible that I did not look at a large enough sample size to say there were no particles, but particles were not abundant on the cell membrane. A few budding particles were observed on the membrane of cells infected with the APPY-AAASA mutant (data not shown). Furthermore, TEMs of cells infected with the double late domain knock-out mutant, AAAA-AAASA, displayed many budding particles (Figure 3.10). Consistent with the classic “late domain phenotype”, the particles exhibited immature morphology with an electron dense ring located just inside the viral membrane and were tethered to the plasma membrane through a membraneous stalk (Figure 3.10B, C). Often particles were seen tethered to

each other (Figure 3.10A, B, and D) and examples of particles budding into apparently internal vesicles were also observed (Figure 3.10D). Cells infected with the AAAA-AAASA, as well other severe late domain mutants, were often vacuolated and generally unhealthy looking (data not shown).

While TEM allows one to look only at a thin slice of the cell (~70 nm), making it easy to miss budding particles, SEM allows a much larger area of the cell surface to be visualized, making this the preferred technique to evaluate budding. SEM was performed by our collaborators, Marc C. Johnson and Devon Gregory (University of Missouri), on DF1 cells transiently transfected with wild-type or late domain mutant proviral DNA. Newly transfected cells proved to be healthier than the infected cells used in my TEM analysis, especially cells infected with the more severe late domain mutants. Budding particles were rarely observed on the surface of the plasma membrane of DF1 cells transfected with wild-type RSV and usually the surface was completely bald (Figure 3.11A and B). Occasionally a few wild-type particles or other cellular protrusions could be seen (data not shown). Although the PPPY-AAASA mutant has only a modest reduction in budding rate and its particles are unobservable by TEM, SEM of the cells transfected with the PPPY-AAASA mutant did show particles. Surfaces of cells transfected with the PPPY-AAASA mutant were decorated with particles tethered to the plasma membrane, indicative of a late budding block and supporting the importance of the LYPSL motif in budding (Figure 3.11C and D). Furthermore, cells transfected with the APPY-LYPSL (E and F), APPY-AAASA (G and H) or AAAA-AAASA (I, J, K and L) mutants exhibited even more densely arranged particles on the surface than the PPPY-AAASA, corresponding to their more severe budding defects. The surface of cells transfected with the double late

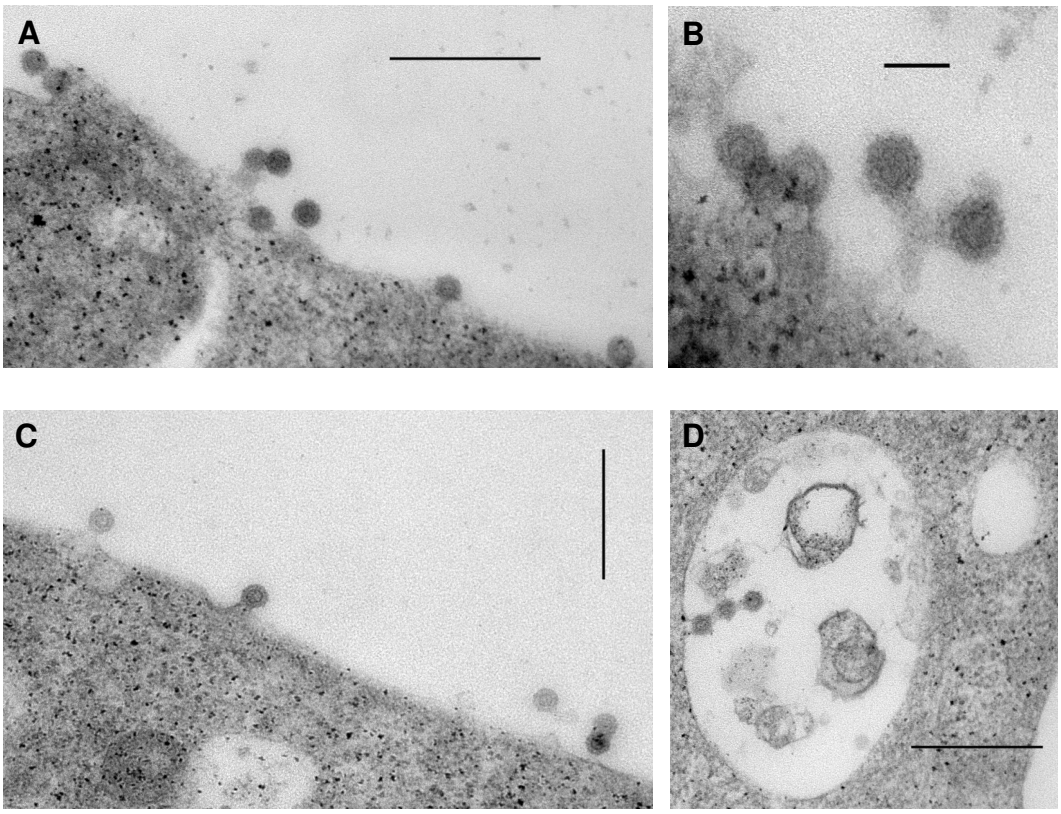

Figure 3.10 Transmission electron micrographs (TEMs) of DF1 cells infected with RSV harboring the double late domain knockout mutant AAAA-AAASA. Bars represent 500 nm in (A), (C), and (D) and 100 nm in (B).

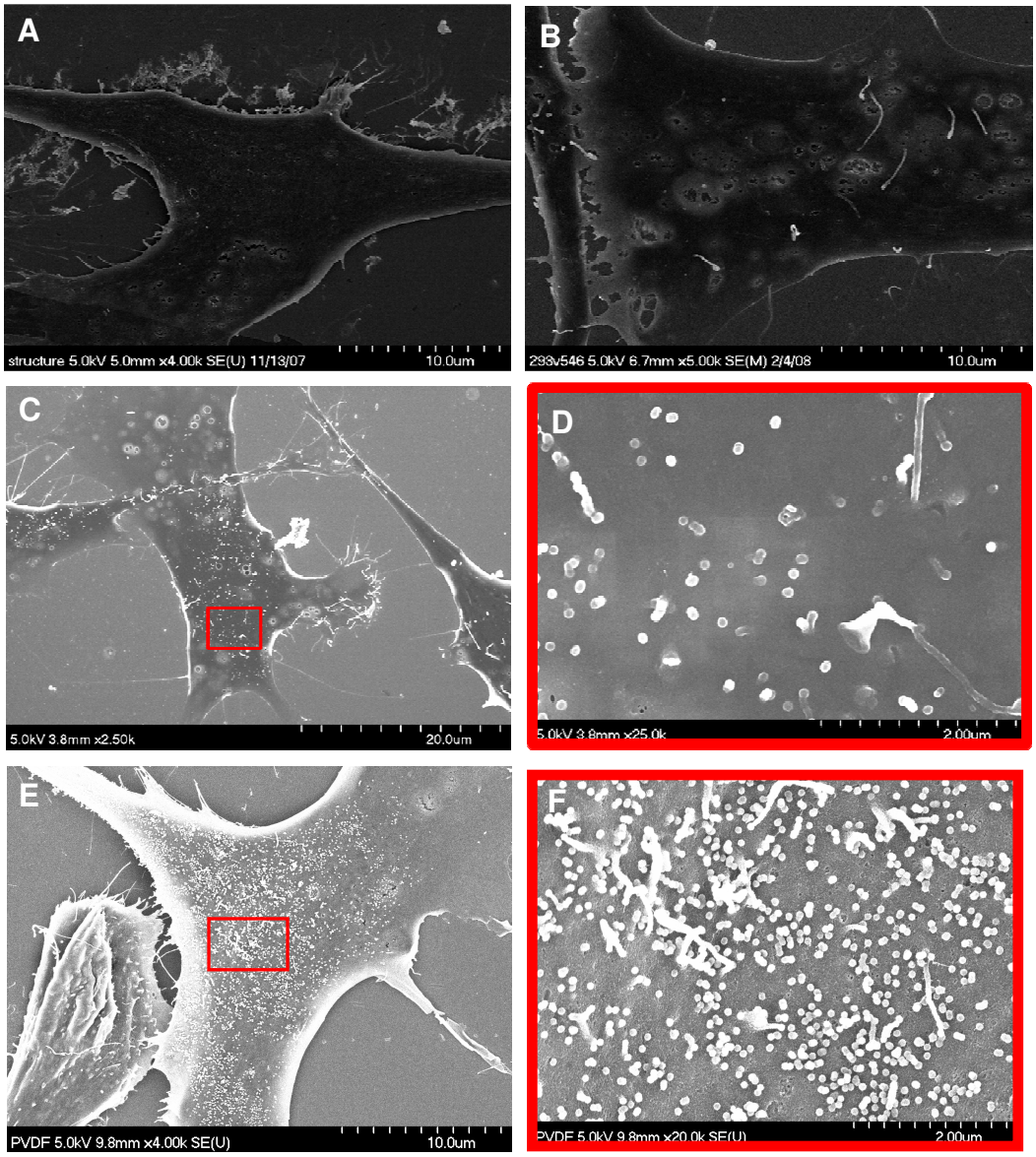

Figure 3.11 Scanning electron micrographs of DF1 cells transfected with late domain mutants. (A) and (B) are transfected with wild-type RSV, (C) and (D) with PPPY-AAASA, (E) and (F) with APPY-LYPSL, (G) and (H) with APPY-AAASA, and (I), (J), (K), (L) with AAAA-AAASA late domain mutants in a proviral construct. Scale bars in lower right of each image represent 20 um in (C); 10 um in (A), (B), (E), (G), (I), and (K); and 2 um in (D), (F), (H), (J), and (L). The area inside the red boxes on the left images correspond to the zoomed-in images to the right. These micrographs were captured by Marc C. Johnson and Devon Gregory.

Figure 3.11 (Continued)

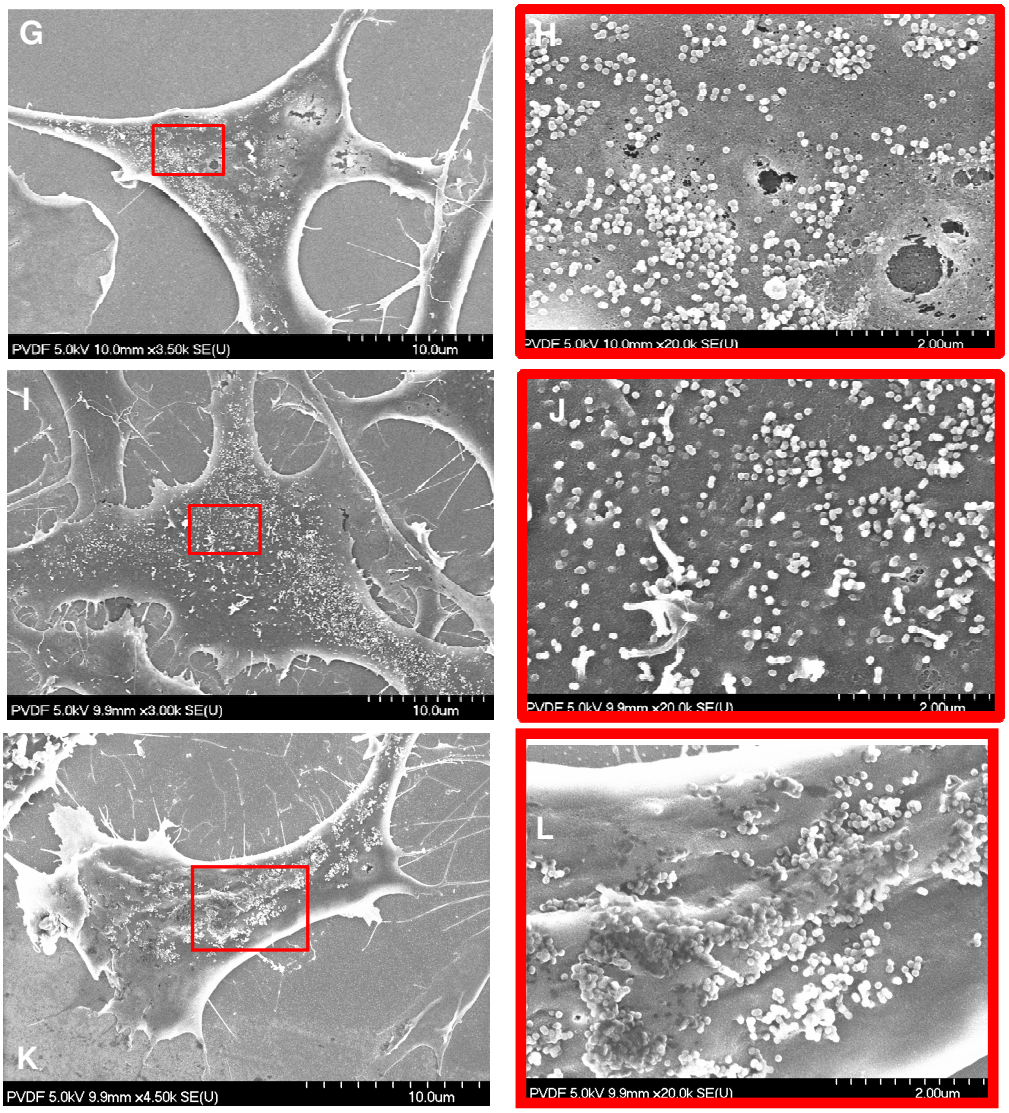

domain knockout, AAAA-AAASA, was not only crowded with fully assembled particles, but also displayed particles that seem to be arrested at various early stages of budding. Some particles appeared to have just begun to induce membrane curvature (Figure 3.11J). The plasma membrane of cells transfected with the double late domain knockout also had virus budding in clusters (Figure 3.11K and L) which was not observed in cells transfected with any of the other mutants.

In summary, the SEM analysis confirmed that the reduction in budding rates measured in the kinetic experiments is most likely due to a delay in the membrane scission step of particle release, not in other pre-assembly steps, as evidenced by the increased number of virions attached to the cell membrane. The qualitative nature of this technique does not allow us to rate the severity of the various late domain mutants. However, there was a general trend of more particles found tethered to cells transfected with the slower budding late domain mutants, with cells transfected with the double late domain mutant, AAAA-AAASA displaying the most severe phenotype of clumps of virus budding at once and particles that appear to be obstructed at earlier steps of at the beginning of the formation of membrane curvature.

Discussion

The results presented in this chapter identify the LYPSL motif in RSV p2b as a late domain. Mutating the LYPSL alone results in a modest but statistically significant reduction in budding rate as measured pulse-chase experiments. Mutating one amino acid of the PPPY motif (APPY) proved to have a larger effect on budding rate than mutating all of the LYPSL motif (AAASA), implying the two late domains exist in a functional hierarchy, with

PPPY as the primary and LYPSL as the secondary late domain. Consistent with this hierarchy, the effect of mutating the LYPSL sequence can be amplified by first weakening the primary PPPY motif. RSV can now join other retroviruses, such as HIV-1, MLV, and HTLV-1, that rely on multiple late domains for optimal budding efficiency (15, 68, 113, 114).

By performing pulse-chase budding analysis on mutants in which heterologous late domains replaced the native PPPY or LYPSL, I confirmed that LYPDL late domain of EIAV is a stronger late domain than the natural LYPSL motif. APPY-LYPDL and AAPY-LYPDL both budded at a faster rate than APPY-LYPSL and AAPY-LYPSL, respectively. Presumably this is a result of LYPDL binding Alix more tightly than LYPSL. The comparison of the LYPLTSL HIV-1 sequence and LYPDL EIAV sequence has suggested that LYPDL binds Alix with a higher affinity. Biosensor experiments measuring dissociate constants showed that the affinity of the bro1 domain through the V-domain of Alix ($Alix_{bro\text{-}V}$) or just the V-domain of Alix ($Alix_V$) was about 60-fold higher for EIAV p9 than it was for HIV-1 p6 (238). Similarly, HIV-1 Gag in which p6 was replaced with EIAV p9 incorporated about 12-fold more Alix into VLPs than HIV-1 (ΔPTAP) Gag (238). EIAV p9 also bound more full-length Alix than HIV-1 p6 in GST pull-down experiments (195). However, these experiments were all done using full-length p9 and p6 domains. It is possible that the sequence surrounding the $LYPX_nL$ motifs could contribute to this difference in Alix-binding ability. Thus, the difference could be attributed solely to the amino acid/s in the X position.

Evolution and virus selection also seems to support the idea that the LYP**D**L sequence is a stronger Alix-binding late domain than LYP**S**L. EIAV is not the only retrovirus that relies completely on a single LYP**D**L motif for late

domain function. Naturally occurring SIVs can harbor a LYP**S**L motif or a LYP**D**L motif. When SIV has a LYP**S**L motif, it also has a PTAP motif. However, when a LYP**D**L is present (such as in SIVdeb), SIV does not contain any other late domain motifs (12), implying LYP**D**L alone is sufficient to support its budding (Table 3.1).

Interestingly the AAPY-LYPDL mutant budded faster than the APPY-LYPDL mutant, despite having a less intact PPPY late domain ($p<0.05$) (Figure 3.4, bars 4 and 6) (Table 3.2, line 11). It is possible that that APPY mutant could bind Nedd4-family members more efficiently than AAPY adding a steric hindrance for Alix binding to the neighboring LYPDL motif. However, if APPY does bind Nedd4 family members more efficiently, it is surprising that APPY-LYPSL does not bud faster than AAPY-LYPSL (Figure 3.4, bars 3 and 5).

Budding experiments also showed that the primary late domain of HIV-1, PTAP, or the SV5 late domain, FPIV, could not functionally replace the primary PPPY late domain. This does not rule out the possibility that heterologous late domains could support RSV budding if placed in their native context with the flanking amino acids of their original source. Despite being modular, there are precedents that late domains can act differently depending on the surrounding amino acids. For example, replacing 11 amino acids of HIV-1 p6 with the 11 amino acids of RSV p2b supports near wild-type budding efficiency. In contrast, just replacing the HIV-1 p6 sequence EPTAP with PPPPY, does not restore budding (148). I went by the assumption that if the PPPY late domain can bind Nedd4 and the LYPSL motif can bind Alix in RSV, then these motifs were displayed and exposed enough for the interaction of alternative late domain binding partners. But the possibility that the context of

the heterologous late domains affected binding, and thus the ability of heterologous late domains to function, cannot be excluded.

Upon identification of the paramyxovirus late domain FPIV, which is not a member of any of the three canonical late domain motifs, there has been speculation that FPIV may belong to the $LYPX_nL$ late domain family and binds Alix. After all, both the $LYPX_nL$ and FPIV fit the ΦPXη consensus, where Φ is a large hydrophobic residue (Y or F), P is a proline, X is any residue, and η is a non-polar residue (V or L). I found that replacing the LYPSL with LFPIV had a moderate, but statistically insignificant effect on budding rate (Table 3.2, line 16). PPPY-LFPIV had an intermediate budding rate in between the rate measured for PPPY-LYPSL (wild-type) and the PPPY-AAASA mutant, making it unclear if FPIV can serve as a YPSL motif. Since the PPPY may be obscure the effects of mutating the LYPSL, the budding rate was measured for a mutant in which the FPIV replaced YPSL in the context of a weakened PPPY motif (APPY-LFPIV). The APPY-LFPIV mutant mediated a higher budding rate than APPY-AAASA (Figure 3.4, bars 8 and 9). Thus it appears that FPIV may be able to support budding in place of LYPSL. However, the budding rate of the APPY-LFPIV mutants was measured only once and spreading data in Chapter 4 shows that this mutant is able to revert readily. Thus, I may have actually been measuring the budding rate of a mixed population of viruses, APPY-LFPIV and PPPY-LFPIV.

Mutating the naturally occurring FPAV sequence in the C-terminal PR domain of Gag reduced the budding rate compared to wild-type RSV (Table 3.2, $p<0.05$). Although follow up studies are required to confirm that this sequence acts as a late domain and to identify its cellular binding partner, it is intriguing to speculate about a possible third late domain in RSV in light of the

ability of the double late domain knock-out (AAAA-AAASA) to spread through tissue culture (Chapter Four, Figure 4.1). A cursory protein BLAST search for FPXV-related motifs uncovered multiple retroviruses that harbor similar motifs including, HIV-1, HTLV-2, EIAV, Walleye dermal sarcoma virus (WDSV), MMTV, and SIVcpz (Table 3.3). Hepatitis A and B virus also have FPAV sequences. Hepatitis B virus is an enveloped virus, but Hepatitis A virus is un-enveloped. The significance of these motifs is unknown.

The importance of the LYPSL motif in RSV budding was tested from two angles. First, as mentioned above, the effects of not having a LYPSL motif on budding were examined by creating the PPPY-AAASA mutant. Second, I took an opposite approach. Since the LYPSL motif is presumed to bind the ESCRT protein Alix, the effects of Alix over-expression on budding rates were also examined. I hypothesized that if the LYPSL mediates budding through the recruitment of Alix, then the over-expression of Alix would rescue the budding defect of primary late domain mutants (APPY-LYPSL and AAAA-LYPSL) as has been shown in HIV-1 (56, 211). Indeed, the APPY-LYPSL and AAAA-LYPSL mutants did bud at a faster rate in the cells that over-expressed hAlix as long as an intact LYPSL is present. However, the over-expression of Alix had no significant effect on the budding rate of wild-type RSV, the PPPY-AAASA or APPY-AAASA mutant. I propose a model in which the LYPSL motif promotes budding by recruiting Alix. Even though LYPSL is a secondary late domain, the positive effect of Alix on budding can be observed when the rate of budding is reduced by PPPY mutations.

TEM and SEM analysis of DF1 cells infected or transfected with wild-type or late domain mutants of RSV supplemented the budding rate data well.

Table 3.3 Viruses that harbor FPIV-like motifs and locations of FPIV-like motifs

Virus	Sequence	Location
PIV (SV5)	FPIV	M
RSV	FPAV	PR
HIV-1	Y/FPIV	MA
FFV	FPIV, FPRV	aa 209, 316 in Gag
HTLV-2	FPIL	aa 136
EIAV	YPIM YPEV	aa 149 aa 361 Pol
Maedi-Visna virus	YPIV FPIV	MA-CA border aa 141, 6aa downstream LYPNL
WDSV	YPAV	aa 343
MPMV	YPAM	aa 150
EFV	YPAM	aa 248
MMTV	FPVV	CA
HAV	FPAV	Core
HBV	FPAV	Core
SIVcpz	FPIV	Gag

PIV(SV5), parainfluenza virus 5; FFV, Feline foamy virus; WDSV, walleye dermal sarcoma virus; MPMV, Mason-Pfizer monkey virus; EFV, Equine foamy virus; MMTV, Mouse mammary tumor virus; HAV, Hepatitis A virus; HBV, Hepatitis B virus.

I was unable to observe particles budding from cells infected with the mutant PPPY-AAASA and APPY-LYPSL by TEM. This is mostly due to the limitations in looking at thin cross-sections of cells. An additional factor could have been expression level. (Chapter 4 discusses the phenomenon of the down expression of viral proteins upon repeated passage of late domain mutants.) However, I was able to observe particles by TEM that assembled from APPY-AAASA and AAAA-AAASA mutant Gag. These particles were tethered to the cell through membraneous stalks and displayed immature morphology that is a signature of particles arrested by late domain defects.

SEM performed by our collaborators, Marc Johnson and Devon Gregory, was more informative and allowed me to look at the entire top surface of the plasma membrane. Wild-type RSV buds very rapidly and was rarely observed in the act of budding from the plasma membrane. This is in contrast to wild-type HIV-1 which is regularly observed in the act of budding, implying RSV buds more quickly than HIV-1. SEM of cells transfected with the PPPY-AAASA mutant, which had only a modest reduction in budding rate compared to wild-type, showed many particles in the process of budding from the plasma membrane. This finding supports the idea that LYPSL functions as a late domain in RSV, and that the reduction in budding rate reflects a block at budding, and not a block at another step in trafficking or assembly. Cells transfected with the APPY-LYPSL mutant exhibited more particles on their surface, implying the PPPY motif is a stronger late domain than the LYPSL motif, also consistent with the budding data. Furthermore, cells transfected with the more severe late domain mutants, APPY-AAASA and AAAA-AAASA, had even more virus particles collected on the cell surface. There was a

general trend more particles on the surface of cells infected with the more severe late domain mutants. However, variation existed among cells transfected with the same mutant, making quantitation of tethered particles useless.

CHAPTER FOUR

REPLICATION OF LATE DOMAIN MUTANTS

Introduction

The subject of viral replication of late domain mutants has been largely neglected. Most studies concerning late domains ignore replication and are limited to the observation and measurement of VLP, but not infectious particle, release. With the exception of a few studies (such as (45, 173)), budding is observed after transient transfection of the Gag protein, without supporting accessory proteins such as Pol (and thus PR), Env, or accessory proteins. In the case of HIV-1, studying infection of late domain mutants is further complicated by the fact that the segment of RNA genome that codes for p6 also codes for Pol in an alternative reading frame, and thus mutations in the late domains could have unintended consequences on Pol function, and thus viral replication. Furthermore, many of the studies characterizing late domains were performed in physiologically-irrelevant cell lines such as 293T, HeLa and COS-1 cells for HIV-1, and 293T and COS-1 cells for RSV because they are easier to transfect.

Following viral spread

In an attempt to determine the effects of late domain mutations on replication, as well as obtain an independent read-out of viral budding, I monitored viral spread through tissue culture. The rate at which a given virus spreads can be useful in comparing late domain defects, as slowed budding should also translate into slower spread through cell culture. RSV infection is non-cytopathic, and since it requires the integration of the provirus into the

host genome, is also permanent. Once an infection begins, it spreads through tissue culture until 100% of the cells are infected. Plotting the percentage of cells infected over time yields a spreading profile for each late domain variant. It is possible for a cell to be infected with more than one virus particle and is termed superinfection. Superinfection is discouraged by the virus and the cell by multiple mechanisms collectively called superinfection resistance (Reviewed in (139)). One such viral strategy to prevent multiple infection events is the Env-mediated down regulation of the cellular receptor for the virus (40).

The spreading assays were performed in a naturally susceptible cell line, DF1 chicken fibroblasts. DF1 cells were transfected with proviral RSV DNA containing either wild-type or mutant late domain motifs and carrying a GFP reporter in the position of the v-src oncogene. One day post-transfection the cells were diluted with a ten-fold excess of non-transfected cells, so that only about 1% of the cell population was expressing GFP (transfected and infected). Cells were split 1:3 daily and sample populations of the cells were taken and fixed for analysis by flow cytometry. The rate of virus spread also depends on cell confluency. Cells plated at a higher density may promote faster spread because cells are closer and thus more likely to be infected from a neighboring cell. However, cells plated at too high of density may also retard virus spread because RSV can only infect dividing cells (the provirus needs access to chromosomes when nuclear envelope dissolves in mitosis). Because of these and other factors, the rate at which a virus spread through tissue culture varied from one experiment to the next. Thus, all of the spreading profiles for a given mutant could not be averaged. However, I found that the mutants consistently fell in the same order, from fastest to

slowest, when tracked in parallel. To report the spreading rates of the late domain mutants, which are only meaningful when compared to each other, I present the spreading profiles in groups that were monitored (split and collected) in parallel.

All mutants were able to spread through DF1 cells. Even a mutant in which both of the late domain consensus sequences were mutated to alanine AAAA-AAASA (Figure 4.1, squares) was able to spread, albeit at a much slower rate than wild-type (Figure 4.1, circles). The spread of the AAAA-AAASA mutant was also confirmed by immunoblot of cell lysates. To address the possibility that infection is occurring through cell-to-cell contact, instead of resulting from released particles, medium was collected from cells infected with the double late domain knockout, filtered to remove cells, and used to reinitiate an infection. The cell-free medium was in fact able to reinitiate infection (data not shown). Although budding of the AAAA-AAASA mutant is inefficient, and cell-to-cell spread cannot be completely ruled out, particle release does occur and results in infectious particles.

Occasionally, the infection of severe late domain mutants, such as AAAA-LYPSL, APPY-AAASA, APPY-LFPIV, and AAAA-AAASA, would not "take hold" and spread. It is not obvious why this happened, but I hypothesize that because the virus spreads so slowly, if not enough cells are initially transfected, it is possible to dilute them too much one day post-transfection, so that the infection never becomes established. This problem was remedied by diluting the cells transfected with the severe late domain mutants less, or not at all, the day after transfection. Alternatively, cells may not be able to tolerate the high expression levels of the slow budding mutants resulting from the transfection, resulting in the killing off of the transfected cells.

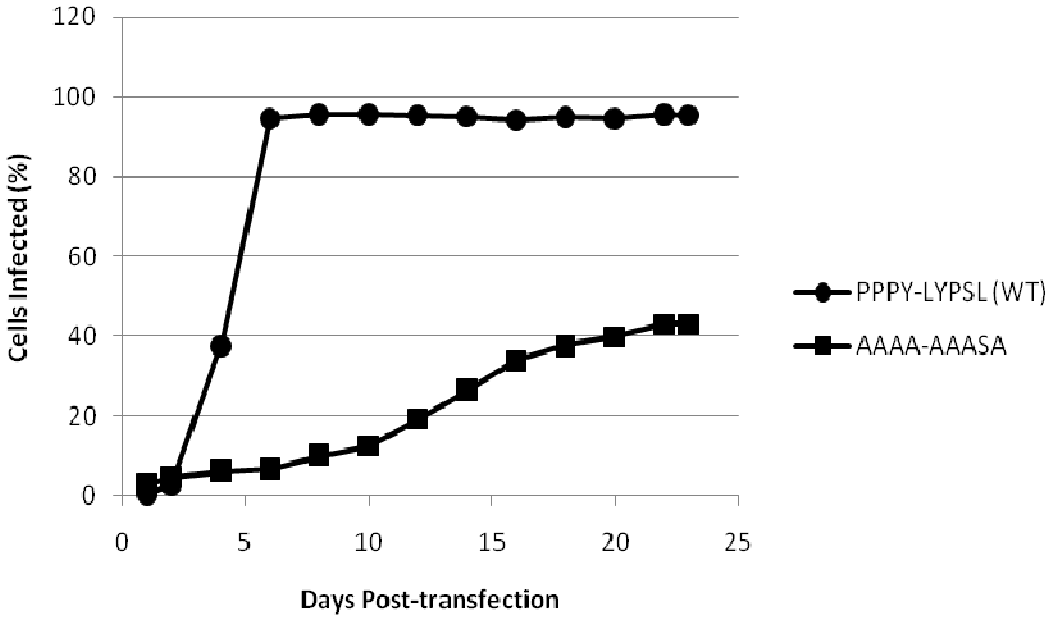

Figure 4.1 Comparison of spreading profiles of wild-type RSV and the AAAA-AAASA mutant in which both late domains are mutated to alanines. DF1 cells were transfected with proviral RSV DNA harboring wild-type late domains or both late domain consensus sequence mutated to alainines. Virus spread was monitored by detection of GFP via flow cytometry.

The LYPSL motif functions in RSV spread

In order examine the effects of mutating the LYPSL motif in RSV replication, I monitored the spread of wild-type or late domain mutants of RSV (PPPY-AAASA, APPY-LYPSL, APPY-AAASA) in parallel, as described above. The spreading profile of the PPPY-AAASA mutant was indistinguishable from that of wild-type (Figure 4.2, compare squares to circles). Thus, the modest reduction in budding rate (Chapter 3, Figure 3.3, bar 2) has no appreciable effect on the rate of virus spread under these conditions. However, the more dramatic budding defect measured for the APPY-LYPSL mutant (Chapter 3, Figure 3.3, bar 3) does translate to slower spread than wild-type (Figure 4.2, compare circles to triangles). Likewise, the APPY-AAASA mutant, which budded too slowly to be reliably measurable with the pulse-chase technique (Chapter 3, Figure 3.3, bar 4) spread more slowly still (Figure 4.2, diamonds). Thus, in the absence of an intact PPPY motif (APPY), the LYPSL then becomes important for virus spread, as APPY-LYPSL spreads more quickly than APPY-AAASA (Figure 4.2, compare squares to diamonds). In summary, these findings illustrate a definite contribution of the LYPSL motif in RSV spreading when the primary PPPY late domain motif is weakened.

Though per particle infectivity of the late domain mutants in principle might be decreased due to incorrect or incomplete Gag processing or RNA splicing (see Discussion), I found that overall the spreading profiles reproducibly correlated with the measured budding rates (Chapter 3). In addition, the spreading assays proved to be more sensitive for comparing the severe late domain mutants since a budding rate below 1/10 of that of wild-type was immeasurable. In contrast, the spreading assay may not be as sensitive for the fast budding mutants, since it could not distinguish between

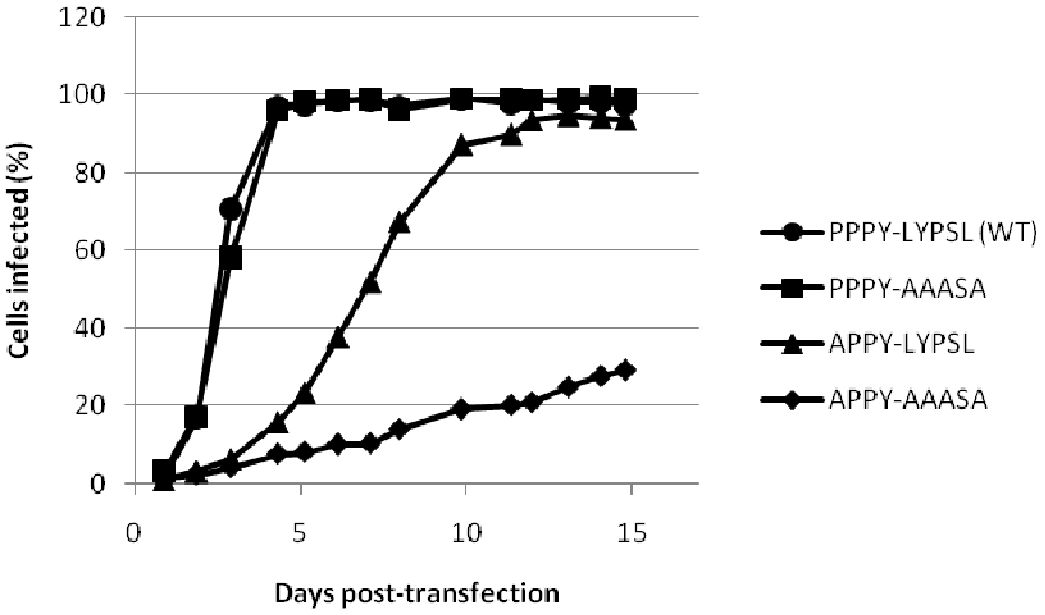

Figure 4.2 Spreading profiles of late domain mutants lacking LYPSL. DF1 cells were transfected with proviral RSV DNA containing the given late domain mutation and then diluted 1:10 with fresh cells the next day. Virus spread was monitored by detection of GFP reporter via flow cytometry. The effect of the absence of the LYPSL motif (AAASA) was examined in the context of an intact and weakened (APPY) PPPY primary late domain.

wild-type and the PPPY-AAASA mutant (Figure 4.2, compare circle and squares).

Heterologous late domains support RSV spreading to varying degrees

Next, I applied the spreading assay to examine the ability of heterologous late domains to functionally replace the LYPSL sequence. First, the EIAV late domain LYPDL was substituted for the LYPSL sequence. To obtain a complete picture of the effects of LYPDL on spreading, it was substituted in three contexts: in the presence of an intact (PPPY), handicapped (APPY), or completely absent (AAAA) PPPY motif. The spread of wild-type, PPPY-LYPDL, APPY-LYPSL, APPY-LYPDL, AAAA-LYPSL, and AAAA-LYPDL mutants was followed in parallel. Consistent with the measured budding rates (Chapter 3, Figure 3.3 bars 1 and 2), wild-type RSV and the PPPY-LYPDL mutant shared similar spreading profiles (Figure 4.3, compare blue diamonds to red squares). Thus, mutating LYPSL to LYPDL, when the primary PPPY motif is present had no effect on the rate of virus spread. However, in the context of a weakened PPPY motif (APPY), LYPDL failed to support a faster spreading rate than the RSV LYPSL sequence (Figure 4.3, compare green triangles to purple crosses). This is in contrast to the budding assay which showed that the APPY-LYPDL mutant buds faster than the APPY-LYPSL mutant (Chapter 3, Figure 3.3, compare bars 3 and 4). The APPY-LYPSL and APPY-LYPDL mutants were compared in four independent spreading experiments. The APPY-LYPSL mutant spread faster than the APPY-LYPDL in three of the four experiments. In the experiment that the APPY-LYPDL mutant spread faster, the transfection of the APPY-LYPSL

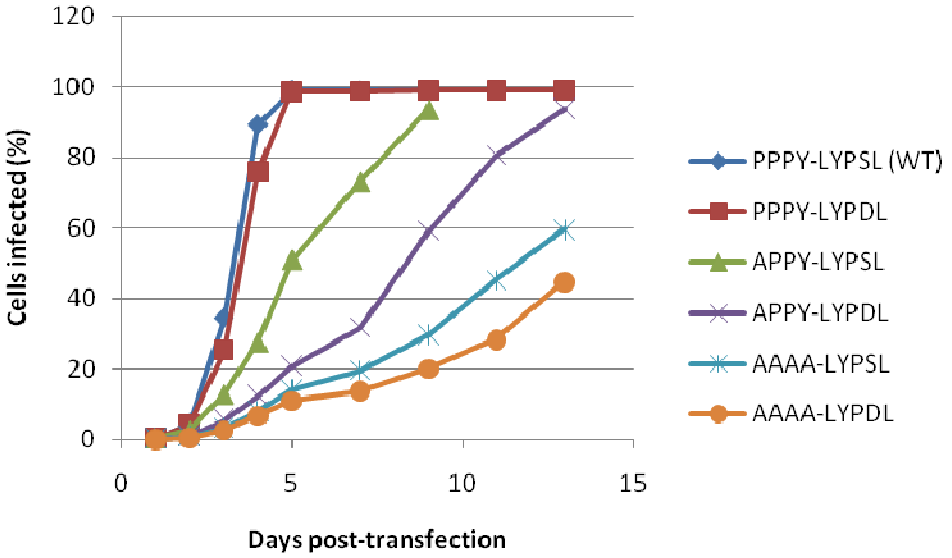

Figure 4.3 Spreading profiles of late domain mutants containing the LYPDL motif from EIAV in place of LYPSL. DF1 cells were transfected with proviral RSV DNA containing the given late domain mutation and then diluted 1:10 with fresh cells the next day. Virus spread was monitored by detection of GFP reporter via flow cytometry.

mutant was insufficient and infection never spread, make a comparison between the two mutants impossible in that case.

To rule out the possibility that APPY-LYPSL spreading faster than APPY-LYPDL was an exception, the LYPDL substitution was also constructed in a more dramatic PPPY mutant background, AAAA. In this context, the LYPSL was still superior over LYPDL for spread (Figure 4.3, compare cyan stars to orange circles). The AAAA-LYPSL and AAAA-LYPDL mutants were not compared in the budding assays because the budding rate of AAAA-LYPSL was below the level of detection (Chapter 3, Figure 3.3, bar 5). I conclude from this set of spreading data that while LYPDL partially rescues the budding rate of APPY and AAPY mutants (Chapter 3, Figure 3.3), it does not rescue the spreading of APPY and AAAA mutants (AAPY was not examined). In conclusion, despite the LYPDL substitution supporting a faster budding rate in RSV, it does not support a faster spreading rate and thus may subject RSV to an unrelated replication disadvantage.

Next I wanted to test whether the paramyxovirus FPIV late domain motif could substitute for the LYPSL motif in the spreading assay. FPIV is a less characterized late domain responsible for the release of the paramyxovirus SV5 (183). The cellular FPIV binding factor remains to be identified. It has been proposed that the FPIV and YPSL motif fit a ΦPXη consensus loosely, where there is a large hydrophobic residue (Φ) followed by a proline (P), any amino acid (X), and then a non-polar residue (η).

The spreading of the PPPY-LFPIV mutant was monitored in parallel with wild-type and the PPPY-AAASA mutant as controls. The PPPY-AAASA spreading profile seemed to lag behind that of wild-type, perhaps because of lower number of cells transfected initially, but their slopes were nearly

indistinguishable, reflecting equal spreading rates (Figure 4.4A, compare blue diamonds to red squares). Wild-type and the PPPY-AAASA mutant consistently showed comparable spreading profiles (Figure 4.2, circles and squares). The PPPY-LFPIV mutant, in contrast, spread more slowly displaying a shallower slope (Figure 4.4A, green triangles). Thus, I conclude that the presence of the FPIV sequence reduces the rate of virus spread compared to wild-type and the PPPY-AAASA mutant, and this difference can be observed even when the primary PPPY motif is intact.

FPIV had a similar effect on spreading when the PPPY motif is weakened. Specifically, the APPY-LFPIV mutant spread more slowly than APPY-LYPSL, and similarly to APPY-AAASA (Figure 4.4B, compare green triangles to red squares and purple crosses). Thus, in the context of a weakened primary PPPY motif, FPIV does not seem to functionally replace LYPSL and rescue spread any better than AAASA.

The spreading profiles displayed for APPY-LFPIV (green triangles) and APPY-AAASA (purple crosses) are examples of severe late domain mutants that failed to spread (or at least spread GFP) through the entire culture (Figure 4.4B). Based on the fact that western blots of cell populations that were positive for Gag expression but were not GFP-positive by flow cytometry analysis, I believe that the virus continued to spread through tissue culture, but that the GFP reporter gene was lost from the provirus (data not shown). GFP is transcribed from a separately spliced mRNA. Loss of GFP, as well as other genes at this site, is well established (80, 161). In my spreading assays that began from transfection, only severe late domain mutants (APPY-AAASA, APPY-LFPIV, AAAA-LYPSL, AAAA-LFPIV, AAAA-AAASA, AAAA-AAASA-GPAV) were observed to lose the GFP marker, observed as the plateauing of

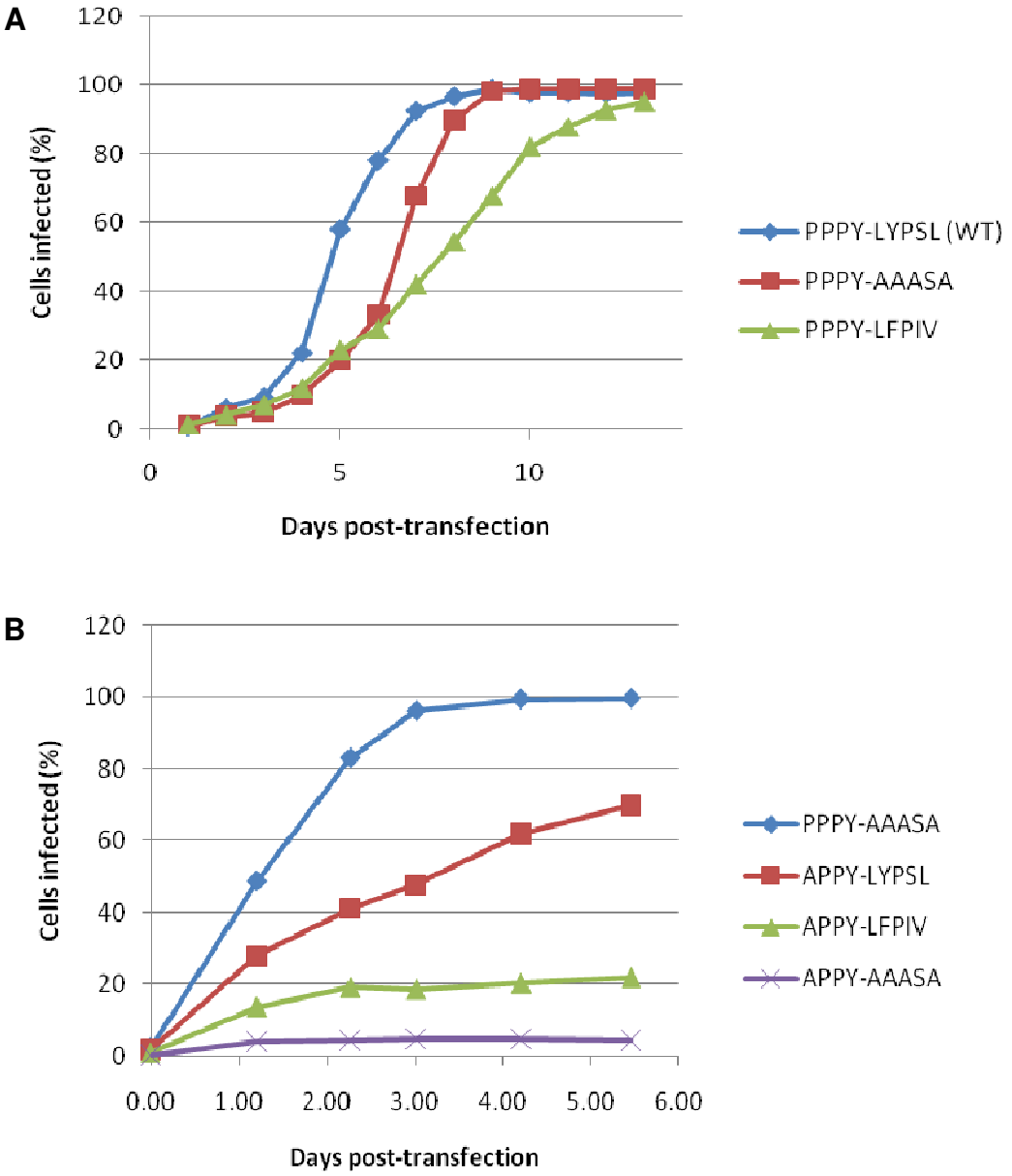

Figure 4.4 The spreading profiles of late domain mutants in which the LYPSL is replaced with the LFPIV motif of parainfluenza 5 (SV5). DF1 cells were transfected with proviral RSV DNA harboring wild-type or mutant late domains. Transfected cells were diluted ~1:10 with fresh cells one day post-transfection and virus spread was monitored by detection of GFP reporter via flow cytometry. The effect of the FPIV sequence in place of the LYPSL motif (AAASA) was examined in the context of an intact and weakened (APPY) PPPY primary late domain.

the spreading curve. However, in preliminary spreading experiments performed by diluting an already fully-infected cell population, loss of GFP occurred even from wild-type RSV. Thus, it appears that over time, and through enough passages, RSV will select against carrying a gene in the GFP position. Loss of the src gene on prolonged passage has been reported previously (100). It seems to take longer for wild-type and mild late domain mutants to lose the GFP and therefore is not observed during the length of a spreading experiment (if started at transfection). However, if cells infected with wild-type and mild mutants are kept long enough and used to initiate new infection the GFP loss is observable.

Both APPY-LFPIV and APPY-AAASA mutants discard the GFP reporter early in the spread started from a transfection, making it difficult to rank them against each other (Figure 4.4B). It is clear, however, that LFPIV does not functionally replace LYPSL since APPY-LFPIV does not significantly increase spreading rate compared to APPY-AAASA. Furthermore, the loss of GFP early after transfection suggests that APPY-LFPIV should be categorized as a severe late domain mutant and FPIV was not functioning as a late domain at this position. This conclusion is in contrast to the budding data which showed that the APPY-LFPIV mutant budded at a faster rate than APPY-AAASA, implying FPIV acted as a late domain in the position. However, the spreading profile of APPY-LFPIV often displayed a switch in spreading rate after extended passaging (Figure 4.5). I attribute this change in spreading rate and the discrepancy of budding and spreading data to the reversion of the APPY-LFPIV mutant to PPPY-LFPIV, since only a single amino acid would need to be changed to restore the wild-type PPPY sequence. I did not verify this hypothesis by reverse transcription of the viral RNA and DNA sequencing.

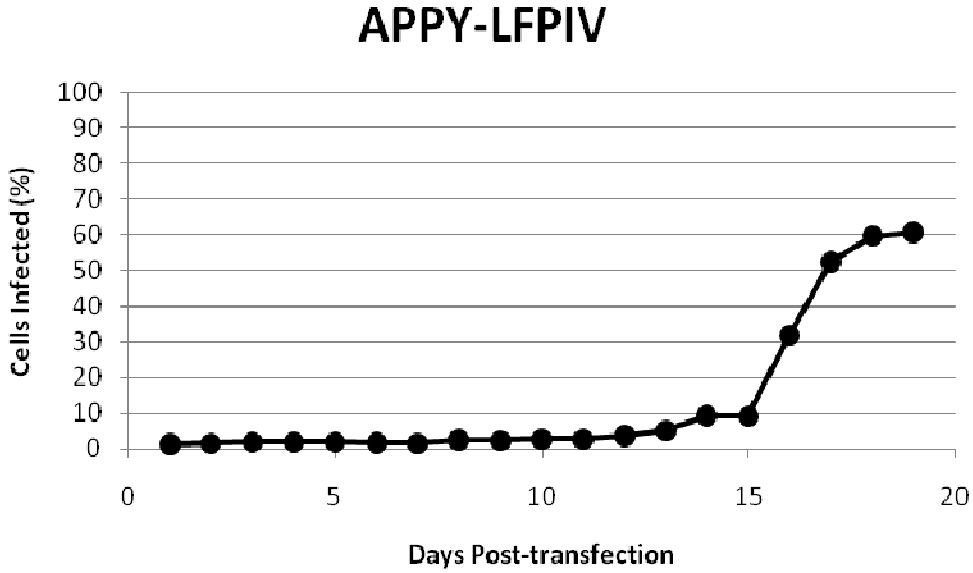

Figure 4.5 Representative spreading profile of the APPY-LFPIV mutant. DF1 cells were transfected with proviral RSV DNA containing the APPY-LFPIV late domain mutation and then diluted 1:10 with fresh cells the next day. Virus spread was monitored by detection of GFP reporter via flow cytometry. The change in spreading slope most likely represents a reversion to PPPY-LFPIV, and was observed multiple times with this mutant.

It is mostly likely that the cells subjected to pulse-chase (Chapter 3, Figure 3.4, bar 8) were actually two populations of cells, those infected with the APPY-LFPIV mutant and those infected with the PPPY-LFPIV revertant, causing the measured budding rate to increase. The fact that the percentage of GFP-positive cells levels off at around 60% implies that the other 40% are infected with virus that has lost the GFP gene (Figure 4.5). Otherwise one would expect the replication rate to continue at that slope until 100% of the cells are infected. Whether the remaining 40% GFP-negative cells are infected with the APPY-LFPIV mutant or a revertant, most likely PPPY-LFPIV, is unknown.

As noted in Chapter 3, RSV harbors its own FPXV motif in PR. Budding experiments showed that mutating FPAV to GPAV caused a two-fold reduction in budding rate (Figure 3.6). The spread of this mutant was monitored in parallel with wild-type and a moderate late domain mutant (PPPY-AAASA). Unfortunately this experiment was initiated by diluting infected cells, not with a fresh transfection, causing wild-type and PPPY-AAASA to lose the GFP reporter gene. Though it looks like the GPAV mutant (squares) spreads similarly to or better than FPAV (wild-type) (circles), while wild-type plateaus because of GFP loss and thus the rate of spread is unknown (Figure 4.6). In conclusion, the GPAV mutant did not exhibit an obvious spreading defect, but the GFP loss of wild-type and PPPY-AAASA, makes it difficult to know for sure.

To further define the late domain requirements of RSV, the spreading assay was employed to test the ability of heterologous late domains to support budding in the place of the primary PPPY late domain. To this end, the spread of the PTAP-LYPSL, FPIV-LYPSL, and AAAA-LYPSL mutants was monitored in parallel. Both the PTAP-LYPSL and the FPIV-LYPSL mutant were

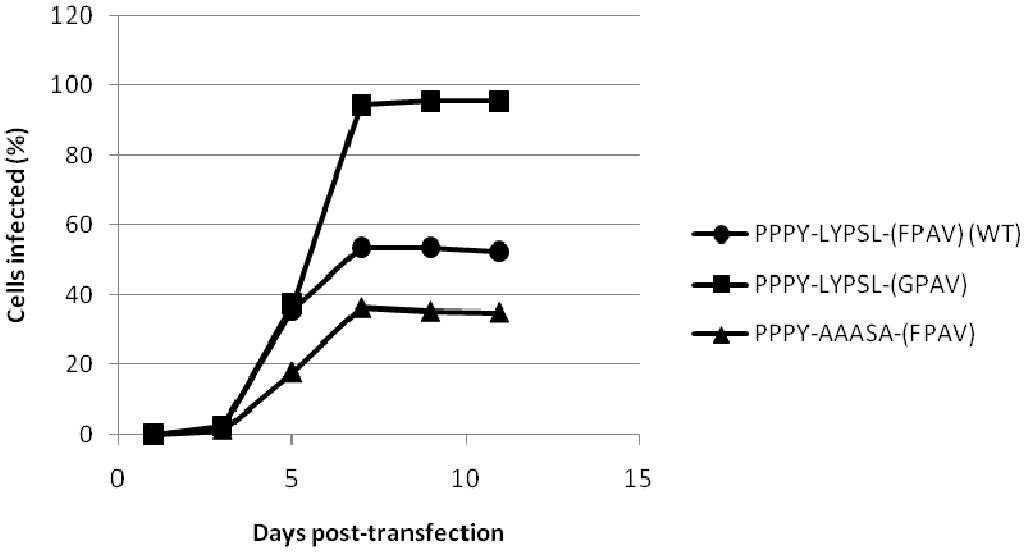

Figure 4.6 Comparison of spreading profiles of wild-type, the modest budding mutant PPPY-AAASA, and mutant of the FPAV (GPAV) sequence in PR.

infectious and able to spread through DF1 cell culture at a rate that was indistinguishable from that of the AAAA-LYPSL mutant (Figure 4.7, blue triangles, blue circles, and blue squares). I therefore conclude that neither the PTAP motif nor the FPIV motif can substitute for the primary late domain of RSV. These data suggest that in the context of RSV p2b, the minimal four-residue PTAP and FPIV late domain motifs do not engage the ESCRT machinery in a way that promotes RSV budding.

Over-expression of Alix rescues spreading of PPPY mutants

The partial but significant rescue of PPPY mutant budding rates upon over-expression of Alix suggests a role for Alix in RSV budding. As an alternative method to measure this rescue, I examined the effects of Alix over-expression on the spread of PPPY mutants.

As a professional adaptor protein, Alix functions in multiple cellular processes including cytokinesis (25, 127, 211) and it has been reported that Alix over-expression slows cell proliferation (227). Since RSV can only infect dividing cells, it is conceivable that a change in cell division frequency could result in a change in the rate of viral spread. To rule out the possibility that the rate of cell division of hAlixDF1 cells differed from that of the control PuroDF1 cells which might affect the rate at which cells are infected in culture, I monitored cell number over time. Regular DF1 cells, DF1 cells transduced with dsRed (dsredDF1) (established by Danso Ako-Adjei), DF1 cells transduced with the puromycin resistance gene (puroDF1), and cells over-expressing hAlix (hAlixDF1) were counted and plated. Each cell type had 4 wells of equal number of cells and the number of cells in a well of each cell type was counted each day. Figure 4.8A shows the number of cells over time

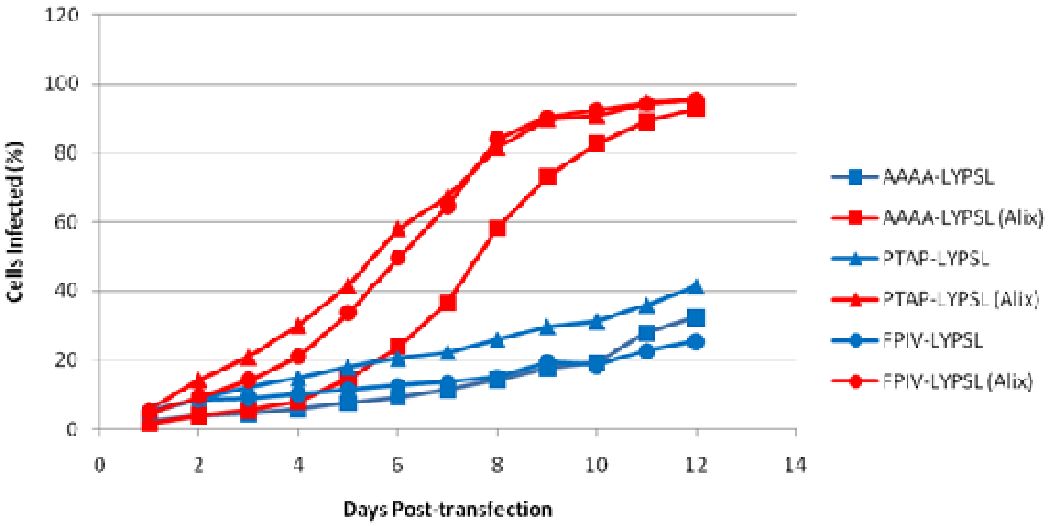

Figure 4.7 Spreading profiles of PPPY late domain mutants in the presence of endogenous levels (blue) or over-expressed (red) levels of Alix. The PPPY late domain is replaced with AAAA (squares), PTAP (triangles), or FPIV (circles). Control puroDF1 (blue) or hAlixDF1(red) cells were transfected with proviral RSV DNA containing the given late domain mutation and then diluted 1:10 with fresh cells the next day. Virus spread was monitored by detection of GFP reporter via flow cytometry.

A

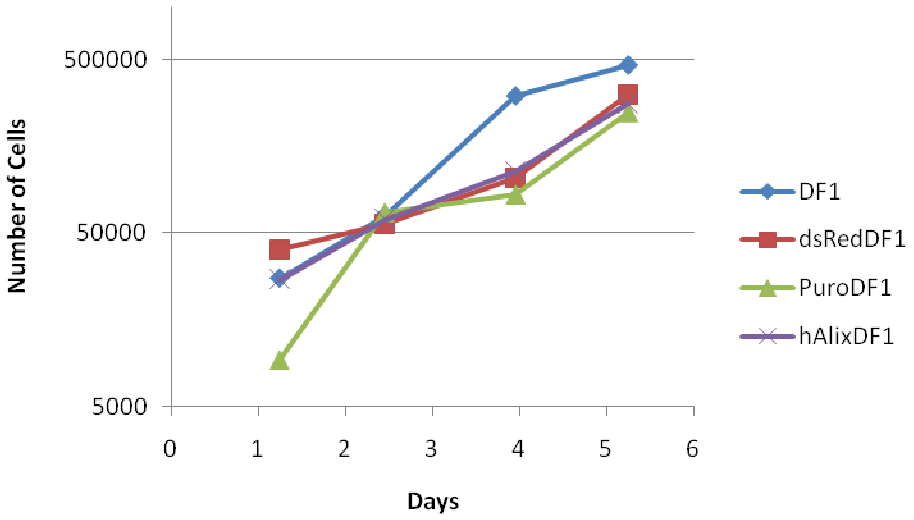

B

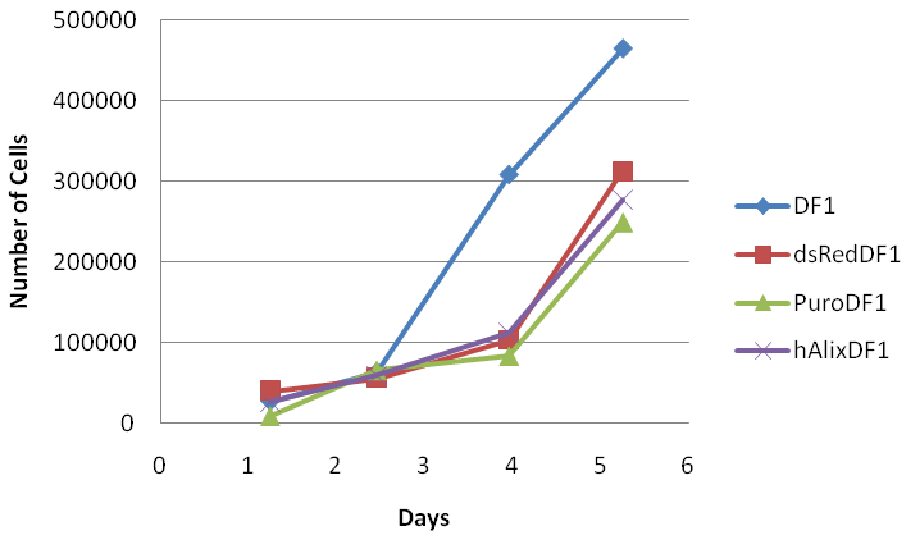

Figure 4.8 Growth curves of DF1 cells, dsRed DF1 cells, PuroDF1 cells, and hAlixDF1 cells. Number of cells over time displayed on a (A) log scale or (B) linear scale.

on a log scale and Figure 4.8B shows the same data on a linear scale. The cells transduced and selected with puromycin, (dsRedDF1, PuroDF1, and hAlix DF1 cells) all proliferated at a similar rate (Figure 4.8A and B). Wild-type DF1 cells also proliferated at a comparable rate to the selected cells, though they did not exhibit the same growth delay seen with the transduced cells when first plated (Figure 4.8B, days 1-4). Perhaps wild-type DF1s require less cell to cell contact for maximal growth rate. Similar growth curves of control PuroDF1 and hAlixFD1 cells allowed us to rule out differences in proliferation as a factor for differences in rate of virus spread.

After establishing that hAlixDF1 cells and control puroDF1 cells divided approximately at equal rates, DF1 cells were transfected with wild-type or late domain mutants. One day post-transfection the cells were split into two groups, one which was diluted approximately 10:1 with hAlixDF1 cells, and the other group of which was diluted 10:1 with control puroDF1 cells. Spread of GFP-positive cells was monitored over time by flow cytometry as described above. The spread of wild-type RSV seemed to be unaffected by the over-expression of hAlix (Figure 4.9A). Similarly, the PPPY-AAASA mutant spread at a similar rate in control puroDF1 cells as it did in hAlixDF1 cells (Figure 4.9B). Both of the PPPY mutants APPY-LYPSL and AAAA-LYPSL, which retained the presumed Alix-binding LYPSL motif showed a faster rate of spread in cells over-expressing hAlix than in the control DF1 cells (Figure 4.9C and D). The viral RNA from the APPY-LYPSL and AAAA-LYPSL mutants from the hAlixDF1 cells was reverse transcribed and sequenced to confirm no reversions had restored the wild-type late domains. Both mutants remained intact. The spreading of the APPY-LYPDL mutant responded to Alix over-expression similarly to, but no better than, the APPY-LYPSL mutant (data not

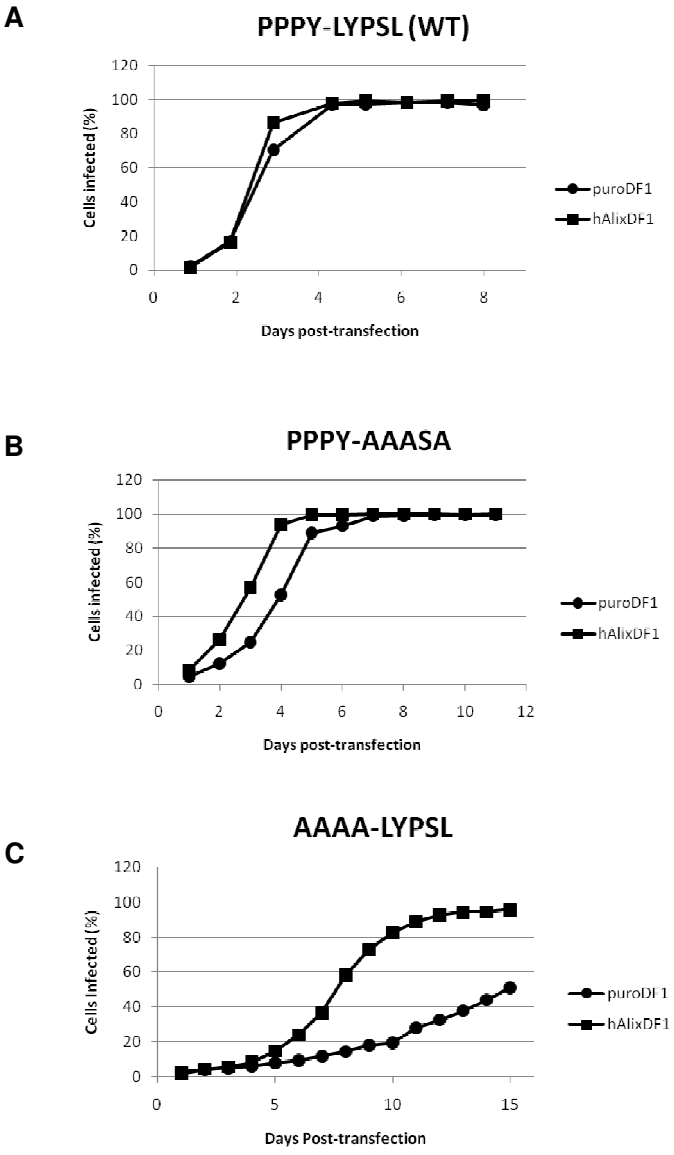

Figure 4.9 Alix over-expression rescues PPPY late domain mutants in the presence of the LYPSL motif. Control puroDF1 (circles) or hAlixDF1 (squares) cells were transfected with proviral RSV DNA containing wild-type late domains or the given late domain mutation and then diluted 1:10 with fresh cells the next day. Virus spread was monitored by detection of GFP via flow cytometry

Figure 4.9 (Continued)

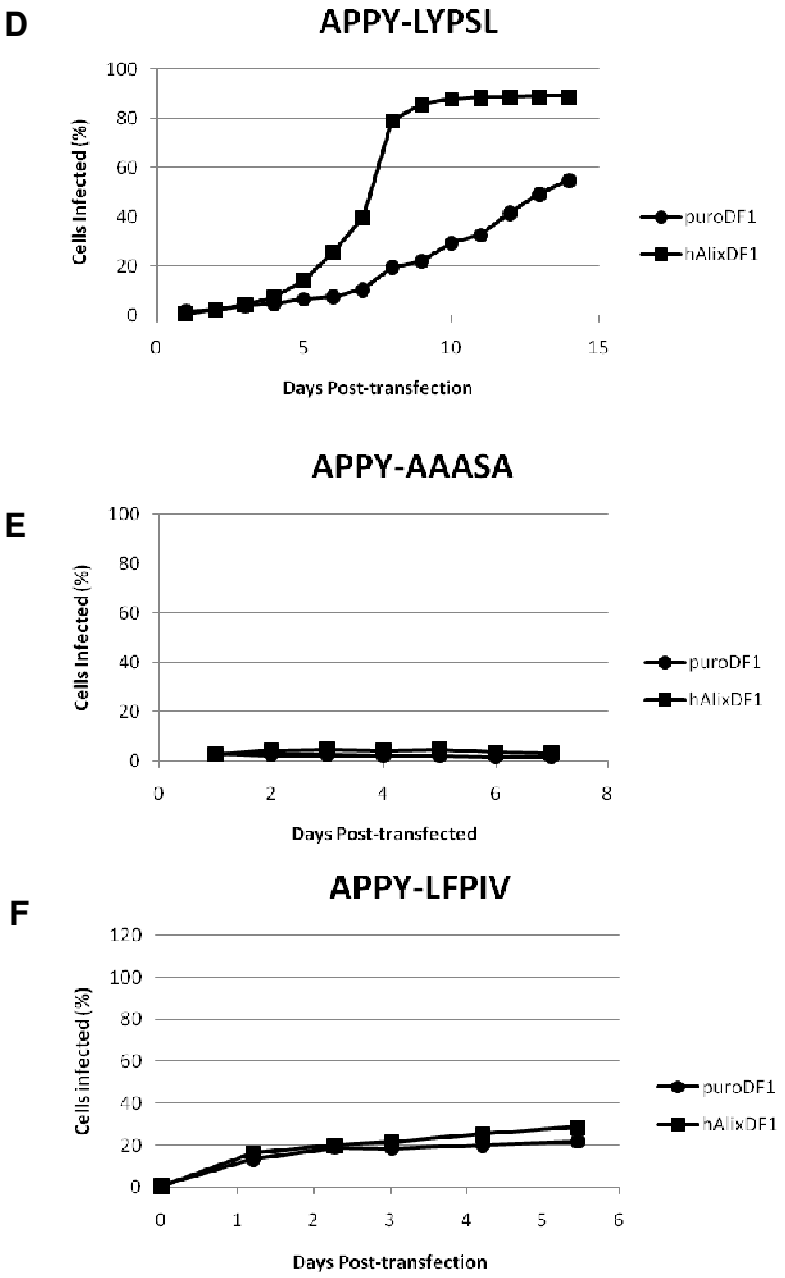

shown). Over-expression of hAlix failed to rescue the spreading rate of the PPPY mutants APPY-AAASA and APPY-LFPIV which lack the Alix binding site (Figure 4.9E and F). These mutants spread equally slowly in control cells and those with an excess of hAlix. Taken together, these data show that over-expression of Alix leads to a LYPSL-dependent rescue of budding and spreading of PPPY mutants.

Furthermore, the rate of spread of the PTAP-LYPSL and FPIV-LYPSL mutants was faster in cells over-expressing hAlix than in control DF1 cells (Figure 4.7, red triangles, and red circles). The rescue observed was comparable to that observed with the AAAA-LYPSL mutant in hAlix over-expressing cells (Figure 4.7, red squares). Thus, the AAAA-LYPSL, PTAP-LYPSL, and FPIV-LYPSL mutants, which all retain the Alix-binding motif, are rescued equally well by hAlix over-expression and thus can be considered equivalent mutants. In other words, PTAP-LYPSL and FPIV-LYPSL spread as if they are completely missing the primary late domain (AAAA-LYPSL). Therefore I conclude that PTAP and FPIV show no evidence of late domain function in the PPPY position.

Low GFP expression is selected for in cells infected with severe late domain mutants

The loss of GFP expression in cells infected with severe late domain mutants led me to examine the absolute intensity of the GFP signal. The data collected from the flow cytometry analysis included a calculated mean GFP intensity of the GFP-positive cells. The average intensity of GFP-positive cells (disregarding cells not expressing GFP at all) was plotted over time as the virus spread through culture (Figure 4.10). The average intensity of GFP-

positive cells varied depending on the severity of the late domain mutation. Viruses fell into one of two categories based on mean GFP intensity of the cells they infected, high intensity (~400) or low intensity (~100), with no infections resulting in cells that had intermediate GFP intensity. Directly after transfection the GFP-intensities of all cells were similar and as the virus spread the average intensity adjusted to either high or to low intensity. Specifically, one day after transfection of all mutants, GFP intensity was relatively high, presumably due to the transfection of multiple DNA molecules into a single cell (Figure 4.10, day 1). Next, the GFP intensity of GFP-positive cells infected with all mutants then dropped, presumably reflecting the dilution of the transfected DNA by cell division (Figure 4.10, days 2-4). After this initial drop, the intensity gradually increased over the next few days in cells infected with wild-type virus or with mutants that have minimal effects on budding rate such as PPPY-AAASA and PPPY-LYPDL (Figure 4.10, blue diamonds, red squares and cyan crosses, days 4-7). The increase in GFP intensity leveled off on about day 7, about 2 days after 100% of the cells were infected, possibly representing superinfection of the cells.

In contrast, the average GFP intensity of cells infected with mutants that exhibit significant reduction in budding rate, such as APPY-LYPSL, APPY-LYPDL, APPY-AAASA , AAAA-LYPSL, and AAAA-AAASA remained low even as the infection spread through the tissue culture (Figure 4.10, green triangles, purple crosses, orange circles, blue lines, and pink lines, days 4-9). Based on the apparent selection of low GFP expression in cells infected with severe late domain mutants, I believe that severe late domain mutants are cytotoxic and cells infected with severe late domain mutant virus express lower levels of GFP, and presumably also lower levels of viral proteins.

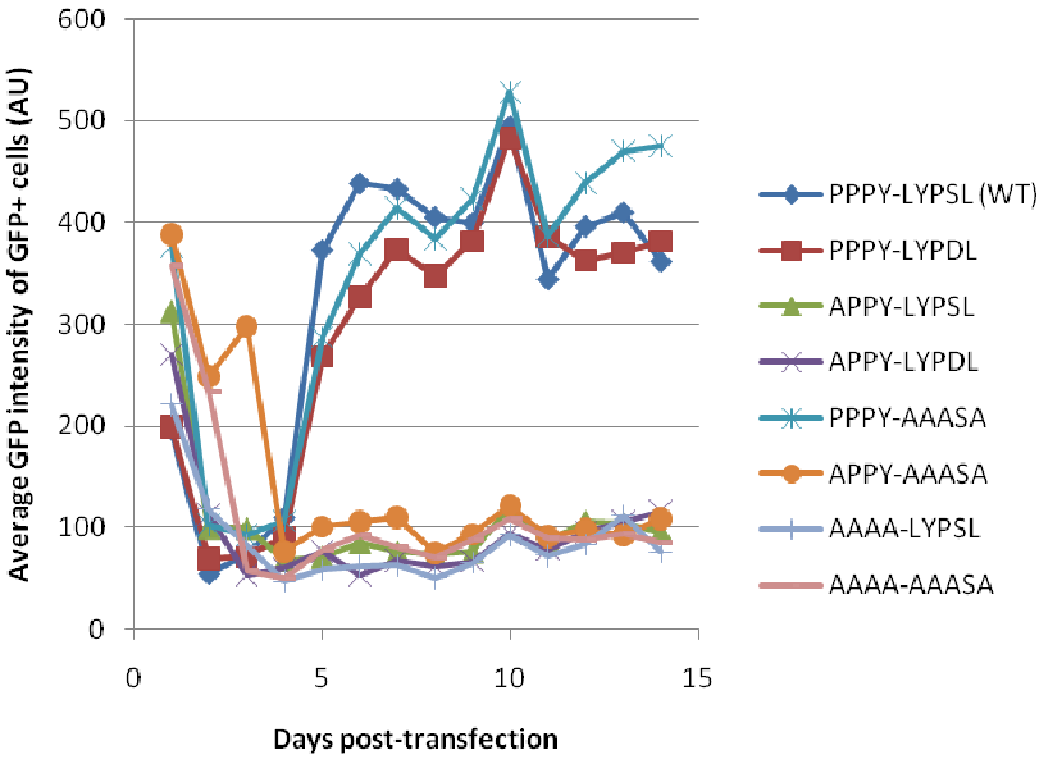

Figure 4.10 Average GFP intensity of GFP-positive cells plotted over time as virus infection spreads through DF1 cells. Data collected from spreading assays shown in Figures 4.1-4.3.

Not only was there a correlation between GFP intensity and the severity of a given late domain mutant, but the GFP intensity of cells infected with a given late domain mutant could be increased by increasing the spreading rate by Alix over-expression. The GFP intensities of the AAAA-LYPSL, PTAP-LYPSL, and FPIV-LYPSL mutants shown in Figure 4.7 were plotted as the infections spread (Figure 4.11). The Alix-mediated rescue of GFP intensity (Figure 4.11) mirrored the rescue of spreading (Figure 4.7). Thus GFP intensity could be considered as another way to evaluate the degree of budding deficiency.

Using GFP intensity as another way of ranking late domain mutants I examined the effects of Alix over-expression on two mutants that lack the LYPSL motif, PPPY-AAASA and APPY-AAASA. Budding and spreading assays showed Alix over-expression had no effect on these two mutants (Figure 3.9 and Figure 4.9). However, cells infected with the PPPY-AAASA mutant had a higher average GFP intensity in cells over-expressing Alix, suggesting that Alix is able to help budding despite a lack of a $LYPX_nL$ motif (Figure 4.12, compare red squares to blue diamonds). Alix over-expression barely had an effect on GFP intensity of cells infected with the APPY-AAASA mutant, although the cells over-expressing Alix did have a slightly higher average intensity (Figure 4.12, compare purple crosses and green triangles). Next the late domain mutants were ranked according to the numerical average GFP intensity at 10 days post-transfection (Table 4.1). All mutants are not included because only mutants followed in parallel can be compared to each other. In general, the GFP intensities decreased as the budding defect increased. The rankings matched the spreading rankings slightly better than the budding rankings. The APPY-LYPSL mutant had higher GFP intensity

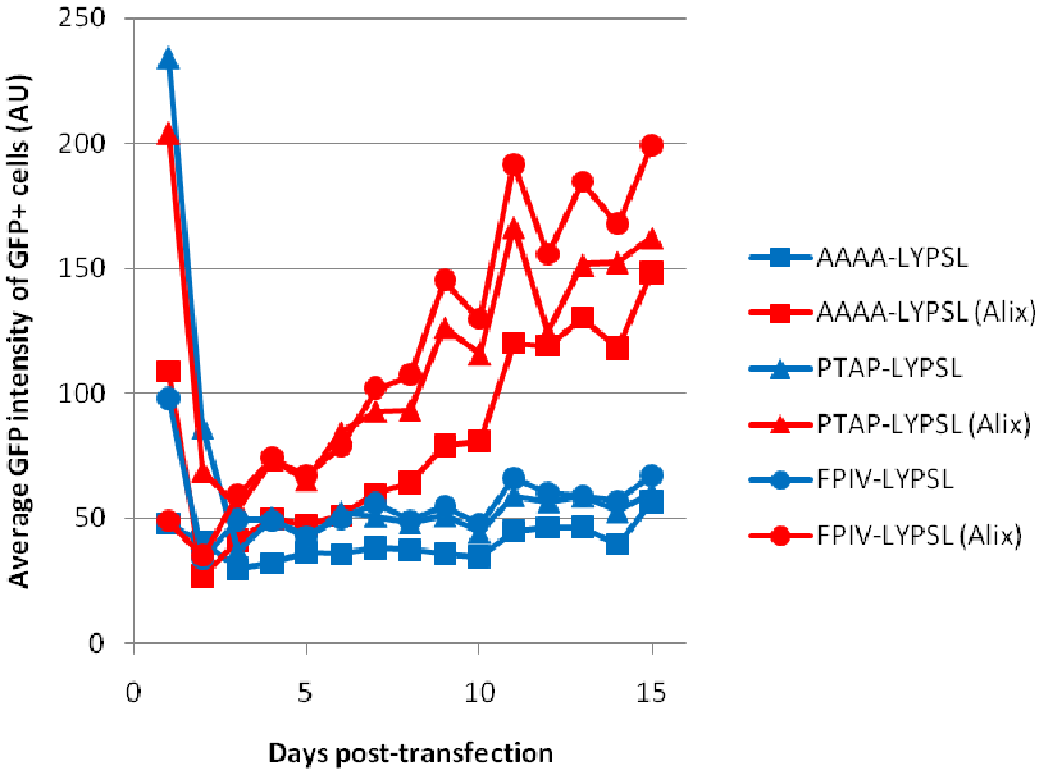

Figure 4.11 Average GFP intensity of GFP-positive cells plotted over time as virus infection spreads through control puroDF1 or hAlixDF1 cells. Data collected from spreading assays shown in Figure 4.6.

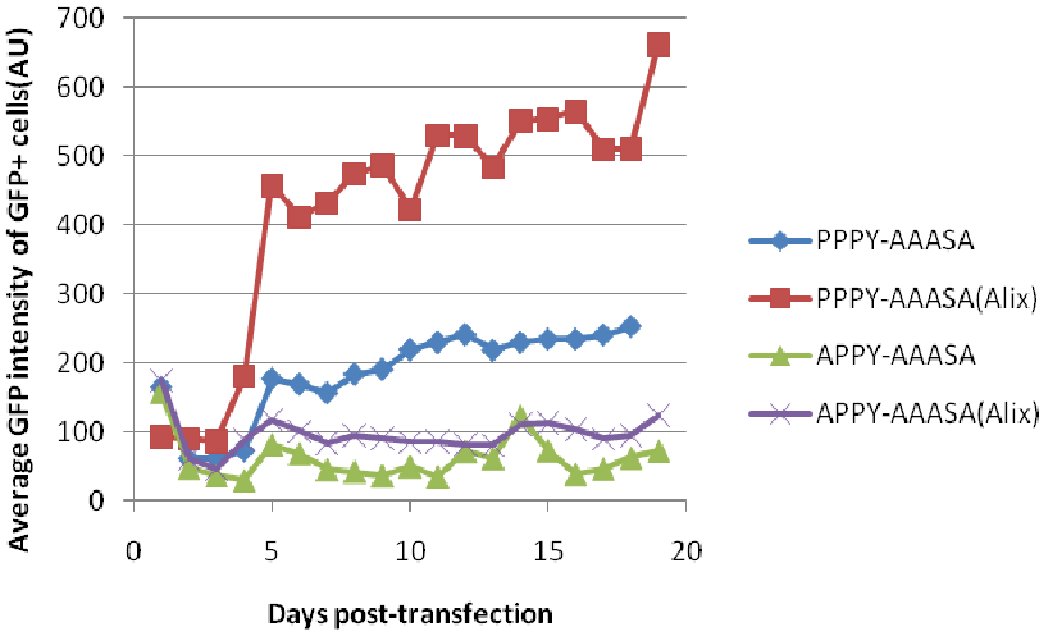

Figure 4.12 Average GFP intensity of GFP-positive cells plotted over time as virus infection spreads through control puroDF1 or hAlixDF1 cells. Data collected from spreading assays shown in Figure 4.8.

than the APPY-LYPDL mutant. One striking outcome was that every mutant had a higher GFP intensity in cells that over-express Alix. This implies that Alix gives budding/replication advantage even in the absence of a $LYPX_nL$ motif, perhaps by binding RSV NC as it binds HIV-1 NC (160).

Many factors can affect the expression of viral genes. Among these 1) splicing, 2) loss of genes from the provirus and 3) the provirus integration site selection can all lead to variable virus gene expression. A combination of these effects could influence the loss and reduction of the GFP expression

The translation of RSV Gag and Gag-Pol occur from the same unspliced RNA transcript. However, the translation of Env and GFP require splicing of that same transcript. The balance of unspliced to spliced RNA does affect the ratio of the viral proteins (Gag, Gag-Pol, Env, GFP) and thus, the fitness of the resulting virus. The importance of maintaining the optimal splicing levels is reflected in the tight regulation of RSV RNA processing and in the frequent loss of the src (or GFP) genes in continued replication of the virus. RSV employs suboptimal env and src (GFP in the constructs used inthis work) splice signals and an element called the negative regulator of slicing (NRS) to maintain levels of unspliced RNA for Gag and Gag-Pol translation. The NRS is a 230 nt element in the *gag* gene (nts 700-930) that seems to prevent over-splicing of the RSV transcript by subverting the splicing machinery to this site (66, 122, 143, 144). Over-splicing, which leads to more Env and Src (GFP), and less Gag and Gag-Pol, places RSV under a replication disadvantage (161). The growth of RSV often selects for viruses lacking the src (or GFP) gene because this additional splice product causes a reduction in replication rate (80, 161). I hypothesize that some of the late

Table 4.1 Ranking of mutants from highest to lowest average GFP intensity of GFP-positive cells

1	PPPY-LYPSL(WT)+**ALIX**
2	PPPY-LYPDL+**ALIX**
3	PPPY-AAASA+**ALIX**
4	PPPY-AAASA
5	PPPY-LYPSL(WT)
6	PPPY-LYPDL
7	APPY-LYPSL+**ALIX**
8	AAAA-LYPSL+**ALIX**
9	APPY+LYPDL+**ALIX**
10	APPY+AAASA+**ALIX**
11	APPY+AAASA
12	APPY-LYPSL
13	AAAA+AAASA+**ALIX**
14	AAAA+AAASA
15	APPY-LYPDL
16	AAAA-LYPSL

domain mutants lost the GFP reporter because of this selection (Figure 4.6 and Figure Figure 4.9, E and F).

The negative regulator of splicing (NRS) does lie in a RNA region that overlaps with the late domain coding sequence. It is possible that mutations in the late domain disrupts the NRS, causes over splicing of RSV RNA and thus puts virus containing other splice products, such as GFP, at more of a disadvantage resulting in the loss of the GFP. However, mutations in the LYPSL alone, which do not have a significant effect on spreading rate, but do overlap the NRS, do not cause a loss of or reduction in GFP. Thus the loss of GFP seems to be directly related to the severity of the late domain defect, not in the disruption of the RNA sequence.

In summary, since GFP loss and intensity reduction mirrored the severity of budding and spreading defects (Figure 4.10, 4.11, and 4.12), and intensity can be represented as a distinct number, it became another way of evaluating and ranking the late domain mutants (Table 4.1).

All viral proteins, Gag, Gag-Pol, Env and the GFP reporter (in place of src), are under the control of the same promoter (in the LTR). RSV integration site selection is fairly random with only a slight preference for transcription units (124, 137). In a given population of infected cells, a distribution of integration sites and thus a distribution of transcription activity from those sites exists. I hypothesize that if a late domain mutant is cytotoxic at high levels, high expressing cells, such as those whose integration site was transcriptionally very active, would die. This killing of cells with high expression of viral proteins would result in a selection of cells with low levels of viral protein expression. This is possibly one reason for the difference in GFP expression between fast budding/spreading and slow budding/spreading

mutants. GPF is a proxy for all viral genes, since they are under control of the same promoter. Lower GFP intensity observed by flow cytometry analysis is reflective of lower expression of all viral proteins. Consistent with this expectation, these mutants also expressed reduced levels of Gag as observed by immunoblot (data not shown).

Cells infected with severe late domain mutants often displayed a “sick” phenotype, often being vacuolated, and they detached from the plate easily. This cytotoxic effect could be the result of the accumulation of massive numbers of unbudded particles (Figure 3.11, E-L). Superinfection and viral DNA accumulation have also been associated with cytotoxicity (167, 217). The ultimate result would be a selection against the cells expressing high levels of the severe late domain mutant viral proteins.

In conclusion, although the mechanism is unclear, I observed both the loss of the GFP expression and a reduction in GFP intensity in cells infected with severe late domain mutants. GFP loss, but not a reduction in GFP intensity, was also observed in cells infected with wild-type RSV and less severe mutants, but only over a long period of time and only if the virus was used to re-initiate infection. GFP could be lost through recombination during reverse transcription followed by selection because of a replication advantage. Low GFP intensity could result from the selection against high expressing cells, because of deleterious effects of late domain defect, whether through integration site selection or through another regulatory mechanism.

Late domain mutants have cleavage defects

RSV particle maturation occurs when the viral protease (PR) dimerizes and liberates itself from the Gag polyprotein and cleaves Gag into its individual

domains, causing a gross morphological change inside the particle. Viral maturation occurs during or shortly after budding from the cell membrane and is required for formation of an infectious particle. Defects in proper Gag cleavage result in reduced infectivity. The mechanism of retroviral protease activation is unknown. It is possible that protease is activated by reaching a threshold concentration in the particle or by the process of budding itself.

TEM images have revealed that late domain mutant particles attached to the surface of the plasma membrane are immature. This is presumably because they have not budded and thus protease has not been activated. However, even late domain mutant particles collected from the medium (and therefore "budded") often show incomplete and incorrect Gag cleavage. HIV-1 late domain mutants are reported to have Gag proteolytic cleavage abnormalities (62, 67, 79, 118).

In RSV, the PPPY and LYPSL motifs both are two amino acids away from a cleavage site that lies between them (Figure 3.1). To address if the observed spreading profiles may reflect cleavage deficiencies, which would affect absolute infectivity in addition to slowed budding, I examined the cleavage profiles of the late domain mutants produced in either control puroDF1 cells (denoted -) or hAlixDF1 cells (denoted +). Filtered medium was collected from cells infected with wild-type or the indicated mutant and the virus was collected by centrifugation. The virus pellets were resolved on SDS-PAGE and subjected to immunoblotting with anti-CANC (Figure 4.13) antiserum.

I found that the more severe the budding defect the less complete proteolysis of Gag. Wild-type virions contain Gag that is fully processed into CA and NC (Figure 4.13, lane 1). Virus produced in cells that over-express

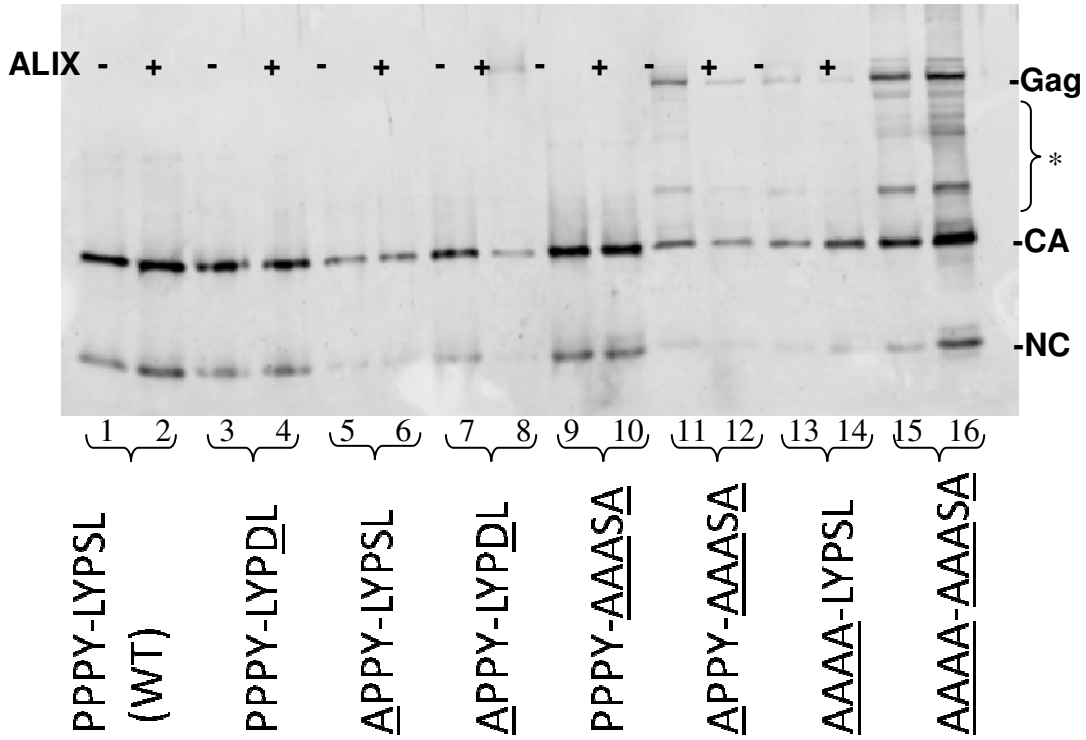

Figure 4.13 Wild-type and late domain mutant Gag in virions from puroDF1 or hAlixDF1 cells. Cell type is denoted by (-) for puroDF1 or (+) for hAlixDF1 cells at the top of the immunoblot. Virions were collected from medium of puroDF1 or hAlixDF1 infected with wild-type of the given late domain mutant. Viral proteins were resolved on SDS-PAGE and immunoblotted with anti-RSV CANC antibody. Partially cleaved products are denoted by *.

hAlix had no effect on wild-type Gag processing (Figure 4.12, lane 2). The processing profiles of Gag from the PPPY-LYPDL and PPPY-AAASA virions, whether produced in control or hAlixDF1 cells, were indistinguishable from that of wild type (Figure 4.13, lanes 3,4,9, and 10). The viral cleavage profiles of the severe late domain mutants APPY-AAASA, AAAA-LYPSL and AAAA-AAASA contained some fully processed CA and NC, but also contained unprocessed Gag and intermediate cleavage products (Figure 4.13, lanes 11-16).

Since the budding of PPPY mutants is more rapid in hAlixDF1 cells, I wanted to investigate if virus produced from hAlixDF1 cells would result in more complete Gag cleavage. I found that hAlixDF1 cells had no significant effect on Gag processing for wild-type, PPPY-LYPDL, APPY-LYPSL, and PPPY-AAASA mutant virions. However, in the mutant whose budding rate and spreading rate was most dramatically rescued by hAlixDF1 cells, AAAA-LYPSL, the ratio of CA:Gag in virions seemed higher than in the virions produced in control DF1 cells (Figure 4.13, lanes 13 and 14). More complete cleavage of Gag in AAAA-LYPSL thus mirrors the budding and spreading rescue.

Detecting Alix incorporation into virions

The initial discovery linking Alix with retroviral budding was the observation that a ~97 kDa protein (Alix) was incorporated into wild-type SIV particles but not into p6 mutant particles (195). Later studies found that the NC domain of HIV-1 also binds Alix, in addition to the $LYPX_nL$ motif in p6 (160). To investigate the effects of various late domain mutations and Alix

over-expression on Alix incorporation into RSV particles, I carried out immunoblots against Alix were performed on wild-type and mutant virus particles from infected hAlixDF1, puroDF1, or DF1 cells. Alix levels were quantified by ImagQuant and normalized to CA levels from same virus samples in parallel CA immunoblots (data not shown). However, measurement of Alix incorporation into particles proved to be complicated by three factors.

First, normalizing the amount of virus loaded by a CA immunoblot was not possible because each late domain mutant had variable levels of Gag processing. Severe late domain mutants exhibited more severe cleavage defects and thus would yield less fully processed CA product per virion (Figure 4.13).

Second, wild-type and late domain mutant particles may not have the same number of Gag molecules. Electron cryotomography has shown that the Gag shell under the membrane of immature HIV-1 particles is discontinuous (58, 222, 225). Recent tomographic analysis of budding sites has revealed that the Gag shell is more complete at budding sites of late domain mutants, presumably because the delay in budding allows more time for a more complete Gag shell to polymerize (23). If late domain mutant particles do in fact contain more Gag molecules than wild-type particles, immunoblots against CA could not be used to normalize for equal number of particles.

Third, the pelleting procedure performed to collect virus yielded Alix even when the medium was collected from uninfected cells (Figure 4.14, lanes 1 and 2). Both uninfected control puroDF1 cells (lane1) and uninfected hAlixDF1 cells (lane2) released Alix into the medium (lane 3). Immunoblots

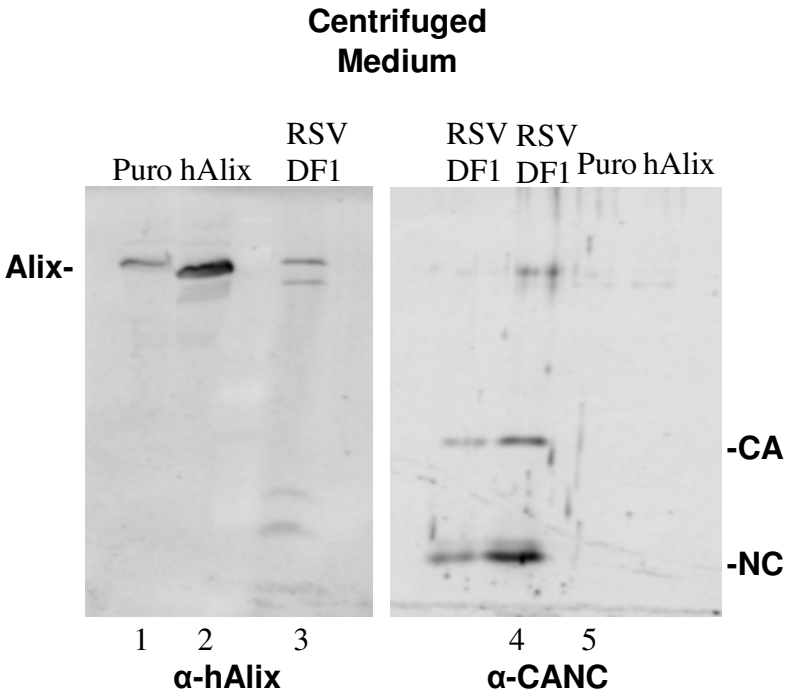

Figure 4.14 Secretion of Alix from uninfected PuroDF1 cells (Puro), uninfected hAlix DF1 cells (hAlix), and infected DF1 cells (RSV DF1). Approximately equal volumes of medium from each cell type was filtered through 0.45 um filter and centrifuged at 70 K rpm for 20 minutes. Proteins in the resulting pellet were resolved by SDS-PAGE. (Puro) uninfected puromycin-resistant DF1 cells; (hAlix) uninfected DF1 cells over-expressing hAlix; (RSV DF1) DF1 cells infected with wild-type RSV were immunoblotted with α-hAlix (left) or α-CANC (right) antibodies. Lanes 1, 2 and 3 all contain 9/10th of the pellets from uninfected puroDF1 cells, uninfected hAlixDF1 cells and DF1 cells infected with wild-type RSV, respectively. Lane 4 (RSV DF1) contains 1/400th of pellet, lane 5 (RSV DF1) contains 1/80th of pellet, and lanes 6 (Puro) and 7 (hAlix) each contain 1/40th of the pellet.

against RSV CANC confirmed that the puroDF1 cells and hAlixDF1 cells were uninfected (Figure 4.14, right blot). Thus, Alix appears to be secreted into the medium in a manner independent of virions, making the immunoblots unrepresentative of the levels of Alix incorporated into virions. Thus, Alix visualized in immunoblots represents all Alix exiting the cell, whether via secretion, in virions, or in exosomes. Alix has been shown to be secreted into the extracellular matrix from the cells and to be important for cell adhesion (151).

The Alix detected from the medium was in the particulate fraction and was not soluble. Instead of secreted Alix, it is more likely that I detected Alix in exosomes. Alix has been detected previously in exosomes (63, 207). Exosomes are 30-100 nm intralumenal vesicles of MVBs that are released when MVBs fuse with the plasma membrane (reviewed in (101)). Proteomic analysis of exosomes released from dendritic cells identified 21 new exosomal resident proteins, including Tsg101 and Alix, Alix being one of the most abundant proteins detected (207). In addition Alix was found to bind to the transferrin receptor (TfR) in exosomes (63). Alix is even regarded as a marker for exosomes (234). Unfortunately exosomes and retroviral particles are similar in size (30-100nm for exosomes, ~100 nm for RSV) and density (1.15 g/ml for exosomes, 1.16-1.18 g/ml for RSV). Cells over-expressing hAlix also excrete more Alix, as shown by immunoblotting comparable volumes of medium from similar amounts of cells (Figure 4.14, left). To fully explore the role of the late domains and possibly NC in incorporation of Alix into virions, virions would have to be separated from secreted Alix by a more stringent method, such as by isopycnic banding or rate zonal centrifugation of particles. Interestingly, the anti-Alix blot reveals a second lower Alix band in the medium

from infected, but not in the medium of uninfected cells. Perhaps this band represents the Alix incorporated into particles and cleaved by the viral protease.

Discussion

In this chapter I have exploited infectious late domain mutants to examine the effects of late domain mutations on RSV replication.
The spreading assay data proved to be a perfect complement to the budding assay data from the previous chapter. For example, the budding assays were able to distinguish between fast budding mutants such as wild-type and PPPY-AAASA mutants. However, the budding rates of the more severe late domain mutants, APPY-AAASA, AAAA-LYPSL, and AAAA-AAASA, were unmeasurable and thus indistinguishable. In contrast, the spreading assay was able to distinguish between the slow budding mutants, but differences in the spreading rates of the fast budding variants (wild-type and PPPY-AAASA) could not detected.

Despite the evolutionary conservation of late domains, the results in this chapter show that RSV can spread through tissue culture, albeit at a reduced rate, when both the PPPY and the LYPSL motif are mutated to alanines. Cell-free medium from cells infected with the double late domain knock-out mutant is able to initiate a new infection, implying the release of infectious particles does occur. This is somewhat surprising considering the incomplete and incorrect Gag cleavage observed in the AAAA-AAASA particles. These data do not exclude the possibility that some spread does occur via cell-to-cell contact, but it shows that infectious particles are “released”.

Spreading profiles corroborated the budding assay data and showed that the LYPSL motif is important, specifically when the PPPY is weakened or absent. Alix over-expression also rescued the spreading retardation of PPPY mutants. The spreading of the AAAA-LYPSL, APPY-LYPSL, PTAP-LYPSL, and FPIV-LYPSL mutants clearly benefited from high Alix levels. By contrast, the spreading rates of mutants that lacked the Alix binding motif (PPPY-AAASA, APPY-AAASA, and APPY-LFPIV) did not significantly improve in cells over-expressing Alix. There are at least two reasons why Alix over-expression was not able to increase the spreading rate of these mutants. One possibility is that these mutants, lacking LYPSL motifs, are unable to recruit Alix. A second possibility is that Alix does help mediate budding of these mutants, either through an interaction with NC or through another ESCRT protein, but the boost from Alix is not observed because the PPPY-AAASA mutant (like wild-type) is already spreading at its maximal rate. A third possibility is that Alix can mediate budding through interaction with other ESCRT proteins, but not through the NC domain. In this case, mutants that have mutations in both late domains (APPY-AAASA, and APPY-LFPIV) would not benefit from Alix over-expression.

To address the question whether Alix can interact with Gag in the absence of the LYPSL motif, Alix incorporation into various late domain mutant particles was measured by immoblotting particles for Alix and normalizing for particle number by immunoblotting aganst CA. Unfortunately, I was unable to measure Alix incorporation because1) Alix is released into the medium via a Gag-independent mechanism (possibly through secretion or in exosomes), 2) late domain mutants undergo variable Gag cleavage making normalization to

CA meaningless, and 3) late domain particles may contain more Gag molecules than wild-type RSV.

A possible clue to whether Alix needs a late domain to mediate budding came in the form of another indicator of viral fitness. Conveniently, the average GFP intensity value provided by the flow cytometry analysis correlated well with the budding and spreading rates. Cells infected with fast budding and spreading mutants had high average GFP intensity and cells infected with slow budding and spreading mutants had low average GFP intensity. Alix over-expression increased the average GFP intensity over every mutant examined, even the double late domain mutant, AAAA-AAASA. If average GFP intensity is a proxy for budding efficiency then it is possible Alix can help mediate budding even in the absence of any late domain, possibly through NC. NC could not be deleted to test its importance on Alix function since it is indispensible for infectivity. The average GFP intensity of cells proved to be a more sensitive method for ranking the mutants, though the significance of the GFP intensity is unclear.

We do know that the expression of viral genes can be affected by at least three factors; 1) viral RNA splicing, 2) loss of viral genes, and 3) integration site selection. It is possible that a combination of these processes led to the loss of the GFP gene and an increase or decrease in GFP expression. Both the loss of the GFP marker and a reduction in GFP intensity was observed in the severe late domain mutants.

For all but one mutant, a slower budding rate in the budding assays translated into a slower spreading rate. This suggests that the spreading assays can be considered another way to assess the severity of late domain mutants. The one exception was the APPY-LYPDL mutant. While the APPY-

LYPDL mutant budded more quickly than the APPY-LYPSL mutant, it consistently spread more slowly than the APPY-LYPSL. Furthermore, the AAAA-LYPSL mutant also spread more quickly than the AAAA-LYPDL mutant. Thus, the aspartic acid does give RSV a replication disadvantage and the modest decrease in viral fitness must be due to factors other than budding rate. I interpret this result to mean that the wild-type suboptimal Alix binding site gives RSV a replication advantage

For the most part heterologous late domains were unable to functionally replace the native late domains at the same positions. FPIV was unable to function as a late domain in place of PPPY or LYPSL. FPIV seemed to be able to substitute for LYPSL (APPY-LFPIV) in the budding assays, but the spreading assays revealed that this mutant often reverted after extended passages. The budding assays most likely were measuring the budding rate of the reverted PPPY-LFPIV mutant. The FPAV sequence in the PR domain of Gag does not seem to be important for spreading. Mutating the phenylalanine to glycine did not reduce the rate of spread compared to wild-type, even though its budding rate was reduced.

PTAP was unable to function as a late domain in place of PPPY. The only heterologous late domain that could function in RSV was the modest one amino acid S→D substitution in LYPSL resulting in the LYPDL motif of EIAV, which supported a faster rate of spread than no late domain (PPPY-AAASA), but not better than LYPSL itself.

Previous work has shown that the context of a late domain contributes to its ability to mediate budding (116, 148). It is possible that the PTAP motif, and even the FPIV motif, can support RSV budding if placed in the correct context that makes it available for binding to its cellular factor.

In summary, the spreading profiles of the late domain mutants supported the model previously constructed based on the budding data. Specifically, the LYPSL motif is important for RSV spreading, especially when the PPPY motif is weakened. The spreading rates of PPPY mutants can be rescued by the over-expression of Alix. Whether Alix needs a LYPSL motif to rescue spread is unclear. Assuming average GFP intensity is a proxy for viral fitness, it appears that Alix over-expression does help all mutants, regardless of the presence of late domains. GFP loss and a reduction in GFP intensity is observed in severe late domain mutants, implying these viruses are under more selection. The spreading assays showed the LYPDL puts the virus at a replication disadvantage over LYPSL, even though it increases budding rate.

CHAPTER FIVE

PERSPECTIVE

The work presented in this thesis examines the requirements, both viral (late domains) and cellular (the ESCRT protein Alix), for RSV budding. The budding rates, spreading rates, and budding phenotypes of infectious RSV late domain mutants were analyzed by pulse-chase, flow cytometry, and EM, respectively. In this chapter, I summarize my results and discuss the impact on our understanding of RSV budding and possible directions for future studies.

Summary

- The LYPSL motif in the p2b domain of Gag is required for maximal RSV budding efficiency. A reduction in budding rate (measured by pulse-chase) and an accumulation of stalled budding particles on the plasma membrane (observed by SEM) occur upon mutation of the LYPSL sequence. Mutating this sequence in the context of a weakened PPPY motif amplifies the budding defect and also slows the rate at which the virus spreads through culture. Despite its contribution to budding, mutating all of the LYPSL motif has less of an effect on budding and spreading than mutating just one amino acid of the PPPY motif.
  Impact: Previous studies have overlooked the role of LYPSL in RSV budding. My comprehensive study that utilized three complementary techniques and examined late domain mutations in various combinations was able to identify LYPSL as a late domain. These data indicate that, like other enveloped viruses, RSV depends on multiple late domains to mediate budding. The two late domains, PPPY and

LYPSL, exist in a functional hierarchy with the PPPY motif being dominant and the LYPSL motif playing a supportive role.

- Alix over-expression partially rescues the slowed budding and spreading rates of PPPY mutants. Alix-mediated rescue of budding rate is measurable only if the LYPSL motif is present. However, the Alix-mediated rescue of the spreading rates of mutants lacking the LYPSL motif, and even both late domains, also exhibit a slight boost from Alix over-expression.

  Impact: The presence of a strong late domain (such as PPPY) can obscure the activity of the secondary late domain (such as LYPSL). I implicate Alix, and thus the LYPSL motif, in RSV budding by showing Alix over-expression boosted the budding and spreading rates of PPPY mutants. Presumably, the compromised PPPY late domain allows RSV to rely more heavily on the weaker LYPSL late domain, which can function better if Alix levels are higher. The Alix-mediated rescue of budding was only apparent when the Alix binding site, LYPSL, was present. However, the subtle improvements in spreading rate of mutants that were missing just the LYPSL late domain or both late domains implies that Alix may be able to aid budding via an interaction with Nedd4 (142), or in the case of the double late domain knockout, with the NC domain as has been shown with HIV-1 (160).
- Heterologous late domains (PTAP and FPIV) proved to be unable to functionally replace the primary PPPY late domain. Nor is FPIV able to functionally replace the YPSL squence. However, the relatively conservative substitution of the EIAV LYPDL motif for the LYPSL sequence does increase the budding rate in the context of a weakened

PPPY late domain. Despite the budding advantage of the APPY-LYPDL mutant over APPY-LYPSL however, it spreads slower than the APPY-LYPSL.

Impact: The HIV-1 late domain (PTAP) and the SV5 late domain (FPIV) do not support budding in the context of RSV Gag. It cannot be ruled out that they could function as active late domains if placed in the right context with surrounding amino acids that make them available for interaction with ESCRT machinery. The inability of FPIV to support budding in place of YPSL implies FPIV does not belong to the YPXL consensus of late domains.

- The spread of late domain mutants through tissue culture was monitored by detection of a GFP marker harbored by the provirus in place of Src. I observed a loss of the GFP marker from the provirus as well as a decrease in average GFP intensity that was proportional to the severity of the late domain defect.

  Impact: Although the loss of Src and GFP from RSV has been reported previously (80, 161), it is unclear why late domain defects would promote the loss and reduce the expression of GFP. Possible explanations for these phenomena include altered splicing resulting in selection against virus with GFP, altered superinfection interference or tolerance, or increased cytotoxicity of severe late domain mutants.

Future Direction

Although my study was one of the most detailed conducted on RSV budding, many unresolved issues remain. One such question is whether the NC domain of RSV Gag possesses the Alix-binding property of the NC domain

of HIV-1 Gag (160). The existence of an alternative Alix-binding site in Gag makes sense in light of the small but repeatable spreading rate (and GFP intensity) boost of mutants that lack LYPSL or both late domains upon Alix over-expression. In support of a role for NC in Alix binding, deletion of either of the two Cys-His motifs in RSV NC results in a late domain-like phenotype of reduced VLP production and immature particles tethered to the membrane (106). This late domain phenotype was not due to a disruption in Nedd4 interaction as a yeast two-hybrid binding assay showed the Cys-His mutants interacted with LDI as well as wild-type Gag.

Since my system relied on infectious RSV, the NC domain was indispensible and I was not able to make the required deletions to test its role in the Alix-mediated rescue of budding and spreading. However, Gag constructs lacking LYPSL and PPPY could be constructed in which the NC is replaced with a leucine zipper, as was done for HIV-1 (160). Co-immunoprecipition of leucine zipper Gag and Alix could help elucidate any role NC has in binding Alix. Given the location of the LYPSL motif in RSV Gag (between MA and CA) compared to the location of the $LYPX_nL$ motif in HIV-1 Gag (C-terminal to NC domain), an Alix/NC interaction in RSV would presumably require different orientations than that in HIV-1.

Alix incorporation into HIV-1 particles was measured by immunoblot (160). Obviously it would be ideal if I could detect Alix incorporation into RSV particles by immunoblot also. This would help address the possibility that Alix is binding Gag via NC or through and interaction with Nedd4 (when PPPY is present). Unfortunately, my method for collecting particles from medium also collected extracellular Alix, even in the absence of Gag (Figure 4.14). Alix in the medium is presumably the result of secretion or more likely an association

with exosomes (63, 151, 207). Subjecting the medium from untransfected HeLa cells to a similar method (culture medium was clarified by low-speed centrifugation and passaged through a 0.45 μm filter and then the virions were pelleted through 20% sucrose cushions), Popov et al. failed to detect Alix in the pellet, even when the cells were transfected with Alix-HA (160). It is unclear why Alix was not pelleted from medium from HeLa cells as it was from my uninfected puroDF1 and hAlixDF1 cells. Perhaps exosome and Alix secretion are cell-type dependent.

Contamination of virus preparations with exosomes or microvesicles can complicate results of a variety of experiments in which pure virions are required. A couple of approaches have been used to exclude these unwanted vesicles. Microvesicles have been immunodepleted from samples using anti-CD45 antibody-linked microbeads (145). Exosomes have been similarly immunodepleted using antibodies against the exosome maker protein acetylcholinesterase (AChE) antibodies (22). Subjecting virus samples to Optiprep velocity gradients has also proved to be a relable method of separating virions from exosomes (22). Considering the inherent uncertainty regarding the purity of virus preparations, it is worth noting that Alix has been observed in budding HIV-1 particles by immunogold labeling (218).

The existence of a third late domain in RSV is another interesting line of investigation considering a mutant lacking both known late domains (AAAA-AAASA) was able to spread through tissue culture. Cells infected with this mutant were releasing infectious particles (versus cell-to-cell spread) as evidenced by the ability of filtered medium from infected cells to reinitiate infection in fresh cells. Attempts to rule out reversion by sequencing the product of the reverse transcription of the viral RNA from this mutant failed,

possibly because of low titers. However, immunoblots of virus and cells infected with this mutant displayed severe Gag cleavage defects, implying the mutations did not revert back to wild-type.

Two candidate sequences for an unidentified late domain in RSV are an ATAP in the p2b domain and a FPAV sequence in PR. The ATAP sequence (T**ASAP**PPPY) is just upstream of the PPPY motif that nearly matches the PTAP consensus. It was previously overlooked as a possible RSV late domain because the first proline proved to be essential for the late domain function of the HIV-1 PTAP motif (79). However, a recent study showed that mutating the first proline to alanine (PTAP→ATAP) in the only late domain of FIV-1 had no effect on budding, suggesting RSV's ASAP sequence deserves a second look (19). The PR domain contains a FPAV sequence that fits the FPXV consensus of the late domain that supports budding in SV5. I found that mutating the FPAV to GPAV reduced the budding rate (Figure 3.6) but not the spreading rate (Figure 4.6) of RSV. Although not a conclusive result, it suggests that the FPAV sequence warrants further study.

An alternative explanation for RSV spreading in the absence of PPPY and LYPSL motifs is that perhaps budding can proceed spontaneously, albeit very slowly, without the aid of cellular factors. It has been postulated that for some viruses the intrinsic associations of viral proteins with microdomains on the plasma membrane are enough to induce curvature and supply the pulling force needed to drive budding (29). Even if it is not efficient, it is possible that the pinching off of an assembled virus particle hanging on by a thin stalk is actually energetically favorable.

The role of phosphorylation of Gag and/or the ESCRT machinery in budding has not been fully examined. It has been demonstrated that the p6

domain of HIV-1 Gag is the major phosphoprotein inside particles (132). Serines, threonines, and tyrosines were all found to be phosphorylated though the specific residues that were phosphorylated were not identified. Given that there is only one tyrosine in p6 and it is the tyrosine located in the $LYPX_nL$ late domain, the phosphorylation of tyrosine can be attributed to this residue. Whether this phosphorylation contributes to the regulation of the $LYPX_nL$ late domain and budding is yet to be determined, as this work was done before the identification of $LYPX_nL$ as a late domain. The significance of p6 as the domain carrying the PTAP late domain was noted by Muller et al., and they point out that the p12 domain of MLV Gag (186) and Mason-Pfizer Monkey Virus pp16 domain (231), both of which harbor the PPPY late domain, have also been shown to be phosphorylated. The major site of RSV phosphorylation in a mature virion is serine 106 in the MA domain. Mutating this serine to alanine prevents almost all of Gag phosphorylation. However, this has no effect on budding or infectivity of RSV (138). It is possible that other transient phosphorylation events occur.

Performing my own cursory phosphorylation motif scan (NetPhos 2.0), RSV is predicted to be phosphorylated at only one of its ten tyrosine residues, PPP**Y**. Interestingly, when the wild type sequence of RSV was entered no phosphorylation was predicted in the LYPSL motif. However, upon substitution of the serine residue with an aspartic acid (L**Y**PDL) the program predicted this Y would be phosphorylated. Thus, it is possible that this mutation created a phosphorylation site, which could have contributed to the phenotype displayed in the budding and spreading assays. Subjecting Alix to the same phosphorylation program yielded no predicted phosphorylation sites in the hydrophobic Gag-binding site of the V-domain, but in P**S**AP the serine residue

is predicted to be phosporylated. In addition, aspartic acid (D) is often used to mimic a constitutively phosphorylated form of serine (S). Thus it is curious that LYPSL (RSV, BIV, some SIV that have PTAP) and LYPDL (EIAV, some SIVs that lack PTAP) are the alternative forms of the motif.

Finally, it should be noted that most of the variable amino acid positions in late domains are filled by amino acids that can be phosphorylated. For example, the variable position of the P**T**/**S**AP motifs can harbor threonines or serines. The X position in LYPX_nL motifs can be a serine (S) at the X position, as is the case with RSV (LYP**S**L) or an aspartic acid (D) as is the case with EIAV (LYP**D**L). Interestingly, aspartic acids (D) have been used to reconstitute a phosphorylated serine (S). Finally, in HIV-1 the X position of the LYPX_nL motif (LYP**LTS**L) is a threonine (T) and serine (S).

The ESCRT-I component MVB12A and MVB12B harbor nine predicted threonine and serine phosphorylation sties (126). Over-expression of MVB12 was shown to inhibit release of HIV-1, but MVB12A mutants in which either five or all nine phosphorylation sites were mutated to alanine had a reduced ability to inhibit particle release despite being able to associate with ESCRT-I as well as wild-type.

Alix interacts with the protein tyrosine kinase Src through its C-terminus (residues 752-757) (182). *Xenopus* Alix, Xp95, and mouse Alix specifically undergo oocyte maturation-dependent phosphorylation in the N-terminus of their proline rich domains (43). Phosphorylation of one of these sites during the induction of mitosis, Threonine745, negatively regulates interaction with SETA as shown by GST pulldown.

Itch, a member of the Nedd4-family of HECT E3 ligases, is auto-inhibited by the interaction of the WW domains with the HECT domain. The

auto-inhibition of Itch is relieved upon phosphorylation by the serine/threonine kinase JNK, which causes a conformational change in Itch and allows it to be activated (60).

Both Hrs (98) and STAM (202) were identified as phosphorylated proteins in growth factor and cytokine stimulated cells. Treating HIV-1 particles with specific kinase inhibitors suggested that ERK2 is responsible for majority of p6 phosphorylation. ERK2/Cdk1 is a mitogen-activated kinase that phosphorylates, among other targets, Cep55 (52) upon mitotic entry. ERK2 has previously been shown to be associated with HIV particles (26). All in all, the regulation of the ESCRT machinery and late domains may be an interesting line of research in the future.

APPENDIX

PRIMERS

Primers used for two-step PCR mutagenesis of late domain mutants

KAD26 (LYPSL→ LYPDL) forward

GGGAGTGGTTTGTATCCTGATCTGGCGGGGGTG

KAD27 (LYPSL→ LYPDL) reverse

CACCCCCGCCAGATCAGGATACAAACCACTCCC

KAD28 (PPPY→ APPY) forward

GCCACAGCCTCGGCCCCTGCACCCCCTTATGTG

KAD29 (PPPY→ APPY) reverse

CACATAAGGGGGTGCAGGGGCCGAGGCTGTGGC

KAD37 (PPPY→ FPIV) forward

GCCTCGGCCCCTTTCCCTATCGTTGTGGGGAGTGGTTTG

KAD38 (PPPY→ FPIV) reverse

CAAACCACTCCCCACAACGATAGGGAAAGGGGCCGAGGC

KAD49 (PPPY→ AAPY) forward

GCCACAGCCTCGGCCCCTGCTGCCCCTTATGTG

KAD50 (PPPY→ AAAA) forward

CGGCCCCTGCTGCCGCAGCAGTGGGGAGTGG

KAD51 (PPPY→ AAPY) reverse

CACATAAGGGGCAGCAGGGGCCGAGGCTGTGGC

KAD52 (PPPY→ AAAA) reverse

CCACTCCCCACTGCTGCGGCAGCAGGGGCCG

KAD65 (PPPY→ PTAP) forward

CCTCGGCCCCTCCTACTGCACCTGTGGGGAGTGGTTTG

KAD66 (PPPY→ PTAP) reverse

CAAACCACTCCCCACAGGTGCAGTAGGAGGGGCCGAGG

KAD67 (FPAV→ APAV) forward

CCCCTGCTCCTCGCCCCCGCAGTCGCTATGG

KAD68 (FPAV→ APAV) reverse

CCATAGCGACTGCGGGGGCGAGGAGCAGGGG

KAD79 (LYPSL→ LFPIV) forward

GGGAGTGGTTTGTTTCCTATTGTGGCGGGGGTG

KAD80 (LYPSL→ LFPIV) reverse

CACCCCCGCCACAATAGGAAACAAACCACTCCC

KAD93 (PPPY→ AAAA, replace KAD50) forward

GCCTCGGCCCCTGCTGCCGCTGCTGTGGGGAGTGGgg

KAD94 (PPPY→ AAAA, replace KAD52) reverse

CCCCACTCCCCACAGCAGCGGCAGCAGGGGCCGAggc

59F (FPAV→ GPAV) (from Danso) forward

GCGACCCCTGCTCCTCGGCCCCGCAGTAGCTATG

59R (FPAV→ GPAV) (from Danso) reverse

CATAGCTACTGCGGGGCCGAGGAGCAGGGGTCGC

KAD111 (LYPSL→ LAAAA) forward

GGGAGTGGTTTGGCTGCTGCCGCGGCGGGGGTGGGAGAGC

KAD112 (LYPSL→ LAAAA) reverse

GCTCTCCCACCCCCGCCGCGGCAGCAGCCAAACCACTCCC

Primers used for reverse transcription of viral RNA

KAD47 (Flanked by XbaI) forward

CATACTTCTAGACCACACCTAAAACCGTTGGCACATC

KAD48 (Flanked by XhoI) reverse

ATGAATCTCGAGCCCCGGTCTTAATAATGCGGCCTGAC

KAD59 (beginning of MA, flanked by XbaI) forward

ACTGATTCTAGACGTCATTAAGGTGATTTCGTCC

KAD60 (beginning of CA, flanked by XbaI) reverse

AGTAGTTCTAGACTCTGTCTTAATCACTACAGGC

REFERENCES

1. **Agromayor, M. and J. Martin-Serrano.** 2006. Interaction of AMSH with ESCRT-III and deubiquitination of endosomal cargo. J. Biol. Chem. **281:**23083-23091.

2. **Ako-Adjei, D., M. C. Johnson, and V. M. Vogt.** 2005. The retroviral capsid domain dictates virion size, morphology, and coassembly of gag into virus-like particles. J. Virol. **79:**13463-13472.

3. **Babst, M.** 2005. A protein's final ESCRT. Traffic **6:**2-9.

4. **Babst, M., D. J. Katzmann, E. J. Estepa-Sabal, T. Meerloo, and S. D. Emr.** 2002. Escrt-III: an endosome-associated heterooligomeric protein complex required for mvb sorting. Dev. Cell. **3:**271-282.

5. **Babst, M., D. J. Katzmann, W. B. Snyder, B. Wendland, and S. D. Emr.** 2002. Endosome-associated complex, ESCRT-II, recruits transport machinery for protein sorting at the multivesicular body. Dev. Cell. **3:**283-289.

6. **Babst, M., T. K. Sato, L. M. Banta, and S. D. Emr.** 1997. Endosomal transport function in yeast requires a novel AAA-type ATPase, Vps4p. EMBO J. **16:**1820-1831.

7. **Babst, M., B. Wendland, E. J. Estepa, and S. D. Emr.** 1998. The Vps4p AAA ATPase regulates membrane association of a Vps protein complex required for normal endosome function. EMBO J. **17:**2982-2993.

8. **Bache, K. G., C. Raiborg, A. Mehlum, and H. Stenmark.** 2003. STAM and Hrs are subunits of a multivalent ubiquitin-binding complex on early endosomes. J. Biol. Chem. **278:**12513-12521.

9. **Baldwin, D. N. and M. L. Linial.** 1998. The roles of Pol and Env in the assembly pathway of human foamy virus. J. Virol. **72:**3658-3665.

10. **Baltimore D.** 1970. RNA-dependent DNA polymerase in virions of RNA tumour viruses

11. **Beyer, A., S. Scheuring, S. Muller, A. Mincheva, P. Lichter, and K. Kohrer.** 2003. Comparative sequence and expression analyses of four mammalian VPS4 genes. Gene **305:**47-59.

12. **Bibollet-Ruche, F., E. Bailes, F. Gao, X. Pourrut, K. L. Barlow, J. P. Clewley, J. M. Mwenda, D. K. Langat, G. K. Chege, H. M. McClure, E. Mpoudi-Ngole, E. Delaporte, M. Peeters, G. M. Shaw, P. M. Sharp, and B. H. Hahn.** 2004. New simian immunodeficiency virus infecting De Brazza's monkeys (Cercopithecus neglectus): evidence for a cercopithecus monkey virus clade. J. Virol. **78:**7748-7762.

13. **Bilodeau, P. S., S. C. Winistorfer, W. R. Kearney, A. D. Robertson, and R. C. Piper.** 2003. Vps27-Hse1 and ESCRT-I complexes cooperate to increase efficiency of sorting ubiquitinated proteins at the endosome. J. Cell Biol. **163:**237-243.

14. **Bork, P. and M. Sudol.** 1994. The WW domain: a signalling site in dystrophin? Trends Biochem. Sci. **19:**531-533.

15. **Bouamr, F., J. A. Melillo, M. Q. Wang, K. Nagashima, M. de Los Santos, A. Rein, and S. P. Goff.** 2003. PPPYVEPTAP motif is the late domain of human T-cell leukemia virus type 1 Gag and mediates its functional interaction with cellular proteins Nedd4 and Tsg101 [corrected]. J. Virol. **77:**11882-11895.

16. **Bowers, K., S. C. Piper, M. A. Edeling, S. R. Gray, D. J. Owen, P. J. Lehner, and J. P. Luzio.** 2006. Degradation of endocytosed epidermal growth factor and virally ubiquitinated major histocompatibility complex class I is independent of mammalian ESCRTII. J. Biol. Chem. **281:**5094-5105.

17. **Bruce, M. C., V. Kanelis, F. Fouladkou, A. Debonneville, O. Staub, and D. Rotin.** 2008. Regulation of Nedd4-2 self-ubiquitination and stability by a PY motif located within its HECT-domain. Biochem. J. **415:**155-163.

18. **Burgdorf, S., P. Leister, and K. H. Scheidtmann.** 2004. TSG101 interacts with apoptosis-antagonizing transcription factor and enhances

androgen receptor-mediated transcription by promoting its monoubiquitination. J. Biol. Chem. **279:**17524-17534.

19. **Calistri, A., C. Del Vecchio, C. Salata, M. Celestino, M. Celegato, H. Gottlinger, G. Palu, and C. Parolin.** 2009. Role of the feline immunodeficiency virus L-domain in the presence or absence of Gag processing: Involvement of ubiquitin and Nedd4-2s ligase in viral egress. J. Cell. Physiol. **218:**175-182.

20. **Callahan, E. M. and J. W. Wills.** 2003. Link between genome packaging and rate of budding for Rous sarcoma virus. J. Virol. **77:**9388-9398.

21. **Campbell, S. and V. M. Vogt.** 1995. Self-assembly in vitro of purified CA-NC proteins from Rous sarcoma virus and human immunodeficiency virus type 1. J. Virol. **69:**6487-6497.

22. **Cantin, R., J. Diou, D. Belanger, A. M. Tremblay, and C. Gilbert.** 2008. Discrimination between exosomes and HIV-1: purification of both vesicles from cell-free supernatants. J. Immunol. Methods **338:**21-30.

23. **Carlson, L. A., J. A. Briggs, B. Glass, J. D. Riches, M. N. Simon, M. C. Johnson, B. Muller, K. Grunewald, and H. G. Krausslich.** 2008. Three-dimensional analysis of budding sites and released virus suggests a revised model for HIV-1 morphogenesis. Cell. Host Microbe **4:**592-599.

24. **Carlton, J. G., M. Agromayor, and J. Martin-Serrano.** 2008. Differential requirements for Alix and ESCRT-III in cytokinesis and HIV-1 release. Proc. Natl. Acad. Sci. U. S. A. **105:**10541-10546.

25. **Carlton, J. G. and J. Martin-Serrano.** 2007. Parallels between cytokinesis and retroviral budding: a role for the ESCRT machinery. Science **316:**1908-1912.

26. **Cartier, C., M. Deckert, C. Grangeasse, R. Trauger, F. Jensen, A. Bernard, A. Cozzone, C. Desgranges, and V. Boyer.** 1997. Association of ERK2 mitogen-activated protein kinase with human immunodeficiency virus particles. J. Virol. **71:**4832-4837.

27. **Chan, D. C., M. T. Bedford, and P. Leder.** 1996. Formin binding proteins bear WWP/WW domains that bind proline-rich peptides and functionally resemble SH3 domains. EMBO J. **15:**1045-1054.

28. **Chatellard-Causse, C., B. Blot, N. Cristina, S. Torch, M. Missotten, and R. Sadoul.** 2002. Alix (ALG-2-interacting protein X), a protein involved in apoptosis, binds to endophilins and induces cytoplasmic vacuolization. J. Biol. Chem. **277:**29108-29115.

29. **Chen, B. J. and R. A. Lamb.** 2007. Mechanisms for enveloped virus budding: Can some viruses do without an ESCRT? Virology

30. **Chen, C., O. Vincent, J. Jin, O. A. Weisz, and R. C. Montelaro.** 2005. Functions of early (AP-2) and late (AIP1/ALIX) endocytic proteins in equine infectious anemia virus budding. J. Biol. Chem. **280:**40474-40480.

31. **Chen, H. I. and M. Sudol.** 1995. The WW domain of Yes-associated protein binds a proline-rich ligand that differs from the consensus established for Src homology 3-binding modules. Proc. Natl. Acad. Sci. U. S. A. **92:**7819-7823.

32. **Cherepanov, P., G. Maertens, P. Proost, B. Devreese, J. Van Beeumen, Y. Engelborghs, E. De Clercq, and Z. Debyser.** 2003. HIV-1 integrase forms stable tetramers and associates with LEDGF/p75 protein in human cells. J. Biol. Chem. **278:**372-381.

33. **Choi, G., S. Park, B. Choi, S. Hong, J. Lee, E. Hunter, and S. S. Rhee.** 1999. Identification of a cytoplasmic targeting/retention signal in a retroviral Gag polyprotein. J. Virol. **73:**5431-5437.

34. **Chow, A. Y. and I. Mellman.** 2005. Old lysosomes, new tricks: MHC II dynamics in DCs. Trends Immunol. **26:**72-78.

35. **Chung, H. Y., E. Morita, U. von Schwedler, B. Muller, H. G. Krausslich, and W. I. Sundquist.** 2008. NEDD4L overexpression rescues the release and infectivity of human immunodeficiency virus type 1 constructs lacking PTAP and YPXL late domains. J. Virol. **82:**4884-4897.

36. **Clague, M. J. and S. Urbe.** 2006. Endocytosis: the DUB version. Trends Cell Biol. **16:**551-559.

37. **Coffin, J. M., S. H. Hughes, and H. Varmus.** 1997. Retroviruses. Cold Spring Harbor Laboratory Press, Plainview, N.Y.

38. **Costa, L. J., N. Chen, A. Lopes, R. S. Aguiar, A. Tanuri, A. Plemenitas, and B. M. Peterlin.** 2006. Interactions between Nef and AIP1 proliferate multivesicular bodies and facilitate egress of HIV-1. Retrovirology **3:**33.

39. **Craven, R. C., A. E. Leure-duPree, R. A. Weldon Jr, and J. W. Wills.** 1995. Genetic analysis of the major homology region of the Rous sarcoma virus Gag protein. J. Virol. **69:**4213-4227.

40. **Crise, B. and J. K. Rose.** 1992. Human immunodeficiency virus type 1 glycoprotein precursor retains a CD4-p56lck complex in the endoplasmic reticulum. J. Virol. **66:**2296-2301.

41. **Dalton, A. K., D. Ako-Adjei, P. S. Murray, D. Murray, and V. M. Vogt.** 2007. Electrostatic interactions drive membrane association of the human immunodeficiency virus type 1 Gag MA domain. J. Virol. **81:**6434-6445.

42. **Dalton, A. K., P. S. Murray, D. Murray, and V. M. Vogt.** 2005. Biochemical characterization of rous sarcoma virus MA protein interaction with membranes. J. Virol. **79:**6227-6238.

43. **Dejournett, R. E., R. Kobayashi, S. Pan, C. Wu, L. D. Etkin, R. B. Clark, O. Bogler, and J. Kuang.** 2007. Phosphorylation of the proline-rich domain of Xp95 modulates Xp95 interaction with partner proteins. Biochem. J. **401:**521-531.

44. **Demirov, D. G., A. Ono, J. M. Orenstein, and E. O. Freed.** 2002. Overexpression of the N-terminal domain of TSG101 inhibits HIV-1 budding by blocking late domain function. Proc. Natl. Acad. Sci. U. S. A. **99:**955-960.

45. **Demirov, D. G., J. M. Orenstein, and E. O. Freed.** 2002. The late domain of human immunodeficiency virus type 1 p6 promotes virus release in a cell type-dependent manner. J. Virol. **76:**105-117.

46. **D'Souza, V. and M. F. Summers.** 2005. How retroviruses select their genomes. Nat. Rev. Microbiol. **3:**643-655.

47. **Duesberg PH, Martin GS, and Vogt PK.** 1970. Glycoprotein components of avian and murine RNA tumor viruses

48. **Dupre, S. and R. Haguenauer-Tsapis.** 2001. Deubiquitination step in the endocytic pathway of yeast plasma membrane proteins: crucial role of Doa4p ubiquitin isopeptidase. Mol. Cell. Biol. **21:**4482-4494.

49. **Eastman, S. W. and M. L. Linial.** 2001. Identification of a conserved residue of foamy virus Gag required for intracellular capsid assembly. J. Virol. **75:**6857-6864.

50. **Einfeld D and Hunter E.** 1988. Oligomeric structure of a prototype retrovirus glycoprotein

51. **Eskelinen, E. L.** 2005. Maturation of autophagic vacuoles in Mammalian cells. Autophagy **1:**1-10.

52. **Fabbro, M., B. B. Zhou, M. Takahashi, B. Sarcevic, P. Lal, M. E. Graham, B. G. Gabrielli, P. J. Robinson, E. A. Nigg, Y. Ono, and K. K. Khanna.** 2005. Cdk1/Erk2- and Plk1-dependent phosphorylation of a centrosome protein, Cep55, is required for its recruitment to midbody and cytokinesis. Dev. Cell. **9:**477-488.

53. **Federspiel, M. J. and S. H. Hughes.** 1997. Retroviral gene delivery. Methods Cell Biol. **52:**179-214.

54. **Finzi, A., A. Orthwein, J. Mercier, and E. A. Cohen.** 2007. Productive human immunodeficiency virus type 1 assembly takes place at the plasma membrane. J. Virol. **81:**7476-7490.

55. **Fischer, N., M. Heinkelein, D. Lindemann, J. Enssle, C. Baum, E. Werder, H. Zentgraf, J. G. Muller, and A. Rethwilm.** 1998. Foamy virus particle formation. J. Virol. **72:**1610-1615.

56. **Fisher, R. D., H. Y. Chung, Q. Zhai, H. Robinson, W. I. Sundquist, and C. P. Hill.** 2007. Structural and biochemical studies of ALIX/AIP1 and its role in retrovirus budding. Cell **128:**841-852.

57. **Fujita, H., Y. Umezuki, K. Imamura, D. Ishikawa, S. Uchimura, A. Nara, T. Yoshimori, Y. Hayashizaki, J. Kawai, K. Ishidoh, Y. Tanaka, and M. Himeno.** 2004. Mammalian class E Vps proteins, SBP1 and mVps2/CHMP2A, interact with and regulate the function of an AAA-ATPase SKD1/Vps4B. J. Cell. Sci. **117:**2997-3009.

58. **Fuller, S. D., T. Wilk, B. E. Gowen, H. G. Krausslich, and V. M. Vogt.** 1997. Cryo-electron microscopy reveals ordered domains in the immature HIV-1 particle. Curr. Biol. **7:**729-738.

59. **Galan, J. M. and R. Haguenauer-Tsapis.** 1997. Ubiquitin lys63 is involved in ubiquitination of a yeast plasma membrane protein. EMBO J. **16:**5847-5854.

60. **Gallagher, E., M. Gao, Y. C. Liu, and M. Karin.** 2006. Activation of the E3 ubiquitin ligase Itch through a phosphorylation-induced conformational change. Proc. Natl. Acad. Sci. U. S. A. **103:**1717-1722.

61. **Ganser-Pornillos, B. K., M. Yeager, and W. I. Sundquist.** 2008. The structural biology of HIV assembly. Curr. Opin. Struct. Biol. **18:**203-217.

62. **Garrus, J. E., U. K. von Schwedler, O. W. Pornillos, S. G. Morham, K. H. Zavitz, H. E. Wang, D. A. Wettstein, K. M. Stray, M. Cote, R. L. Rich, D. G. Myszka, and W. I. Sundquist.** 2001. Tsg101 and the vacuolar protein sorting pathway are essential for HIV-1 budding. Cell **107:**55-65.

63. **Geminard, C., A. De Gassart, L. Blanc, and M. Vidal.** 2004. Degradation of AP2 during reticulocyte maturation enhances binding of hsc70 and Alix to a common site on TFR for sorting into exosomes. Traffic **5:**181-193.

64. **Goff, A., L. S. Ehrlich, S. N. Cohen, and C. A. Carter.** 2003. Tsg101 control of human immunodeficiency virus type 1 Gag trafficking and release. J. Virol. **77:**9173-9182.

65. **Goila-Gaur, R., D. G. Demirov, J. M. Orenstein, A. Ono, and E. O. Freed.** 2003. Defects in human immunodeficiency virus budding and endosomal sorting induced by TSG101 overexpression. J. Virol. **77:**6507-6519.

66. **Gontarek, R. R., M. T. McNally, and K. Beemon.** 1993. Mutation of an RSV intronic element abolishes both U11/U12 snRNP binding and negative regulation of splicing. Genes Dev. **7:**1926-1936.

67. **Gottlinger, H. G., T. Dorfman, J. G. Sodroski, and W. A. Haseltine.** 1991. Effect of mutations affecting the p6 gag protein on human immunodeficiency virus particle release. Proc. Natl. Acad. Sci. U. S. A. **88:**3195-3199.

68. **Gottwein, E., J. Bodem, B. Muller, A. Schmechel, H. Zentgraf, and H. G. Krausslich.** 2003. The Mason-Pfizer monkey virus PPPY and PSAP motifs both contribute to virus release. J. Virol. **77:**9474-9485.

69. **Gottwein, E., S. Jager, A. Habermann, and H. G. Krausslich.** 2006. Cumulative mutations of ubiquitin acceptor sites in human immunodeficiency virus type 1 gag cause a late budding defect. J. Virol. **80:**6267-6275.

70. **Gromley, A., C. Yeaman, J. Rosa, S. Redick, C. T. Chen, S. Mirabelle, M. Guha, J. Sillibourne, and S. J. Doxsey.** 2005. Centriolin anchoring of exocyst and SNARE complexes at the midbody is required for secretory-vesicle-mediated abscission. Cell **123:**75-87.

71. **Hanson, P. I., R. Roth, Y. Lin, and J. E. Heuser.** 2008. Plasma membrane deformation by circular arrays of ESCRT-III protein filaments. J. Cell Biol. **180:**389-402.

72. **Harada, F., R. C. Sawyer, and J. E. Dahlberg.** 1975. A primer ribonucleic acid for initiation of in vitro Rous sarcarcoma virus deoxyribonucleic acid synthesis. J. Biol. Chem. **250:**3487-3497.

73. **Hartmann, C., M. Chami, U. Zachariae, B. L. de Groot, A. Engel, and M. G. Grutter.** 2008. Vacuolar protein sorting: two different functional states of the AAA-ATPase Vps4p. J. Mol. Biol. **377:**352-363.

74. **Harty, R. N., M. E. Brown, G. Wang, J. Huibregtse, and F. P. Hayes.** 2000. A PPxY motif within the VP40 protein of Ebola virus interacts physically and functionally with a ubiquitin ligase: implications for filovirus budding. Proc. Natl. Acad. Sci. U. S. A. **97:**13871-13876.

75. **Harty, R. N., J. Paragas, M. Sudol, and P. Palese.** 1999. A proline-rich motif within the matrix protein of vesicular stomatitis virus and rabies virus interacts with WW domains of cellular proteins: implications for viral budding. J. Virol. **73:**2921-2929.

76. **Henderson, L. E., H. C. Krutzsch, and S. Oroszlan.** 1983. Myristyl amino-terminal acylation of murine retrovirus proteins: an unusual post-translational proteins modification. Proc. Natl. Acad. Sci. U. S. A. **80:**339-343.

77. **Hofmann, K. and L. Falquet.** 2001. A ubiquitin-interacting motif conserved in components of the proteasomal and lysosomal protein degradation systems. Trends Biochem. Sci. **26:**347-350.

78. **Howard, T. L., D. R. Stauffer, C. R. Degnin, and S. M. Hollenberg.** 2001. CHMP1 functions as a member of a newly defined family of vesicle trafficking proteins. J. Cell. Sci. **114:**2395-2404.

79. **Huang, M., J. M. Orenstein, M. A. Martin, and E. O. Freed.** 1995. p6Gag is required for particle production from full-length human immunodeficiency virus type 1 molecular clones expressing protease. J. Virol. **69:**6810-6818.

80. **Hughes, S. H.** 2004. The RCAS vector system. Folia Biol. (Praha) **50:**107-119.

81. **Hurley, J. H. and S. D. Emr.** 2006. The ESCRT complexes: structure and mechanism of a membrane-trafficking network. Annu. Rev. Biophys. Biomol. Struct. **35:**277-298.

82. **Ichioka, F., M. Horii, K. Katoh, Y. Terasawa, H. Shibata, and M. Maki.** 2005. Identification of Rab GTPase-activating protein-like protein (RabGAPLP) as a novel Alix/AIP1-interacting protein. Biosci. Biotechnol. Biochem. **69:**861-865.

83. **Irion, U. and D. St Johnston.** 2007. bicoid RNA localization requires specific binding of an endosomal sorting complex. Nature **445:**554-558.

84. **Joshi, A., U. Munshi, S. D. Ablan, K. Nagashima, and E. O. Freed.** 2008. Functional Replacement of a Retroviral Late Domain by Ubiquitin Fusion. Traffic

85. **Jouvenet, N., P. D. Bieniasz, and S. M. Simon.** 2008. Imaging the biogenesis of individual HIV-1 virions in live cells. Nature **454:**236-240.

86. **Jouvenet, N., S. J. Neil, C. Bess, M. C. Johnson, C. A. Virgen, S. M. Simon, and P. D. Bieniasz.** 2006. Plasma membrane is the site of productive HIV-1 particle assembly. PLoS Biol. **4:**e435.

87. **Kato, M., K. Miyazawa, and N. Kitamura.** 2000. A deubiquitinating enzyme UBPY interacts with the Src homology 3 domain of Hrs-binding protein via a novel binding motif PX(V/I)(D/N)RXXKP. J. Biol. Chem. **275:**37481-37487.

88. **Katoh, K., H. Shibata, K. Hatta, and M. Maki.** 2004. CHMP4b is a major binding partner of the ALG-2-interacting protein Alix among the three CHMP4 isoforms. Arch. Biochem. Biophys. **421:**159-165.

89. **Katoh, K., H. Shibata, H. Suzuki, A. Nara, K. Ishidoh, E. Kominami, T. Yoshimori, and M. Maki.** 2003. The ALG-2-interacting protein Alix associates with CHMP4b, a human homologue of yeast Snf7 that is involved in multivesicular body sorting. J. Biol. Chem. **278:**39104-39113.

90. **Katzmann, D. J., M. Babst, and S. D. Emr.** 2001. Ubiquitin-dependent sorting into the multivesicular body pathway requires the function of a conserved endosomal protein sorting complex, ESCRT-I. Cell **106:**145-155.

91. **Katzmann, D. J., C. J. Stefan, M. Babst, and S. D. Emr.** 2003. Vps27 recruits ESCRT machinery to endosomes during MVB sorting. J. Cell Biol. **162:**413-423.

92. **Kenney, S. P., T. L. Lochmann, C. L. Schmid, and L. J. Parent.** 2008. Intermolecular interactions between retroviral Gag proteins in the nucleus. J. Virol. **82:**683-691.

93. **Kikonyogo, A., F. Bouamr, M. L. Vana, Y. Xiang, A. Aiyar, C. Carter, and J. Leis.** 2001. Proteins related to the Nedd4 family of ubiquitin protein ligases interact with the L domain of Rous sarcoma virus and are required for gag budding from cells. Proc. Natl. Acad. Sci. U. S. A. **98:**11199-11204.

94. **Kim, H. T., K. P. Kim, F. Lledias, A. F. Kisselev, K. M. Scaglione, D. Skowyra, S. P. Gygi, and A. L. Goldberg.** 2007. Certain pairs of ubiquitin-conjugating enzymes (E2s) and ubiquitin-protein ligases (E3s) synthesize nondegradable forked ubiquitin chains containing all possible isopeptide linkages. J. Biol. Chem. **282:**17375-17386.

95. **Kim, J., S. Sitaraman, A. Hierro, B. M. Beach, G. Odorizzi, and J. H. Hurley.** 2005. Structural basis for endosomal targeting by the Bro1 domain. Dev. Cell. **8:**937-947.

96. **Knejzlik, Z., M. Strohalm, L. Sedlackova, M. Kodicek, M. Sakalian, and T. Ruml.** 2004. Isolation and characterization of the Mason-Pfizer monkey virus p12 protein. Virology **324:**204-212.

97. **Komada, M. and N. Kitamura.** 2005. The Hrs/STAM complex in the downregulation of receptor tyrosine kinases. J. Biochem. **137:**1-8.

98. **Komada, M. and N. Kitamura.** 1995. Growth factor-induced tyrosine phosphorylation of Hrs, a novel 115-kilodalton protein with a structurally conserved putative zinc finger domain. Mol. Cell. Biol. **15:**6213-6221.

99. **Kranz, A., A. Kinner, and R. Kolling.** 2001. A family of small coiled-coil-forming proteins functioning at the late endosome in yeast. Mol. Biol. Cell **12:**711-723.

100. **Lai MM, Hu SS, and Vogt PK.** 1977. Occurrence of partial deletion and substitution of the src gene in the RNA genome of avian sarcoma virus

101. **Lakkaraju, A. and E. Rodriguez-Boulan.** 2008. Itinerant exosomes: emerging roles in cell and tissue polarity. Trends Cell Biol. **18:**199-209.

102. **Langelier, C., U. K. von Schwedler, R. D. Fisher, I. De Domenico, P. L. White, C. P. Hill, J. Kaplan, D. Ward, and W. I. Sundquist.** 2006. Human ESCRT-II complex and its role in human immunodeficiency virus type 1 release. J. Virol. **80:**9465-9480.

103. **Larson, D. R., M. C. Johnson, W. W. Webb, and V. M. Vogt.** 2005. Visualization of retrovirus budding with correlated light and electron microscopy. Proc. Natl. Acad. Sci. U. S. A. **102:**15453-15458.

104. **Lata, S., M. Roessle, J. Solomons, M. Jamin, H. G. Gottlinger, D. I. Svergun, and W. Weissenhorn.** 2008. Structural basis for autoinhibition of ESCRT-III CHMP3. J. Mol. Biol. **378:**816-825.

105. **Lazert, C., N. Chazal, L. Briant, D. Gerlier, and J. C. Cortay.** 2008. Refined study of the interaction between HIV-1 p6 late domain and ALIX. Retrovirology **5:**39.

106. **Lee, E. G. and M. L. Linial.** 2006. Deletion of a Cys-His motif from the Alpharetrovirus nucleocapsid domain reveals late domain mutant-like budding defects. Virology **347:**226-233.

107. **Lee, S., A. Joshi, K. Nagashima, E. O. Freed, and J. H. Hurley.** 2007. Structural basis for viral late-domain binding to Alix. Nat. Struct. Mol. Biol. **14:**194-199.

108. **Leung, K. F., J. B. Dacks, and M. C. Field.** 2008. Evolution of the multivesicular body ESCRT machinery; retention across the eukaryotic lineage. Traffic **9:**1698-1716.

109. **Lewinski, M. K., M. Yamashita, M. Emerman, A. Ciuffi, H. Marshall, G. Crawford, F. Collins, P. Shinn, J. Leipzig, S. Hannenhalli, C. C. Berry, J. R. Ecker, and F. D. Bushman.** 2006. Retroviral DNA integration: viral and cellular determinants of target-site selection. PLoS Pathog. **2:**e60.

110. **Licata, J. M., M. Simpson-Holley, N. T. Wright, Z. Han, J. Paragas, and R. N. Harty.** 2003. Overlapping motifs (PTAP and PPEY) within the Ebola virus VP40 protein function independently as late budding domains: involvement of host proteins TSG101 and VPS-4. J. Virol. **77:**1812-1819.

111. **Life, R. B., E. G. Lee, S. W. Eastman, and M. L. Linial.** 2008. Mutations in the amino terminus of foamy virus Gag disrupt morphology and infectivity but do not target assembly. J. Virol. **82:**6109-6119.

112. **Macias, M. J., M. Hyvonen, E. Baraldi, J. Schultz, M. Sudol, M. Saraste, and H. Oschkinat.** 1996. Structure of the WW domain of a kinase-associated protein complexed with a proline-rich peptide. Nature **382:**646-649.

113. **Marcucci, K. T., Y. Martina, F. Harrison, C. A. Wilson, and D. R. Salomon.** 2008. Functional hierarchy of two L domains in porcine endogenous retrovirus (PERV) that influence release and infectivity. Virology **375:**637-645.

114. **Martin-Serrano, J. and P. D. Bieniasz.** 2003. A bipartite late-budding domain in human immunodeficiency virus type 1. J. Virol. **77:**12373-12377.

115. **Martin-Serrano, J., S. W. Eastman, W. Chung, and P. D. Bieniasz.** 2005. HECT ubiquitin ligases link viral and cellular PPXY motifs to the vacuolar protein-sorting pathway. J. Cell Biol. **168:**89-101.

116. **Martin-Serrano, J., D. Perez-Caballero, and P. D. Bieniasz.** 2004. Context-dependent effects of L domains and ubiquitination on viral budding. J. Virol. **78:**5554-5563.

117. **Martin-Serrano, J., A. Yarovoy, D. Perez-Caballero, and P. D. Bieniasz.** 2003. Divergent retroviral late-budding domains recruit vacuolar protein sorting factors by using alternative adaptor proteins. Proc. Natl. Acad. Sci. U. S. A. **100:**12414-12419.

118. **Martin-Serrano, J., T. Zang, and P. D. Bieniasz.** 2001. HIV-1 and Ebola virus encode small peptide motifs that recruit Tsg101 to sites of particle assembly to facilitate egress. Nat. Med. **7:**1313-1319.

119. **Maytal-Kivity, V., N. Reis, K. Hofmann, and M. H. Glickman.** 2002. MPN+, a putative catalytic motif found in a subset of MPN domain proteins from eukaryotes and prokaryotes, is critical for Rpn11 function. BMC Biochem. **3:**28.

120. **McCullough, J., M. J. Clague, and S. Urbe.** 2004. AMSH is an endosome-associated ubiquitin isopeptidase. J. Cell Biol. **166:**487-492.

121. **McCullough, J., P. E. Row, O. Lorenzo, M. Doherty, R. Beynon, M. J. Clague, and S. Urbe.** 2006. Activation of the endosome-associated ubiquitin isopeptidase AMSH by STAM, a component of the multivesicular body-sorting machinery. Curr. Biol. **16:**160-165.

122. **McNally, M. T., R. R. Gontarek, and K. Beemon.** 1991. Characterization of Rous sarcoma virus intronic sequences that negatively regulate splicing. Virology **185:**99-108.

123. **Missotten, M., A. Nichols, K. Rieger, and R. Sadoul.** 1999. Alix, a novel mouse protein undergoing calcium-dependent interaction with the apoptosis-linked-gene 2 (ALG-2) protein. Cell Death Differ. **6:**124-129.

124. **Mitchell, R. S., B. F. Beitzel, A. R. Schroder, P. Shinn, H. Chen, C. C. Berry, J. R. Ecker, and F. D. Bushman.** 2004. Retroviral DNA integration: ASLV, HIV, and MLV show distinct target site preferences. PLoS Biol. **2:**E234.

125. **Mölling K, Bolognesi DP, Bauer H, Büsen W, Plassmann HW, and Hausen P.** 1971. Association of viral reverse transcriptase with an enzyme degrading the RNA moiety of RNA-DNA hybrids

126. **Morita, E., V. Sandrin, S. L. Alam, D. M. Eckert, S. P. Gygi, and W. I. Sundquist.** 2007. Identification of human MVB12 proteins as ESCRT-I subunits that function in HIV budding. Cell. Host Microbe **2:**41-53.

127. **Morita, E., V. Sandrin, H. Y. Chung, S. G. Morham, S. P. Gygi, C. K. Rodesch, and W. I. Sundquist.** 2007. Human ESCRT and ALIX proteins interact with proteins of the midbody and function in cytokinesis. EMBO J. **26:**4215-4227.

128. **Mortuza, G. B., L. F. Haire, A. Stevens, S. J. Smerdon, J. P. Stoye, and I. A. Taylor.** 2004. High-resolution structure of a retroviral capsid hexameric amino-terminal domain. Nature **431:**481-485.

129. **Mosser, E. A., J. D. Kasanov, E. C. Forsberg, B. K. Kay, P. A. Ney, and E. H. Bresnick.** 1998. Physical and functional interactions between the transactivation domain of the hematopoietic transcription factor NF-E2 and WW domains. Biochemistry **37:**13686-13695.

130. **Mothes W, Boerger AL, Narayan S, Cunningham JM, and Young JA.** 2000. Retroviral entry mediated by receptor priming and low pH triggering of an envelope glycoprotein

131. **Mukai, A., E. Mizuno, K. Kobayashi, M. Matsumoto, K. I. Nakayama, N. Kitamura, and M. Komada.** 2008. Dynamic regulation of ubiquitylation and deubiquitylation at the central spindle during cytokinesis. J. Cell. Sci. **121:**1325-1333.

132. **Muller, B., T. Patschinsky, and H. G. Krausslich.** 2002. The late-domain-containing protein p6 is the predominant phosphoprotein of human immunodeficiency virus type 1 particles. J. Virol. **76:**1015-1024.

133. **Munshi, U. M., J. Kim, K. Nagashima, J. H. Hurley, and E. O. Freed.** 2007. An Alix fragment potently inhibits HIV-1 budding: characterization of binding to retroviral YPXL late domains. J. Biol. Chem. **282:**3847-3855.

134. **Murk, J. L., B. M. Humbel, U. Ziese, J. M. Griffith, G. Posthuma, J. W. Slot, A. J. Koster, A. J. Verkleij, H. J. Geuze, and M. J. Kleijmeer.** 2003. Endosomal compartmentalization in three dimensions: implications for membrane fusion. Proc. Natl. Acad. Sci. U. S. A. **100:**13332-13337.

135. **Muziol, T., E. Pineda-Molina, R. B. Ravelli, A. Zamborlini, Y. Usami, H. Gottlinger, and W. Weissenhorn.** 2006. Structural basis for budding by the ESCRT-III factor CHMP3. Dev. Cell. **10:**821-830.

136. **Nara, A., N. Mizushima, A. Yamamoto, Y. Kabeya, Y. Ohsumi, and T. Yoshimori.** 2002. SKD1 AAA ATPase-dependent endosomal transport is involved in autolysosome formation. Cell Struct. Funct. **27:**29-37.

137. **Narezkina, A., K. D. Taganov, S. Litwin, R. Stoyanova, J. Hayashi, C. Seeger, A. M. Skalka, and R. A. Katz.** 2004. Genome-wide analyses of avian sarcoma virus integration sites. J. Virol. **78:**11656-11663.

138. **Nelle, T. D., M. F. Verderame, J. Leis, and J. W. Wills.** 1998. The major site of phosphorylation within the Rous sarcoma virus MA protein is not required for replication. J. Virol. **72:**1103-1107.

139. **Nethe, M., B. Berkhout, and A. C. van der Kuyl.** 2005. Retroviral superinfection resistance. Retrovirology **2:**52.

140. **Nickerson, D. P., M. R. Russell, and G. Odorizzi.** 2007. A concentric circle model of multivesicular body cargo sorting. EMBO Rep. **8:**644-650.

141. **Nikko, E. and B. Andre.** 2007. Evidence for a direct role of the Doa4 deubiquitinating enzyme in protein sorting into the MVB pathway. Traffic **8:**566-581.

142. **Nikko, E. and B. Andre.** 2007. Split-ubiquitin two-hybrid assay to analyze protein-protein interactions at the endosome: application to Saccharomyces cerevisiae Bro1 interacting with ESCRT complexes, the Doa4

ubiquitin hydrolase, and the Rsp5 ubiquitin ligase. Eukaryot. Cell. **6:**1266-1277.

143. **Ogert, R. A., L. H. Lee, and K. L. Beemon.** 1996. Avian retroviral RNA element promotes unspliced RNA accumulation in the cytoplasm. J. Virol. **70:**3834-3843.

144. **O'Sullivan, C. T., T. S. Polony, R. E. Paca, and K. L. Beemon.** 2002. Rous sarcoma virus negative regulator of splicing selectively suppresses SRC mRNA splicing and promotes polyadenylation. Virology **302:**405-412.

145. **Ott, D. E.** 2009. Purification of HIV-1 virions by subtilisin digestion or CD45 immunoaffinity depletion for biochemical studies. Methods Mol. Biol. **485:**15-25.

146. **Ott, D. E., L. V. Coren, E. N. Chertova, T. D. Gagliardi, and U. Schubert.** 2000. Ubiquitination of HIV-1 and MuLV Gag. Virology **278:**111-121.

147. **Ott, D. E., L. V. Coren, T. D. Copeland, B. P. Kane, D. G. Johnson, R. C. Sowder 2nd, Y. Yoshinaka, S. Oroszlan, L. O. Arthur, and L. E. Henderson.** 1998. Ubiquitin is covalently attached to the p6Gag proteins of human immunodeficiency virus type 1 and simian immunodeficiency virus and to the p12Gag protein of Moloney murine leukemia virus. J. Virol. **72:**2962-2968.

148. **Ott, D. E., L. V. Coren, T. D. Gagliardi, and K. Nagashima.** 2005. Heterologous late-domain sequences have various abilities to promote budding of human immunodeficiency virus type 1. J. Virol. **79:**9038-9045.

149. **Ott, D. E., L. V. Coren, R. C. Sowder 2nd, J. Adams, K. Nagashima, and U. Schubert.** 2002. Equine infectious anemia virus and the ubiquitin-proteasome system. J. Virol. **76:**3038-3044.

150. **Ott, D. E., L. V. Coren, R. C. Sowder 2nd, J. Adams, and U. Schubert.** 2003. Retroviruses have differing requirements for proteasome function in the budding process. J. Virol. **77:**3384-3393.

151. **Pan, S., R. Wang, X. Zhou, J. Corvera, M. Kloc, R. Sifers, G. E. Gallick, S. H. Lin, and J. Kuang.** 2008. Extracellular Alix regulates integrin-mediated cell adhesions and extracellular matrix assembly. EMBO J. **27:**2077-2090.

152. **Pan, S., R. Wang, X. Zhou, G. He, J. Koomen, R. Kobayashi, L. Sun, J. Corvera, G. E. Gallick, and J. Kuang.** 2006. Involvement of the conserved adaptor protein Alix in actin cytoskeleton assembly. J. Biol. Chem. **281:**34640-34650.

153. **Panet, A., W. A. Haseltine, D. Baltimore, G. Peters, F. Harada, and J. E. Dahlberg.** 1975. Specific binding of tryptophan transfer RNA to avian myeloblastosis virus RNA-dependent DNA polymerase (reverse transcriptase). Proc. Natl. Acad. Sci. U. S. A. **72:**2535-2539.

154. **Parent, L. J., R. P. Bennett, R. C. Craven, T. D. Nelle, N. K. Krishna, J. B. Bowzard, C. B. Wilson, B. A. Puffer, R. C. Montelaro, and J. W. Wills.** 1995. Positionally independent and exchangeable late budding functions of the Rous sarcoma virus and human immunodeficiency virus Gag proteins. J. Virol. **69:**5455-5460.

155. **Patnaik, A., V. Chau, F. Li, R. C. Montelaro, and J. W. Wills.** 2002. Budding of equine infectious anemia virus is insensitive to proteasome inhibitors. J. Virol. **76:**2641-2647.

156. **Patnaik, A. and J. W. Wills.** 2002. In vivo interference of Rous sarcoma virus budding by cis expression of a WW domain. J. Virol. **76:**2789-2795.

157. **Peters, G., F. Harada, J. E. Dahlberg, A. Panet, W. A. Haseltine, and D. Baltimore.** 1977. Low-molecular-weight RNAs of Moloney murine leukemia virus: identification of the primer for RNA-directed DNA synthesis. J. Virol. **21:**1031-1041.

158. **Peters, G. G. and J. Hu.** 1980. Reverse transcriptase as the major determinant for selective packaging of tRNA's into Avian sarcoma virus particles. J. Virol. **36:**692-700.

159. **Piper, R. C. and D. J. Katzmann.** 2007. Biogenesis and function of multivesicular bodies. Annu. Rev. Cell Dev. Biol. **23:**519-547.

160. **Popov, S., E. Popova, M. Inoue, and H. G. Gottlinger.** 2007. Human Immunodeficiency Virus Type 1 Gag Engages the Bro1 Domain of ALIX/AIP1 through Nucleocapsid. J. Virol.

161. **Portsmouth, D., D. Deitermann, B. Salmons, W. H. Gunzburg, and M. Renner.** 2008. Transgene expression facilitated by the v-src splice acceptor can impair replication kinetics and lead to genomic instability of Rous sarcoma virus-based vectors. J. Virol. **82:**1610-1614.

162. **Puffer, B. A., L. J. Parent, J. W. Wills, and R. C. Montelaro.** 1997. Equine infectious anemia virus utilizes a YXXL motif within the late assembly domain of the Gag p9 protein. J. Virol. **71:**6541-6546.

163. **Puffer, B. A., L. J. Parent, J. W. Wills, and R. C. Montelaro.** 1997. Equine infectious anemia virus utilizes a YXXL motif within the late assembly domain of the Gag p9 protein. J. Virol. **71:**6541-6546.

164. **Pullan, L., S. Mullapudi, Z. Huang, P. R. Baldwin, C. Chin, W. Sun, S. Tsujimoto, S. J. Kolodziej, J. K. Stoops, J. C. Lee, M. N. Waxham, A. J. Bean, and P. A. Penczek.** 2006. The endosome-associated protein Hrs is hexameric and controls cargo sorting as a "master molecule". Structure **14:**661-671.

165. **Putterman, D., R. B. Pepinsky, and V. M. Vogt.** 1990. Ubiquitin in avian leukosis virus particles. Virology **176:**633-637.

166. **Raiborg, C., K. G. Bache, D. J. Gillooly, I. H. Madshus, E. Stang, and H. Stenmark.** 2002. Hrs sorts ubiquitinated proteins into clathrin-coated microdomains of early endosomes. Nat. Cell Biol. **4:**394-398.

167. **Rainey, G. J. and J. M. Coffin.** 2006. Evolution of broad host range in retroviruses leads to cell death mediated by highly cytopathic variants. J. Virol. **80:**562-570.

168. **Ratner, L., W. Haseltine, R. Patarca, K. J. Livak, B. Starcich, S. F. Josephs, E. R. Doran, J. A. Rafalski, E. A. Whitehorn, and K. Baumeister.** 1985. Complete nucleotide sequence of the AIDS virus, HTLV-III. Nature **313:**277-284.

169. **Row, P. E., H. Liu, S. Hayes, R. Welchman, P. Charalabous, K. Hofmann, M. J. Clague, C. M. Sanderson, and S. Urbe.** 2007. The MIT domain of UBPY constitutes a CHMP binding and endosomal localization signal required for efficient epidermal growth factor receptor degradation. J. Biol. Chem. **282:**30929-30937.

170. **Row, P. E., I. A. Prior, J. McCullough, M. J. Clague, and S. Urbe.** 2006. The ubiquitin isopeptidase UBPY regulates endosomal ubiquitin dynamics and is essential for receptor down-regulation. J. Biol. Chem. **281:**12618-12624.

171. **Rusten, T. E., T. Vaccari, K. Lindmo, L. M. Rodahl, I. P. Nezis, C. Sem-Jacobsen, F. Wendler, J. P. Vincent, A. Brech, D. Bilder, and H.**

Stenmark. 2007. ESCRTs and Fab1 regulate distinct steps of autophagy. Curr. Biol. **17:**1817-1825.

172. **Saad, J. S., J. Miller, J. Tai, A. Kim, R. H. Ghanam, and M. F. Summers.** 2006. Structural basis for targeting HIV-1 Gag proteins to the plasma membrane for virus assembly. Proc. Natl. Acad. Sci. U. S. A. **103:**11364-11369.

173. **Sabo, Y., N. Laham-Karam, and E. Bacharach.** 2008. Basal budding and replication of the murine leukemia virus are independent of the gag L domains. J. Virol. **82:**9770-9775.

174. **Sachse, M., S. Urbe, V. Oorschot, G. J. Strous, and J. Klumperman.** 2002. Bilayered clathrin coats on endosomal vacuoles are involved in protein sorting toward lysosomes. Mol. Biol. Cell **13:**1313-1328.

175. **Sakalian, M. and N. D. Rapp.** 2006. Rescue of internal scaffold-deleted Mason-Pfizer monkey virus particle production by plasma membrane targeting. Virology **345:**317-327.

176. **Saksena, S., J. Sun, T. Chu, and S. D. Emr.** 2007. ESCRTing proteins in the endocytic pathway. Trends Biochem. Sci. **32:**561-573.

177. **Sawyer, R. C. and H. Hanafusa.** 1979. Comparison of the small RNAs of polymerase-deficient and polymerase-positive Rous sarcoma virus and another species of avian retrovirus. J. Virol. **29:**863-871.

178. **Scheifele, L. Z., R. A. Garbitt, J. D. Rhoads, and L. J. Parent.** 2002. Nuclear entry and CRM1-dependent nuclear export of the Rous sarcoma virus Gag polyprotein. Proc. Natl. Acad. Sci. U. S. A. **99:**3944-3949.

179. **Scheifele, L. Z., E. P. Ryan, and L. J. Parent.** 2005. Detailed mapping of the nuclear export signal in the Rous sarcoma virus Gag protein. J. Virol. **79:**8732-8741.

180. **Schleinkofer, K., U. Wiedemann, L. Otte, T. Wang, G. Krause, H. Oschkinat, and R. C. Wade.** 2004. Comparative structural and energetic analysis of WW domain-peptide interactions. J. Mol. Biol. **344:**865-881.

181. **Schmidt, M. H., B. Chen, L. M. Randazzo, and O. Bogler.** 2003. SETA/CIN85/Ruk and its binding partner AIP1 associate with diverse cytoskeletal elements, including FAKs, and modulate cell adhesion. J. Cell. Sci. **116:**2845-2855.

182. **Schmidt, M. H., I. Dikic, and O. Bogler.** 2005. Src phosphorylation of Alix/AIP1 modulates its interaction with binding partners and antagonizes its activities. J. Biol. Chem. **280:**3414-3425.

183. **Schmitt, A. P., G. P. Leser, E. Morita, W. I. Sundquist, and R. A. Lamb.** 2005. Evidence for a new viral late-domain core sequence, FPIV, necessary for budding of a paramyxovirus. J. Virol. **79:**2988-2997.

184. **Schroder, A. R., P. Shinn, H. Chen, C. Berry, J. R. Ecker, and F. Bushman.** 2002. HIV-1 integration in the human genome favors active genes and local hotspots. Cell **110:**521-529.

185. **Scott, A., H. Y. Chung, M. Gonciarz-Swiatek, G. C. Hill, F. G. Whitby, J. Gaspar, J. M. Holton, R. Viswanathan, S. Ghaffarian, C. P. Hill, and W. I. Sundquist.** 2005. Structural and mechanistic studies of VPS4 proteins. EMBO J. **24:**3658-3669.

186. **Sen, A., C. J. Sherr, and G. J. Todaro.** 1977. Phosphorylation of murine type C viral p12 proteins regulates their extent of binding to the homologous viral RNA. Cell **10:**489-496.

187. **Shih, S. C., D. J. Katzmann, J. D. Schnell, M. Sutanto, S. D. Emr, and L. Hicke.** 2002. Epsins and Vps27p/Hrs contain ubiquitin-binding domains that function in receptor endocytosis. Nat. Cell Biol. **4:**389-393.

188. **Shim, S., L. A. Kimpler, and P. I. Hanson.** 2007. Structure/function analysis of four core ESCRT-III proteins reveals common regulatory role for extreme C-terminal domain. Traffic **8:**1068-1079.

189. **Sommerfelt, M. A., S. S. Rhee, and E. Hunter.** 1992. Importance of p12 protein in Mason-Pfizer monkey virus assembly and infectivity. J. Virol. **66:**7005-7011.

190. **Spearman, P., R. Horton, L. Ratner, and I. Kuli-Zade.** 1997. Membrane binding of human immunodeficiency virus type 1 matrix protein in vivo supports a conformational myristyl switch mechanism. J. Virol. **71:**6582-6592.

191. **Spidel, J. L., R. C. Craven, C. B. Wilson, A. Patnaik, H. Wang, L. M. Mansky, and J. W. Wills.** 2004. Lysines close to the Rous sarcoma virus late domain critical for budding. J. Virol. **78:**10606-10616.

192. **Spitzer, C., S. Schellmann, A. Sabovljevic, M. Shahriari, C. Keshavaiah, N. Bechtold, M. Herzog, S. Muller, F. G. Hanisch, and M. Hulskamp.** 2006. The Arabidopsis elch mutant reveals functions of an ESCRT component in cytokinesis. Development **133:**4679-4689.

193. **Staub, O., S. Dho, P. Henry, J. Correa, T. Ishikawa, J. McGlade, and D. Rotin.** 1996. WW domains of Nedd4 bind to the proline-rich PY motifs in the epithelial Na+ channel deleted in Liddle's syndrome. EMBO J. **15:**2371-2380.

194. **Stauffer, D. R., T. L. Howard, T. Nyun, and S. M. Hollenberg.** 2001. CHMP1 is a novel nuclear matrix protein affecting chromatin structure and cell-cycle progression. J. Cell. Sci. **114:**2383-2393.

195. **Strack, B., A. Calistri, S. Craig, E. Popova, and H. G. Gottlinger.** 2003. AIP1/ALIX is a binding partner for HIV-1 p6 and EIAV p9 functioning in virus budding. Cell **114:**689-699.

196. **Strack, B., A. Calistri, and H. G. Gottlinger.** 2002. Late assembly domain function can exhibit context dependence and involves ubiquitin residues implicated in endocytosis. J. Virol. **76:**5472-5479.

197. **Stuchell, M. D., J. E. Garrus, B. Muller, K. M. Stray, S. Ghaffarian, R. McKinnon, H. G. Krausslich, S. G. Morham, and W. I. Sundquist.** 2004. The human endosomal sorting complex required for transport (ESCRT-I) and its role in HIV-1 budding. J. Biol. Chem. **279:**36059-36071.

198. **Stuchell-Brereton, M. D., J. J. Skalicky, C. Kieffer, M. A. Karren, S. Ghaffarian, and W. I. Sundquist.** 2007. ESCRT-III recognition by VPS4 ATPases. Nature **449:**740-744.

199. **Sudol, M.** 1994. Yes-associated protein (YAP65) is a proline-rich phosphoprotein that binds to the SH3 domain of the Yes proto-oncogene product. Oncogene **9:**2145-2152.

200. **Sudol, M., P. Bork, A. Einbond, K. Kastury, T. Druck, M. Negrini, K. Huebner, and D. Lehman.** 1995. Characterization of the mammalian YAP (Yes-associated protein) gene and its role in defining a novel protein module, the WW domain. J. Biol. Chem. **270:**14733-14741.

201. **Sun, Z., J. Pan, W. X. Hope, S. N. Cohen, and S. P. Balk.** 1999. Tumor susceptibility gene 101 protein represses androgen receptor transactivation and interacts with p300. Cancer **86:**689-696.

202. **Takeshita, T., T. Arita, H. Asao, N. Tanaka, M. Higuchi, H. Kuroda, K. Kaneko, H. Munakata, Y. Endo, T. Fujita, and K. Sugamura.** 1996. Cloning of a novel signal-transducing adaptor molecule containing an SH3 domain and ITAM. Biochem. Biophys. Res. Commun. **225:**1035-1039.

203. **Tamai, K., N. Tanaka, A. Nara, A. Yamamoto, I. Nakagawa, T. Yoshimori, Y. Ueno, T. Shimosegawa, and K. Sugamura.** 2007. Role of Hrs in maturation of autophagosomes in mammalian cells. Biochem. Biophys. Res. Commun. **360:**721-727.

204. **Tanaka, N., M. Kyuuma, and K. Sugamura.** 2008. Endosomal sorting complex required for transport proteins in cancer pathogenesis, vesicular transport, and non-endosomal functions. Cancer. Sci. **99:**1293-1303.

205. **Tang, C., E. Loeliger, P. Luncsford, I. Kinde, D. Beckett, and M. F. Summers.** 2004. Entropic switch regulates myristate exposure in the HIV-1 matrix protein. Proc. Natl. Acad. Sci. U. S. A. **101:**517-522.

206. **Temin HM and Mizutani S.** 1970. RNA-dependent DNA polymerase in virions of Rous sarcoma virus

207. **Thery, C., M. Boussac, P. Veron, P. Ricciardi-Castagnoli, G. Raposo, J. Garin, and S. Amigorena.** 2001. Proteomic analysis of dendritic cell-derived exosomes: a secreted subcellular compartment distinct from apoptotic vesicles. J. Immunol. **166:**7309-7318.

208. **Tommasi di Vignano, A., G. Di Zenzo, M. Sudol, G. Cesareni, and L. Dente.** 2000. Contribution of the different modules in the utrophin carboxy-terminal region to the formation and regulation of the DAP complex. FEBS Lett. **471:**229-234.

209. **Tritel, M. and M. D. Resh.** 2000. Kinetic analysis of human immunodeficiency virus type 1 assembly reveals the presence of sequential intermediates. J. Virol. **74:**5845-5855.

210. **Tsang, H. T., J. W. Connell, S. E. Brown, A. Thompson, E. Reid, and C. M. Sanderson.** 2006. A systematic analysis of human CHMP protein interactions: additional MIT domain-containing proteins bind to multiple components of the human ESCRT III complex. Genomics **88:**333-346.

211. **Usami, Y., S. Popov, and H. G. Gottlinger.** 2007. Potent rescue of human immunodeficiency virus type 1 late domain mutants by ALIX/AIP1 depends on its CHMP4 binding site. J. Virol. **81:**6614-6622.

212. **Vana, M. L., Y. Tang, A. Chen, G. Medina, C. Carter, and J. Leis.** 2004. Role of Nedd4 and ubiquitination of Rous sarcoma virus Gag in budding of virus-like particles from cells. J. Virol. **78:**13943-13953.

213. **VerPlank, L., F. Bouamr, T. J. LaGrassa, B. Agresta, A. Kikonyogo, J. Leis, and C. A. Carter.** 2001. Tsg101, a homologue of ubiquitin-conjugating (E2) enzymes, binds the L domain in HIV type 1 Pr55(Gag). Proc. Natl. Acad. Sci. U. S. A. **98:**7724-7729.

214. **Vito, P., L. Pellegrini, C. Guiet, and L. D'Adamio.** 1999. Cloning of AIP1, a novel protein that associates with the apoptosis-linked gene ALG-2 in a Ca2+-dependent reaction. J. Biol. Chem. **274:**1533-1540.

215. **von Schwedler, U. K., M. Stuchell, B. Muller, D. M. Ward, H. Y. Chung, E. Morita, H. E. Wang, T. Davis, G. P. He, D. M. Cimbora, A. Scott, H. G. Krausslich, J. Kaplan, S. G. Morham, and W. I. Sundquist.** 2003. The protein network of HIV budding. Cell **114:**701-713.

216. **Waters, L. C., B. C. Mullin, T. Ho, and W. K. Yang.** 1975. Ability of tryptophan tRNA to hybridize with 35S RNA of avian myeloblastosis virus and to prime reverse transcription in vitro. Proc. Natl. Acad. Sci. U. S. A. **72:**2155-2159.

217. **Weller, S. K., A. E. Joy, and H. M. Temin.** 1980. Correlation between cell killing and massive second-round superinfection by members of some subgroups of avian leukosis virus. J. Virol. **33:**494-506.

218. **Welsch, S., A. Habermann, S. Jager, B. Muller, J. Krijnse-Locker, and H. G. Krausslich.** 2006. Ultrastructural analysis of ESCRT proteins suggests a role for endosome-associated tubular-vesicular membranes in ESCRT function. Traffic **7:**1551-1566.

219. **Welsch, S., O. T. Keppler, A. Habermann, I. Allespach, J. Krijnse-Locker, and H. G. Krausslich.** 2007. HIV-1 buds predominantly at the plasma membrane of primary human macrophages. PLoS Pathog. **3:**e36.

220. **Wernimont, A. K. and W. Weissenhorn.** 2004. Crystal structure of subunit VPS25 of the endosomal trafficking complex ESCRT-II. BMC Struct. Biol. **4:**10.

221. **Wiesner, S., A. A. Ogunjimi, H. R. Wang, D. Rotin, F. Sicheri, J. L. Wrana, and J. D. Forman-Kay.** 2007. Autoinhibition of the HECT-type ubiquitin ligase Smurf2 through its C2 domain. Cell **130:**651-662.

222. **Wilk, T., I. Gross, B. E. Gowen, T. Rutten, F. de Haas, R. Welker, H. G. Krausslich, P. Boulanger, and S. D. Fuller.** 2001. Organization of immature human immunodeficiency virus type 1. J. Virol. **75:**759-771.

223. **Williams, R. L. and S. Urbe.** 2007. The emerging shape of the ESCRT machinery. Nat. Rev. Mol. Cell Biol. **8:**355-368.

224. **Wills, J. W., C. E. Cameron, C. B. Wilson, Y. Xiang, R. P. Bennett, and J. Leis.** 1994. An assembly domain of the Rous sarcoma virus Gag protein required late in budding. J. Virol. **68:**6605-6618.

225. **Wright, E. R., J. B. Schooler, H. J. Ding, C. Kieffer, C. Fillmore, W. I. Sundquist, and G. J. Jensen.** 2007. Electron cryotomography of immature HIV-1 virions reveals the structure of the CA and SP1 Gag shells. EMBO J. **26:**2218-2226.

226. **Wu, X., Y. Li, B. Crise, and S. M. Burgess.** 2003. Transcription start regions in the human genome are favored targets for MLV integration. Science **300:**1749-1751.

227. **Wu, Y., S. Pan, W. Luo, S. H. Lin, and J. Kuang.** 2002. Hp95 promotes anoikis and inhibits tumorigenicity of HeLa cells. Oncogene **21:**6801-6808.

228. **Xiang, Y., C. E. Cameron, J. W. Wills, and J. Leis.** 1996. Fine mapping and characterization of the Rous sarcoma virus Pr76gag late assembly domain. J. Virol. **70:**5695-5700.

229. **Xiao, J., H. Xia, K. Yoshino-Koh, J. Zhou, and Z. Xu.** 2007. Structural characterization of the ATPase reaction cycle of endosomal AAA protein Vps4. J. Mol. Biol. **374:**655-670.

230. **Xie, W., L. Li, and S. N. Cohen.** 1998. Cell cycle-dependent subcellular localization of the TSG101 protein and mitotic and nuclear abnormalities associated with TSG101 deficiency. Proc. Natl. Acad. Sci. U. S. A. **95:**1595-1600.

231. **Yasuda, J. and E. Hunter.** 1998. A proline-rich motif (PPPY) in the Gag polyprotein of Mason-Pfizer monkey virus plays a maturation-independent role in virion release. J. Virol. **72:**4095-4103.

232. **Yoshimori, T., F. Yamagata, A. Yamamoto, N. Mizushima, Y. Kabeya, A. Nara, I. Miwako, M. Ohashi, M. Ohsumi, and Y. Ohsumi.** 2000. The

mouse SKD1, a homologue of yeast Vps4p, is required for normal endosomal trafficking and morphology in mammalian cells. Mol. Biol. Cell **11:**747-763.

233. **Yuan, B., S. Campbell, E. Bacharach, A. Rein, and S. P. Goff.** 2000. Infectivity of Moloney murine leukemia virus defective in late assembly events is restored by late assembly domains of other retroviruses. J. Virol. **74:**7250-7260.

234. **Yuyama, K., N. Yamamoto, and K. Yanagisawa.** 2008. Accelerated release of exosome-associated GM1 ganglioside (GM1) by endocytic pathway abnormality: another putative pathway for GM1-induced amyloid fibril formation. J. Neurochem. **105:**217-224.

235. **Zabransky, A., M. Sakalian, and I. Pichova.** 2005. Localization of self-interacting domains within betaretrovirus Gag polyproteins. Virology **332:**659-666.

236. **Zamborlini, A., Y. Usami, S. R. Radoshitzky, E. Popova, G. Palu, and H. Gottlinger.** 2006. Release of autoinhibition converts ESCRT-III components into potent inhibitors of HIV-1 budding. Proc. Natl. Acad. Sci. U. S. A. **103:**19140-19145.

237. **Zhadina, M., M. O. McClure, M. C. Johnson, and P. D. Bieniasz.** 2007. Ubiquitin-dependent virus particle budding without viral protein ubiquitination. Proc. Natl. Acad. Sci. U. S. A. **104:**20031-20036.

238. **Zhai, Q., R. D. Fisher, H. Y. Chung, D. G. Myszka, W. I. Sundquist, and C. P. Hill.** 2008. Structural and functional studies of ALIX interactions with YPX(n)L late domains of HIV-1 and EIAV. Nat. Struct. Mol. Biol. **15:**43-49.

239. **Zhao, W. M., A. Seki, and G. Fang.** 2006. Cep55, a microtubule-bundling protein, associates with centralspindlin to control the midbody integrity and cell abscission during cytokinesis. Mol. Biol. Cell **17:**3881-3896.

240. **Zhou, W. and M. D. Resh.** 1996. Differential membrane binding of the human immunodeficiency virus type 1 matrix protein. J. Virol. **70:**8540-8548.

241. **Zhou, X., S. Pan, L. Sun, J. Corvera, S. H. Lin, and J. Kuang.** 2008. The HIV-1 p6/EIAV p9 docking site in Alix is autoinhibited as revealed by a conformation-sensitive anti-Alix monoclonal antibody. Biochem. J. **414:**215-220.